APPLICATION OF SURFACE ENHANCED RAMAN SPECTROSCOPY TO FOOD SAFETY ISSUES

A Dissertation

presented to

the Faculty of the Graduate School

at the University of Missouri

In Partial Fulfillment

of the Requirements for the Degree

Doctor of Philosophy

---

by

LILI HE

Dr. Mengshi Lin, Dissertation Supervisor

DECEMBER 2009

The undersigned, appointed by the dean of the Graduate School,

have examined the thesis entitled

APPLICATION OF SURFACE ENHANCED RAMAN SPECTROSCOPY TO FOOD SAFETY ISSUES

presented by Lili He,

a candidate for the degree of Doctor of Philosophy,

and hereby certify that, in their opinion, it is worthy of acceptance.

Mengshi Lin, Ph.D., Department of Food Science

Azlin Mustapha, Ph.D., Department of Food Science

Ingolf Gruen, Ph.D., Department of Food Science

Hao Li, Ph.D., Department of Mechanical and Aerospace Engineering

ACKNOWLEDGEMENTS

I would like to express my deep and sincere gratitude to my advisor, Dr. Mengshi Lin, for his advising and support that greatly helped me finish my study and research at the University of Missouri. I am deeply grateful to Dr. Hao Li for his guidance to my research. I would also like to thank Dr. Azlin Mustapha and Dr. Ingolf Gruen for kindly serving on my committee and supporting me to complete my study and research.

I appreciate Dr. Joseph Awika, Dr. Nam-Jung King, and Dr. David Ledoux for their collaboration in my projects.

I want to thank all the help from Jian Shi, Xin Sun for nanofabrication work, Liyi and Lecdoux for HPLC work, and my labmates, Cui Fan, Charis Chiu, and Bin Liu.

Last but not least, I want to express my most sincere thanks to all of my family members, especially to my husband, Yang (Alex) Liu, my mother, Wenjuan He, my grandmother, Wanzhen Lou, and my cats Waiwai and Manman, for their love, endless support, and encouragement.

TABLE OF CONTENTS

LIST OF FIGURES

Figure **Page**

LIST OF TABLES

Table **Page**

APPLICATION OF SURFACE ENHANCED RAMAN SPECTROSCOPY TO FOOD SAFETY ISSUES

Lili He

Dr. Mengshi Lin, Dissertation Supervisor

ABSTRACT

In recent years, food safety issues caused by contamination of chemical substances or microbial species have raised a great deal of concern in the United States. Conventional chromatography-based methods for detection of chemical contaminants and microbial plating methods for detection of food-borne pathogens are time-consuming and labor-intensive. In this project, we explored the feasibility of using surface enhanced Raman spectroscopy (SERS) coupled with a variety of substrates (e.g. commercial gold substrates, fractal-like gold nanoaggregates, silver dendrites, and gold-coated zinc oxide nanonecklaces) for detection of various chemical and microbiological food contaminants, including melamine and its analogues, restricted antibiotics and prohibited dyes, and *Bacillus* spores. Our results demonstrate that SERS is capable of detecting, characterizing, and differentiating chemical and microbiological contaminants in foods quickly and accurately. The limit of detection of SERS could reach a single spore or parts per billion level for chemical samples. These results indicate a great potential of using SERS techniques for rapid detection, classification, and quantification of chemical and biochemical contaminants in food products.

CHAPTER 1

INTRODUCTION

1.1 Background

There has been mounting concern in recent years about intentional adulteration of imported foods and food ingredients coming into the United States through the global food chain. In 2007, melamine was implicated in the pet and human food recalls (Cianciolo and others 2008; Brown and others 2007a) and in the global food safety scares in 2008 involving milk and milk-derived products (Ingelfinger 2008; Xin and Stone 2008; Chan and others 2008). In those food safety incidents, melamine was intentionally added to foods and animal feed to boost the protein content. In 2008, the U.S. Food and Drug Administration (FDA) concluded that levels of melamine and its analogues below 2.5 ppm in foods and levels of melamine or one of its analogues alone below 1.0 ppm in infant formula do not raise public health concerns (FDA 2008a,b). Until the 2007 pet food recalls, however, melamine contamination was not routinely monitored since there was no reason to suspect that a supplier would intentionally commit this type of economic fraud.

Other forms of intentional contamination have also impacted the safety of imported foods, particularly seafood, which also received heightened scrutiny in 2007 due to the presence of harmful substances and unapproved drug residues, including fluoroquinolones (FQs), malachite green, gentian violet, etc. From October, 2006 to May, 2007, FDA conducted increased testing of farmed seafood from China for illegal drugs and found that over 15% of the tested products were contaminated with one or more of

these illegal substances. None of these substances are approved for use in aquatic foods sold in the US. The manufacturers of contaminated seafood were primarily from China and Southeast Asia, but also included Mexico and Venezuela.

Recent safety scares with imported products have raised significant concerns in the U.S. about threats to the 1.2 trillion dollar food industry, and to the billions of dollars of imported foods entering the U.S. each year. Imports have increased dramatically by 67% from 2000 until 2006 with total values of all imported goods increasing from $1.17 trillion to $1.95 trillion dollars. The number of shipments has increased by 33% from 23.5 million to 31.3 million shipments. Projections are that the amount of imported goods will increase three-fold between now and 2015 and 40% of these imports will be from China (Leavitt 2007).

Currently, only about 1% of imported foods are randomly inspected by federal agencies primarily due to limited resources and time-consuming protocols required for testing (USAToday 2007). Current analytical methods for testing prohibited substances are mainly HPLC-based that are time-consuming, expensive, and labor-intensive, requiring complex procedures of sample pretreatment and well-trained technicians to operate the instrumentation. Therefore, it is of paramount importance to develop simpler, quicker, but sensitive, and cost-effective methods for monitoring the safety of our imported foods.

1.2 Objectives

The overall goal of this project was to develop surface enhanced Raman spectroscopy (SERS) methods coupled with novel nanosubstrates and evaluate their performance in

detection, characterization, and quantification of different substances involved in recent food safety incidents. We evaluated the performance of SERS methods for detecting chemical and biological contaminants using commercial and home-made substrates in both standard solutions and real food matrix; and verified SERS results using HPLC protocols and other traditional methods. The outline of SERS tests is shown in Figure 1.

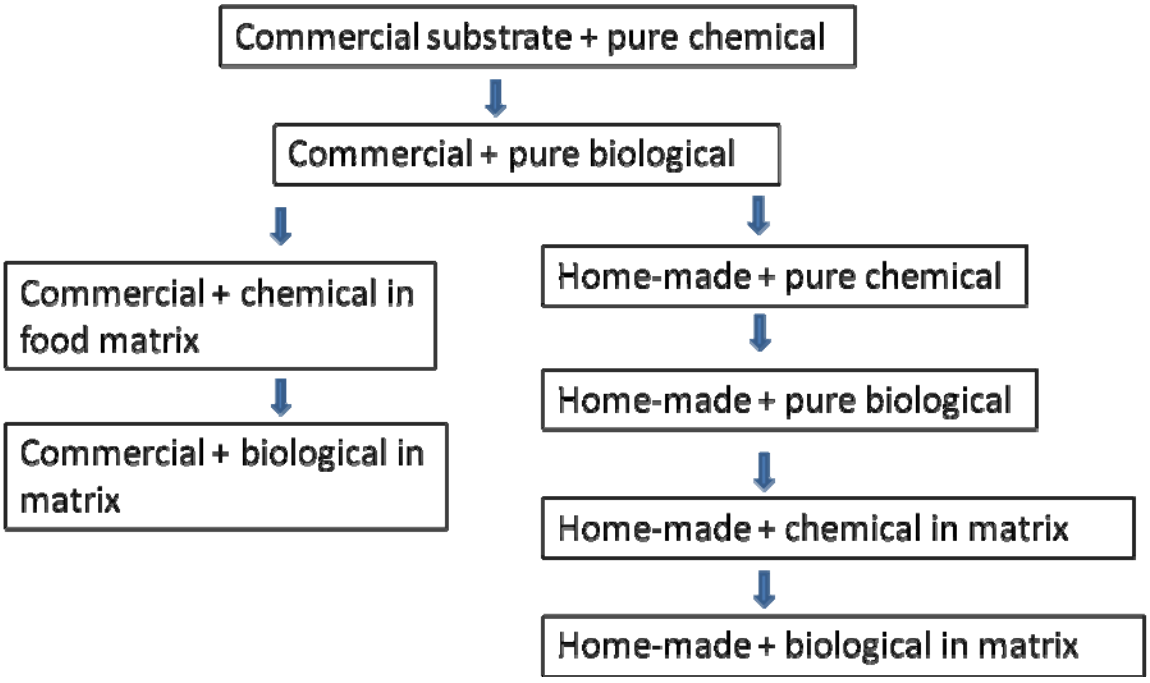

Figure 1. The outline of SERS tests

Several technical questions must be addressed to complete this project:

- Do different nanosubstrates yield different spectra for the same analyte?
- Is a nanosubstrate suitable for testing all different kinds of samples (including complex biological samples)?
- How do nanosubstrate fabrication procedure and conditions affect the performance of nanosubstrates in SERS measurement?
- How to make nanosubstrates that show consistent SERS activities using "bottom-up" technology?
- Which type of nanostructure has the highest sensitivity and best reproducibility?
- How to simplify the extraction procedure for food contaminates? Is the simplified extraction procedure suitable for all different kinds of foods.
- How to simplify SERS detection procedure and data analysis?
- What are the advantages and disadvantages of SERS compared with HPLC and other methods?
- How to combine SERS and HPLC or other methods for solving food safety issues?

To answer the aforementioned questions, we conducted systematic studies and carefully-designed experiments. The details of this project are shown in the next chapters.

CHAPTER 2

LITERATURE REVIEW

2.1 Food contaminants

2.1.1 Chemical contaminants

Since early 2007, there has been mounting concern about melamine contamination in pet food, human foods, food ingredients, and other milk-derived products. In the notorious pet food incident, melamine was intentionally added to wheat gluten and other protein ingredients and incorporated into a variety of animal and human foods. By November 2007, 244 cases of pet deaths and 348 cases of kidney diseases in pets had been confirmed in the United States (MSNBC 2007). Detection of this problem prompted massive recalls of pet foods, livestock feeds, and feeds for commercial aquaculture and hatcheries. The economic impact on the pet food market and the food industry has been enormous. In 2008, milk and milk-derived products contaminated by melamine caused global food safety scares. By December 2008, nearly 300,000 people were ill, more than 50,000 infants were hospitalized, and six infant died in China. In late 2008, trace amounts of melamine and cyanuric acid were detected separately in US-made infant formula products (Cohn 2008; Mendoza 2009). Melamine (2,4,6-triamino-1,3,5-triazine), along with its derivative compounds (*e.g.* cyanuric acid, melamine cyanurate, etc.), was implicated in these food contamination incidents. Melamine is a common industrial chemical often combined with formaldehyde to produce melamine resin, a heat tolerant polymer used in kitchenware and fire retardant fabrics (Sugita and others 1990). Melamine or cyanuric acid was intentionally added to food ingredients to boost protein

content since both melamine and cyanuric acid are high in nitrogen. Although neither melamine nor cyanuric acid are thought to be highly toxic to humans, a current hypothesis is that the toxicity increases when melamine and cyanuric acid are present together (Brown and others 2007). Melamine and cyanuric acid can form extremely insoluble "spoke-like" crystals which contain melamine, cyanuric acid and melamine cyanurate (Perdigao and others 2006) and serve as a biomarker for melamine contamination (Yi and others 1990). These crystals formed in animal kidneys and were suspected of compromising kidney function, leading to acute renal failure.

Recently, imported seafood, primarily from Southeast Asia, China, Mexico, and Venezuela, have received heightened scrutiny by the FDA due to the presence of harmful substances and unapproved drug residues such as crystal violet (CV), malachite green (MG), fluoroquinolones (FQs), and other illegal drugs (FDA 2007a, b). CV and MG are inexpensive triphenylmethane dyes effective against fungal and parasite infections in fish (Alderman 1982). Due to their mutagenic and teratogenic effect to humans, however, they are not approved for use in aquaculture (Culp and Beland 1996). Currently, the FDA and other federal agencies routinely monitor seafood for prohibited dye residues. Zero tolerance policy applies to all residues of CV and MG including its main metabolite leucomalachite green (LMG) in fish. The European Commission requires that methods used must be able to determine the sum of MG and LMG residues at the minimum performance limit of 2 parts per billion (ppb) (Anonymous 2004). FQs (e.g. enrofloxacin, and ciprofloxacin) and chloramphenicol are antibiotics effective in the treatment of various bacterial diseases in aquaculture (Roybal and others 2003). However, residues of FQs in food products are of great concern because of the potential to develop antibacterial resistance to these drugs in humans (Smith and others 1999). As the consumption of

farmed seafood products increases in the US and in other markets around the world, concerns about product safety, particularly of imports, increases. The FDA is concerned that non-compliant and potentially unsafe products will enter the country in greater quantities if the use of unapproved new animal drugs and the misuse of approved new animal drugs remain unchecked. Because of this risk, an import alert was issued on July 27, 2007, permitting FDA District offices to detain, without physical examination, products from firms that have a history of using unapproved drugs.

2.1.2 Food-born microbes

Microbial agencies such as food-borne bacteria and fungi always are involved in food safety and quality issues. For example, food-borne outbreaks caused by *Salmonella* Saintpaul began in April 2008 when thousands of people throughout the United States and Canada got sick after eating contaminated food. *Salmonella* is a gram-negative, rod-shaped bacilli that can cause diarrhea in humans. They are microscopic living organisms that pass from the feces of people or animals to other people or other animals. Salmonellosis is an infection caused by *Salmonella*. According to the Centers for Disease Control and Prevention (CDC), salmonellosis causes an estimated 1.4 million cases of food-borne illness and more than 500 deaths annually in the United States. The investigation by CDC showed that jalapeño peppers, serrano peppers, and tomatoes that were grown and packed in Mexico were a major source of contamination in the outbreak.

Outbreaks due to food-borne pathogen *Escherichia coli* O157:H7 have increased in frequency since the recognition of food-borne illness caused by this microorganism

(Riley and others 1983). In the fall of 2006, spinach leaves from the Salinas Valley in California contaminated with *E. coli* O157:H7 infected 204 persons across the United States, in which 3 people died from this outbreak. *E. coli* O157:H7 can extensively survive in acidic foods, and its infective dose is as low as 10 - 100 cells (Lin and others 1996). The reported sources of infection have included minced beef, vegetables, apple cider and water (Nastasijevic and others 2008). Therefore, an efficient and safe antibacterial agent preventing this microorganism is highly needed.

Detection of *Bacillus* spores is of considerable importance in solving environmental, industrial and clinical issues. In the agricultural and food industries, the ubiquity of these spore-forming bacteria allows them to potentially threaten the safety of a wide range of foods, including dairy products, meats, cereals, vegetables, spices, and ready-to-eat meals. In addition, *Bacillus* spores can survive standard processing and sanitation treatments for foods and food processing equipment. As a consequence, germination of *Bacillus* spores may potentially lead to food-borne illnesses or outbreaks. Pathogenecity of *Bacillus* species has been mainly related to *B. cereus* and *B. anthracis* species (Turnbull 1996). *B. cereus* is a well-known food-transmitted pathogen that may cause illness through the production of either an emetic (vomit-inducing) or diarrheal toxin (Granum and Lund 1997). The infectious dose is thought to be between 10^5 to 10^8 cells or spores per gram of food (Granum and Lund 1997). *B. anthracis*, the etiological agent of anthrax, is a highly virulent pathogen for higher animals and a potential biological warfare agent. The Center for Disease Control and Prevention (CDC) estimates that inhalation of 10,000 *B. anthracis* spores or 100 nanograms would be lethal to 50% of an exposed population (Inglesby and others 2002). Spores of *B. anthracis* species were used in the 2001

bioterrorism attacks against the United States government and others and impacted postal service for many months (Rasco and Bledsoe 2005).

2.2 Conventional approaches of detecting food contaminants

2.2.1 Chromatography-based methods

Chromatography is a technique for the separation of mixtures. It involves samples dissolved in a mobile phase, which may be a gas or a liquid. The mobile phase is then forced through a stationary phase, which may be a liquid film on the surface of an inert support material or a solid surface. Interaction between different analytes in the sample and the stationary phase allows different analytes to move at differing rates, resulting in the separation (Braithwaite and Smith 1996). Based on a different solid matrix, chromatography can be classified into paper chromatography, thin layer chromatography, and column chromatography (e.g. gas chromatography and liquid chromatography). Based on different interaction between analytes and stationary phase, chromatography can be classified into gel filtration chromatography (differences in size), ion exchange chromatography (differences in charge), affinity chromatography (recognition of specific ligands), hydrophobic interaction chromatography (differences in hydrophobic residues), etc. (Cazes and Scott 2002).

Gas and liquid chromatography coupled with different detectors (e.g. UV and MS) are the most versatile and widespread techniques employed in modern analytical chemistry. These techniques are sensitive, accurate, and relatively fast. Therefore, chromatography-based techniques have been widely used as standard methods by the FDA and other federal agencies, industrial sectors, and academia as well. For examples, HPLC/UV (FDA

2007c), LC-MS (Turnipseed and others 1998; Andersen and others 2006), LC/MS/MS (Smoker and Krynitsky 2008), and GC/MS (Litzau and others 2008) have been used by the FDA for detection and identification of melamine and many illegal drugs in food products. Generally, the limit of detection (LOD) for melamine using chromatography-based methods could reach the ppb level.

2.2.2 Conventional plating methods for food-borne microbes

Conventional methods for detection of food-borne bacteria involve cultural enrichment and isolation in non-selective and selective media. The procedure usually involves cultivation, isolation, screening and confirmation. Cultivation consists of pre-enrichment and selective enrichment. Pre-enrichment is to restore the injured target microorganisms in a non-selective environment. Selective enrichment facilitates the growth of target bacteria and suppresses the non-target ones. In the isolation step, enriched cultures are streaked onto a selective agar medium. Usually, the target bacteria will be selected based on their unique color or shape. Subsequent confirmation steps include biochemical tests that are based on whether or not the bacterial isolates can utilize a specific substrate during growth with color changes or gas production. The FDA Bacteriological Analytical Manual (BAM) is a widely used microbiological manual for food pathogen detection.

Other advanced technologies such as polymerase chain reaction (PCR), 16S rDNA/RNA analysis, immunomagnetic separation (IMS), and various microscopic methods are more complex, cumbersome, and often requiring highly trained technicians to conduct the tests. For example, IMS requires additional non-selective and selective pre-enrichment steps. PCR could give results within a few hours, but it relies on primers

designed to yield specific PCR product formations (Kroll and others 1993). Therefore, it is of paramount importance to develop simpler, quicker, but sensitive, and cost-effective methods for detection and monitoring food contaminates.

2.3 Vibrational spectroscopy

Vibrational spectroscopy is a spectroscopic method for studying molecule vibration. A molecular vibration occurs when atoms in a molecule are in periodic motion while the molecule as a whole has constant translational and rotational motion. A molecular vibration is excited when the molecule absorbs a quantum of energy, E, corresponding to the vibration's frequency, ν, according to the relation $E = h\nu$, where h is Planck's constant. A fundamental vibration is excited when the energy is absorbed by the molecule in its ground state. There are two types of vibrational spectroscopy: infrared spectroscopy and Raman spectroscopy.

2.3.1 Infrared spectroscopy

Infrared radiation spans a section of the electromagnetic spectrum having wavenumbers from roughly 13,000 to 10 cm^{-1}, or wavelengths from 0.78 to 1000 μm. The infrared portion of the electromagnetic spectrum is divided into three regions; the near-, mid- and far- infrared, named for their relation to the visible spectrum.

Infrared absorption information is generally presented in the form of a spectrum with wavelength or wavenumber as the x-axis and absorption intensity or percent transmittance as the y-axis. Transmittance, T, is the ratio of radiant power transmitted by

the sample (I) to the radiant power incident on the sample (I_0). Absorbance (A) is the logarithm to the base 10 of the reciprocal of the T.

$$A = \log_{10}(1/T) = -\log_{10}T = -\log_{10}I/\ I_0 \qquad (2\text{-}1)$$

Infrared spectroscopy exploits the fact that molecules have specific frequencies at which they rotate or vibrate corresponding to discrete energy levels (vibrational modes). These resonant frequencies are determined by the shape of the molecular potential energy surfaces, the masses of the atoms and, by the associated vibronic coupling. In order for a vibrational mode in a molecule to be IR active, it must be associated with changes in the permanent dipole. The natural frequency of vibration of a bond is given by

$$\tilde{\nu} = \frac{1}{2\pi c}\sqrt{\frac{K}{\mu}} \qquad (2\text{-}2)$$

which is derived from Hooke's Law for vibrating springs. The reduced mass, μ, of the system is given by

$$\mu = \frac{m1m2}{m1 + m2} \qquad (2\text{-}3)$$

K is the constant that varies from one bond to another. Thus, the resonant frequencies can be in a first approach related to the strength of the bond, and the mass of the atoms at either end of it. The frequency of the vibrations can be associated with a particular bond type.

The general regions of the infrared spectrum in which various kinds of vibrational bands are observed are outlined in Figure 2 (Cited from http://www.cem.msu.edu/~reusch/VirtualText/Spectrpy/Images/irspect.gif). Note that the blue colored sections above the dashed line refer to stretching vibrations, and the green colored band below the line encompasses bending vibrations. The complexity of infrared spectra in the 1450 to 600 cm^{-1} region makes it difficult to assign all the absorption bands, and because of the unique patterns found there, it is often called the fingerprint region.

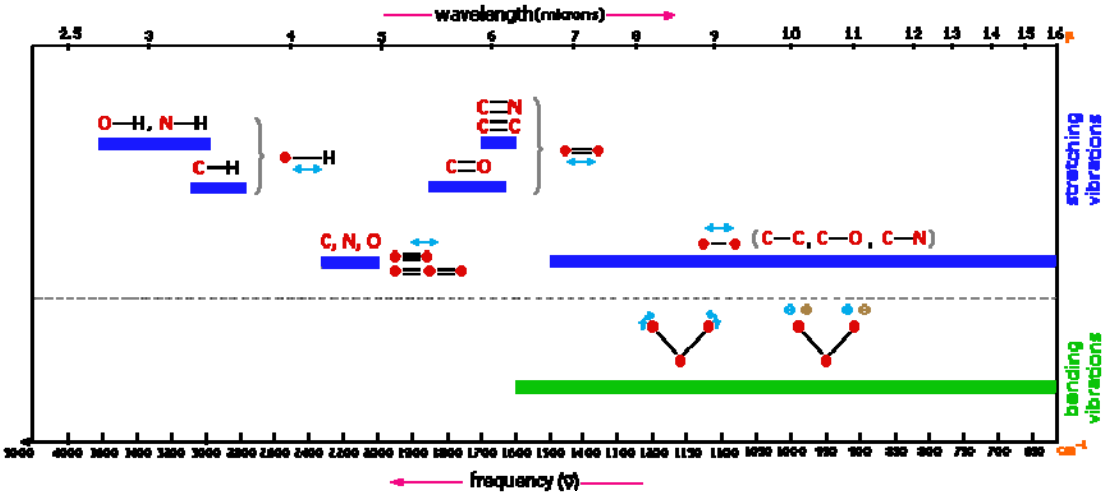

Figure 2. Infrared spectrum

There are a number of advanced types of IR spectroscopy, including Fourier transform infrared spectrometer (FTIR) and two-dimensional (2D) infrared correlation spectroscopy. In FTIR, instead of recording the amount of energy absorbed when the frequency of the IR light is varied (monochromator), the IR light is guided through an interferometer. Performing a mathematical Fourier transform on this signal results in a spectrum identical to that from conventional (dispersive) infrared spectroscopy. Two-dimensional infrared correlation spectroscopy is the application of 2D correlation analysis on infrared spectra. By extending the spectral information of a perturbed sample, spectral analysis is simplified and resolution is enhanced.

2.3.2 Raman spectroscopy

Raman spectroscopy is a spectroscopic technique for studying vibrational, rotational, and other low-frequency modes in a system. It relies on inelastic scattering, or Raman scattering, of monochromatic light, usually from a laser in the visible, IR, or near ultraviolet (UV) range. The laser light interacts with phonons or other excitations in the system, resulting in the energy of the laser photons being shifted up or down. The shift in energy gives information about the phonon modes in the system (McCreery 2000). Samples can be measured non-destructively, on-line, and in real-time. IR spectroscopy yields similar but complementary information to Raman spectroscopy. Spontaneous Raman scattering is typically very weak, and as a result the main difficulty of Raman spectroscopy is separating the weak inelastically scattered light from the intense Rayleigh scattered light.

The Raman effect occurs when light impinges upon a molecule and interacts with the electron cloud of the bonds of that molecule. The incident photon excites one of the phonons into a virtual state. For the spontaneous Raman effect, the molecule will be excited from the ground state to a virtual energy state, and relax into a vibrational excited state, which generates Stokes Raman scattering (McCreery 2000). If the molecule was already in an elevated vibrational energy state, the Raman scattering is then called anti-Stokes Raman scattering (Figure 3).

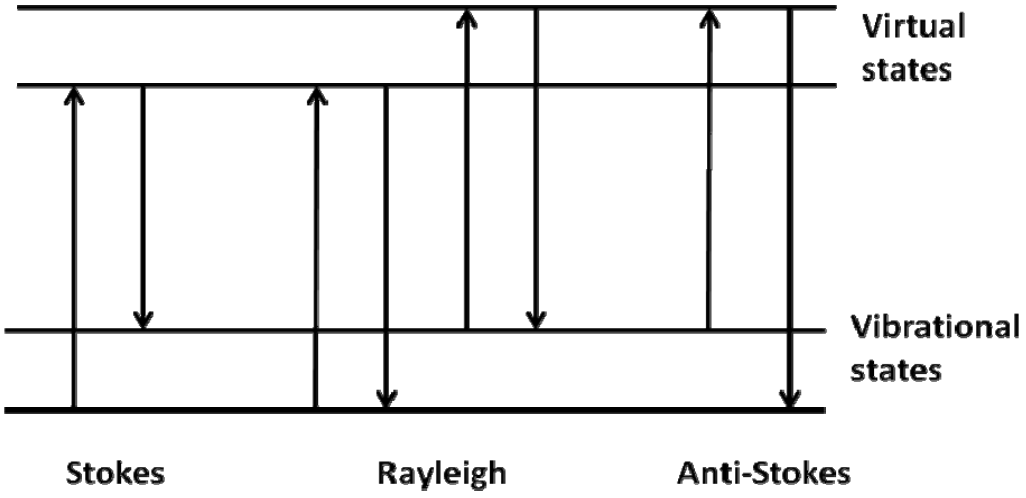

Figure 3. Raman and Rayleigh effects

Numerically, the energy difference between the initial and final vibrational levels, or Raman shift in wave numbers (cm^{-1}), is calculated through

$$\bar{\nu} = \frac{1}{\lambda_{inc}} - \frac{1}{\lambda_{sc}} \quad (2\text{-}4)$$

in which λ_{inc} and λ_{sc} are the wavelengths (in cm) of the incident and Raman scattered photons, respectively. The vibrational energy is ultimately dissipated as heat. Because of the low intensity of Raman scattering, the heat dissipation does not cause a measurable temperature rise in a material.

Raman scattering occurs because a molecular vibration can change the polarizability. The polarizability measures the ease with which the electron cloud around a molecule can be distorted. The change is described by the polarizability derivative, $\frac{da}{dQ}$, where a is the polarizability of the molecule, Q is the normal coordinate of the vibration.

There are a number of advanced types of Raman spectroscopy, including surface enhanced Raman, tip-enhanced Raman, resonance Raman, transmission Raman, etc.

2.3.2.1 Surface enhanced Raman spectroscopy

Surface enhanced Raman spectroscopy (SERS) is a variant of Raman spectroscopy that exploits nanoscale phenomena. As mentioned above, Raman signals are normally very weak and can only be used for bulk samples or concentrated solutions. Metallic nanostructures (typically gold and silver) could tremendously enhance the Raman cross-section of the sample molecules that are in a certain proximity of the metal surface due to the large electromagnetic field induced by localized surface plasmon resonance (Haynes

and others 2005a). Therefore, LOD of SERS could reach the ppb or a single molecule level.

SERS phenomena were first discovered from measuring pyridine adsorbed on electrochemically roughened silver materials in 1974 by Martin Fleischman and his colleagues at Southampton University (Southampton, England). However, they concluded that the greatly enhanced signals were from the increased surface area. In 1977, Richard Van Duyne and his group at Northwestern University (Chicago, IL, USA) confirmed the SERS phenomena and firstly proposed the electromagnetic enhancement mechanism. Later, Albrecht and Creighton proposed a charge-transfer effect to the mechanisms behind the SERS phenomena (Haynes and others 2005b). Both Nie and Kneipp groups achieved single-molecule detection independently with different experimental conditions. The Nie study included a correlated topographical and optical characterization of unaggregated silver nanoparticles dosed with Rhodamine 6G (R6G) molecules. They concluded that the single-molecule enhancement was 10^6–10^7 larger than the population-averaged enhancement (Doering and Nie 2002). The Kneipp research group, on the other hand, probed small (100-150 nm) silver colloid aggregates dosed with crystal violet molecules. The large (10^{14}) single-molecule enhancement is hypothetically attributed to large electromagnetic fields generated by fractal-pattern clusters of silver colloid nanoparticles (Kneipp and Kneipp 2006).

2.3.2.1.1 SERS mechanisms

Basically, there are two models that explain SERS mechanisms, “electromagnetic (EM) model” and “charge transfer (CT) model”.

2.3.2.1.1.1 EM model

According to the EM model, the increase in the Raman intensity is caused by extremely high local electromagnetic fields that arise from localized surface plasmon resonance (LSPR), where it is called “hot-spots”. Surface plasmons are oscillating conduction electron of the electromagnetic fields on a metal interface. In order to produce surface plasmon, the dielectric constant of the metal must be negative. Typical metals that support surface plasmons are silver, gold, copper, platinum, titanium, and chromium. Generally, silver generates more surface plasmon than other metals due to its large negativity of dielectric constant. On smooth surfaces, plasmon excitation energy escapes and is lost as heat. Rough surfaces with localized space could accumulate some of the plasmons so that the plasma energy is radiated and generate high local electromagnetic fields. Roughness is not affected by a single factor, but a combination of several factors such as particle size, shape, and gap, etc. Typically, the optimum roughness is in the nanometer range (10 to 100 nm). Resonance occurs when an electric field (laser light) at a certain incident wavelength excites the localized surface plasmons in strong light scattering, resulting in the appearance of intense surface plasmon absorption bands and an enhancement of the local electromagnetic fields. The frequency and intensity of the surface plasmon absorption bands depend on the type of metal, nanostructure size, size distribution, and shape, as well as the environments which surround them (Willets and VanDuyne 2007).

Suppose a molecule in the vicinity of the sphere (2r) with the distance d is exposed to a field E. The electromagnetic enhancement factor G_{SERS} can be expressed as

$$G_{SERS}(r_m, v) = \left|\frac{E(r_m, v)}{E_{inc}(v)}\right|^4 \sim \left|\frac{\varepsilon_m - \varepsilon_0}{\varepsilon_m + 2\varepsilon_0}\right|^4 \left(\frac{r}{r+d}\right)^{12} \quad (2\text{-}5)$$

where $E(r_m,v)$ is the total electric field at the molecule location r_m, $E_{inc}(v)$ is the incident excitation field, and v is the laser frequency. ε_m is the wavelength-dependent dielectric constant of the metal composing the sphere, and ε_0 is the dielectric constant of the local environment around the sphere (Haynes and others 2005a; Kneipp and others 2002).

This relation reveals that when $\varepsilon_m = -2\varepsilon_0$, which can be achieved for silver and gold at certain wavelengths in the visible and NIR, the magnitude of the electric field at the surface of the sphere becomes very large. This field enhancement is induced by satisfying the LSPR condition. Similar relations can be derived for the extinction and scattering cross sections of the nanoparticles. Maximization of these cross sections at resonant wavelengths yields the spectroscopic signature of exciting the LSPR. Generally, electromagnetic enhancement relies on Raman-active molecules being confined within these electromagnetic fields and contributes an average enhancement factor of ≥10,000.

2.3.2.1.1.2 CT model

According to the CT model, an incident photon excites an electron from the metal surface into an adsorbed molecule, creating a negatively charged excited molecule. The molecular geometry of this excited molecule differs from that of the neutral species. This charge transfer induces a nuclear relaxation within the excited molecule so that the electron returns to the metal surface and creates an excited neutral molecule and the emission of a wavelength shifted (Raman) photon. This mechanism is site-specific and

analyte-dependent. Molecules must be directly adsorbed to the roughened surface (Haynes and others 2005a). Some chemicals like methanol doesn't show any SERS enhancement (Kneipp and others 2002). Others like rhodamine 6G, crystal violet, pyridine, and benzotriazole were shown to have large enhancement in SERS (Le Ru and others 2007). This enhancement factor is thought to contribute an average of 100 fold.

2.3.3 SERS-active substrates

A well-performing SERS substrate is the key in SERS applications as well as understanding the SERS mechanism. To date, various types of SERS-active substrates have been developed, including silver colloid (Xu and Fang 2004), silver nanowires (Tao and others 2003), silver/gold fractal aggregates (Qiu and others 2008b), silver dendrite (Song and others 2006), roughened gold film electrode (Sauer and others 2004), gold-coated laser-ablated silicon plate (Alexander and Le 2007b), silver-coated microarray platform (Allain and Vo-Dinh 2002), etc. Many of the existing SERS substrates were fabricated by "bottom-up" techniques (e.g. self-assembly of chemicals) (He and others 2008a), which can usually provide tremendously enhanced Raman signals. However, a common problem with these "bottom-up" substrates is that they often give inconsistent performance when spot-to-spot or substrate-to-substrate tests are conducted. This is mainly because of a lack of structural uniformity and integrity over the entire area of the substrate. Other substrates fabricated by "top-down" techniques (e.g. electro-beam lithography) (Alexander and Le 2007b), however, often produce weaker signals although reproducible signals can be obtained. Additionally, most "top-down" techniques involve the use of expensive equipment and/or complex procedures. Therefore, a better method is

needed to fabricate substrates that are reproducible, stable, easy-to-make, economic, and can provide satisfactory signal enhancement. However, it is very difficult to make a substrate possessing a high enhancement factor and high reproducibility at the same time. Some compromises are required between these two parameters. For real-world applications, reproducibility is considered more important than enhancement factors (Brown and Milton 2008).

2.4.4 SERS applications in food science

Nanoscaled silver and gold materials are two commonly used nanomaterials to enhance Raman scattering due to the large electromagnetic field induced by localized surface plasmon resonance (Haynes and others 2005a). The unique "fingerprint-like" and sensitive properties make this technique promising in rapid, accurate, and sensitive detecting of chemical and biological agents in food products. Various silver and gold-based nanosubstrates have been developed. SERS has been explored in characterization and measurement of various food components and contaminants, such as Vitamin A (Wang and others 2004) and C (Panicker and others 2006), food dye E102 (Peica and others 2005), flavone (Teslova and others 2007), sodium benzoate (Peica and others 2007), dimethyl formamide (Mishra and others 2007), melamine and its analogues (He and others 2008b; Lin and others 2008), Sudan dyes (Wu and others 2006), crystal violet dyes (He and others 2008a), and food-borne microbes (Chu and others 2008; He and others 2007).

CHAPTER 3

MATERIALS AND METHODS

3.1 Food contaminants

3.1.1 Melamine and its analogues

3.1.1.1 Preparation of melamine and its analogues in standard solution

Melamine and cyanuric acid were purchased from Fisher Scientific Inc. (Pittsburgh, PA, USA). Both melamine and cyanuric acid are poorly soluble in water. For example, at 25°C, the solubility of melamine and cyanuric acid is about 2.5×10^{-2} and 2.0×10^{-2} mol L^{-1}, respectively (Seifer 2002). In this study, a series of concentrations (10^{-2}, 10^{-3}, 10^{-4} 10^{-5}, and 10^{-6} mol L^{-1}) of melamine in water were prepared. An aqueous solution of cyanuric acid (10^{-3} mol L^{-1}) was also prepared by dissolving in water with stirring; when cyanuric acid particles were completely dissolved, the solution was analyzed immediately by SERS. Melamine cyanurate was prepared by adding equal amounts (10^{-3} mol L^{-1}) of melamine and cyanuric acid together in a glass container.

3.1.1.2 Preparation of melamine in food matrices

3.1.1.2.1 Wheat gluten

Wheat gluten was purchased from a local oriental grocery store. Melamine was incorporated into wheat gluten at the levels of 2.0, 1.0, 0.5, 0.1, and 0% (w/w). Duplicate samples were prepared for each treatment.

3.1.1.2.2 Chicken feed

A commercial type chicken basal diet was prepared using corn (52.7%), soybean meal (28.7%), pork meal (4.5%), fish meal (3.5%), corn oil (6%), mineral (0.1%), vitamin premixes (0.08%), others (4.4%). The basal diet was formulated to include 3% sand. Melamine was substituted for sand in the basal diet to achieve the desired melamine concentrations so that each diet had the same amount of nutrients. Melamine was incorporated into chicken feed at levels of 2.0, 1.0, 0.5, 0.1 0.05, and 0% (w/w). Duplicate samples were prepared for each treatment.

3.1.1.2.3 Cake

To determine how food processing conditions affect melamine recovery in foods made with contaminated food ingredients, two food models, home-baked cake and noodles, were selected.

Commercial premium cake mix (J. M. Smucker Company, Orrville, OH, USA), cooking oils, large farm eggs and table salt were purchased from a local supermarket. Melamine was added into five batches of cake mix (34.5 g) at the levels of 2.0, 1.0, 0.5, 0.1 and 0% (w/w), respectively. A mixture of tap water (100 mL), oil (26 mL) and one egg (egg white and egg yolk, 40 g) was prepared by hand whisking and then divided evenly into five portions. Each portion (32.76 g) was blended with the cake mix (34.5 g) containing different concentrations of melamine. Melamine content in each batter was estimated to be 1.020, 0.508, 0.256, 0.051, and 0% (w/w), respectively. These percentages were calculated as the weight of added melamine in each batter divided by the total weight of cake mix, liquid portion (water, oil, and egg), and the added melamine. Each cake batter was then baked in an oven at 170^{o}C for 15 min. After baking, cakes

were air-dried for 24 h and ground with a mortar and pestle before extraction. The dry basis of melamine content in each batter was estimated to be 1.680, 0.841, 0.424, 0.085, and 0%, respectively. Duplicate samples were prepared for each treatment.

3.1.1.2.3 Noodle

Noodles were made from wheat gluten spiked with different concentrations of melamine (2.0, 1.0, 0.5, and 0.1% w/w), tap water, and salt (gluten: water: salt = 100: 25: 3.6 w/v/w). All ingredients were then put in a blender (Kitchen Aid, St. Joseph, MI, USA) and mixed at low speed for 1 min and at high speed for 4 min to allow dough formation. Melamine contents in dough were estimated to be 1.30, 0.65, 0.31, and 0.07% (w/w), respectively. These percentages were calculated as the weight of added melamine divided by the total weight of the dough. The dough was hand-kneaded for 1 min, shaped into a rectangular form and stored inside a closed plastic bag at room temperature for 1 h. The dough sheets were passed through the sheeting rolls (Kitchen Aid) three times at increasing roll settings of 1 to 3 to 5 to produce a 5-mm-thick dough sheet. Raw noodles were air-dried for 24 h and ground with a mortar and pestle before extraction. The dry basis of melamine content in each batter was estimated to be 2.513, 1.088, 0.547, 0.110, and 0%, respectively. Duplicate samples were prepared for each treatment.

3.1.1.3 Melamine extraction from food matrices

Extraction of melamine in samples was based upon a standard FDA method for melamine detection with some modifications (FDA, 2007b). Briefly, 50% (v/v) acetonitrile in water was used to extract melamine from all tested samples. For wheat

gluten and chicken feed samples, melamine was extracted at a ratio of 0.1 g sample to 10 mL extraction solvent. The samples were then sonicated using an ultrasonic processor equipped with a 6.5 mm tapered microtip (Sonics & Materials, Inc. Newtown, CT) for 2 min with 30 s working and 30 s interval at an amplitude of 36%. For cake and noodle samples, melamine was extracted at the ratio of 2.0 g sample with 15 ml extraction solvent, and sonicated for 3 min with 1 min working and 1 min interval at amplitude of 36%.

For SERS analysis, samples were set for 30 s to allow for the setting of large particles, then 0.3 μL of the upper layer of the extract was deposited onto a substrate. For HPLC analysis, extracts were further purified by centrifugation at 2,266 × *g* for 20 min. The supernatant of each sample was then diluted with 0.1 N HCl and filtered through a 0.45 μm nylon syringe filter. Melamine standard stock solution (1.0 mg/mL) was prepared with an acetonitrile: water (60: 40 v/v). A series of concentrations of standard melamine solutions were prepared by diluting the stock solution with 0.1 N HCl to obtain concentrations of 1, 5, 10, 25, 50, 75, 100, 200, 300, 400 μg/mL, respectively.

3.1.2 Prohibited antifungal dyes

Crystal violet (CV) was purchased from Fisher Scientific (Rochester, NY, USA) and malachite green (MG) from MP Biomedicals (Solon, OH, USA). Standard solutions for CV and MG were prepared and diluted in 50% ethanol solution in the range of 0.2 ppb to 2000 ppb.

3.1.3 Restricted antibiotics

Enrofloxacin (ENRO), ciprofloxacin (CIP), and chloramphenicol (CHL) were purchased from Fisher Scientific (Rochester, NY, USA). Standard solutions of ENRO and CHL were prepared and diluted in 50% ethanol solution in the range of 20 ppb to 200 ppm. CIP was prepared and diluted in hydrochloric acid solution (pH = 5) in the range of 20 ppb to 200 ppm.

3.1.4 *Bacillus* spores

Bacillus species are rod-shaped, Gram-positive, spore-forming aerobic or facultatively anaerobic bacteria. Under stressed conditions such as lack of key nutrients, certain *Bacillus* cells in the vegetative state will spontaneously develop into a dormant state known as an endospore (Turnbull 1996). The spore is organized into a series of concentrically arranged structures (Figure 4), each of which contribute in a different way to resist against environmental stresses such as heat, radiation, desiccation and chemical disinfectants (Turnbull 1996). Particularly, the central core of spores carries the constituents of future vegetative cell, accompanied by dipicolinic acid (DPA) which is essential to the heat resistance. Up to 15% of the dry weight of the spore consists of calcium dipicolinate (CaDPA). CaDPA or its acid form, DPA, can be used as a biomarker of bacterial spores since it is found in almost all bacterial spores but not in pollen and mold spores (Farquharson and others 2004; Janssen and others 1958).

Bacillus strains used in this study were obtained from the culture collection in the Food Microbiology laboratory at the University of Missouri, Columbia, MO. They included *B. cereus* ATCC 13061, *B. cereus* ATCC 10876, *B. cereus* sp. *B. subtilis* sp., and *B. stearothermophilus* sp. Bacteria were activated by transferring vegetative cells

from refrigerated slant to tryptic soy agar (TSA) (Difco, MD, USA), followed by incubating at 37°C for 48 h. A representative colony was then picked, cultured on TSA and incubated at 37°C for 7 days until cells turned into spores due to the depletion of nutrients. The spores were then washed from the plates with sterile water, followed by centrifuging at 12,000 g for 10 min. This procedure was repeated five times to obtain pure spores.

Dipicolinic acid (2, 6-pyridinedicarboxylic acid, DPA), dodecylamine (DDA) were purchased from Fisher Scientific Inc. (Pittsburgh, PA, USA). The extraction of DPA from *B. subtilis* sp. followed the method of Farquharson (2004). Briefly, 100 µl of DDA solution (50 mM) in ethanol was pre-heated to 78°C and then added to ~10 µg *B. subtilis* spores to digest the spore coat. After 1 min, the resultant solution was drawn and deposited onto the substrate for Raman measurement.

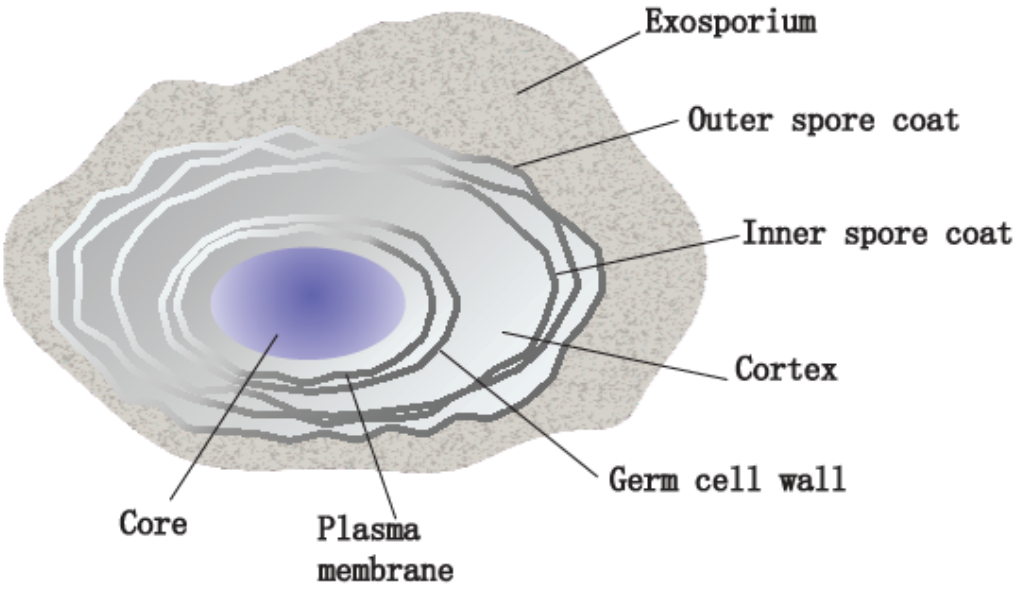

Figure 4. Graphic structure of a typical *Bacillus* spore

3.2 SERS-active substrates

3.2.1 Commercial Klarite^{TM} gold substrate

Klarite^{TM} SERS-active gold nanosubstrates (D3technologies Ltd, Glasgow, UK) were used in this study. Klarite^{TM} devices were fabricated on silicon wafers coated with 100 nm gold. A 6 mm × 10 mm chip including a 4 mm × 4 mm patterned SERS-active area and an unpatterned gold reference area is adhered to a standard microscope slide. Scanning electron microscopy (SEM) micrograph taken by FEI Quanta 600F Environmental SEM (FEI Company, Hillsboro, Oregon, USA) was used to show the patterned gold surface under high vacuum and secondary electron mode.

3.2.2 Home-made nanosubstrates

3.2.2.1 Gold fractal nanoaggregates

Gold nanostructures were fabricated through a self-assembly process using gold (Au) nanoparticles as building blocks. First, gold nanoparticles with size between 30 and 50 nm were produced by a hydrothermal citrate-reduction method. Sodium citrate (0.05 M) was used to reduce the gold (III) ions in 1 mM of HAuCl4 aqueous solution (Sigma-Aldrich Chemicals, St Louis, MO, USA) by continuously stirring with a magnetic stir bar at 300 rpm at boiling temperature. The formation of gold nanoparticles was confirmed by the change of solution color from initially fainted-yellow to finally wine-red. The gold nanoparticle solution appeared to be stable over several months because citrate serves as a capping agent at room temperature and is capable of controlling the particle size and morphology. A small quantity (5 mL) of cetyltrimethylammonium bromide (CTAB) solution (10^{-2} M) was then introduced to the gold nanoparticle suspension in a plastic

cuvette (5 mL). The color of the suspension changed immediately from wine-red to blue-purple, reflecting the onset of particle aggregation. As the nanoparticle aggregation proceeded, the dark-brown precipitate was gradually accumulated at the bottom of vessel over a few hours. The precipitate was then carefully taken up by a pipette and deposited onto a clean gold-coated glass slide (Thermo Electron, Waltham, MA, USA) and a brief annealing treatment (~ 300^{o}C, 2 h in air) was followed to provide a clean SERS-active area.

The prepared nanostructure was examined by Field Emission Scanning Electron Microscopy (FESEM, FEI Quanta, OR, USA) to verify the formation of Au nanostructures deposited on the gold coated glass slide. A SEM scan was performed at high vacuum mode at 10 kV of electron acceleration voltage.

3.2.2.2 Silver dendrites

Silver nanostructures were prepared through a simple replacement reaction involving both zinc (Zn) and silver nitrate ($AgNO_3$):

$$Zn + AgNO_3 \rightarrow Ag + ZnNO_3 \qquad (3\text{-}1)$$

$AgNO_3$ aqueous solution was prepared by dissolving $AgNO_3$ (Fisher Scientific, Rochester, NY, USA) in de-ionized water. The Zinc plate (Fisher Scientific, Rochester, NY, USA) was first cleaned by diluted hydrochloric acid (0.02 mol/L) to remove surface contamination and then rinsed with de-ionized water and dried by cold air. The zinc plate was then immersed into the $AgNO_3$ solution. Silver nanostructures with different morphologies were obtained quickly by adjusting the silver ion concentrations. The nanostructure products were carefully peeled off the zinc plate with tweezers and put into

a glass bottle. The nanostructure products were then rinsed several times using de-ionized water to remove excessive chemicals like Zn^{2+} and NO_3^-. Finally, the silver nanostructures were collected and deposited onto a clean gold-coated glass slide (Thermo Electron, Waltham, MA, USA). The final nanosubstrate with multiple spots of silver nanostructure could be used under Raman spectroscopy directly. The nanostructures were examined by Field Emission Scanning Electron Microscopy (FESEM, FEI Quanta, OR, USA) and SEM scan was performed at high vacuum mode at 10 kV of electron acceleration voltage.

3.2.2.3 Gold-coated zinc oxide nanonecklaces (ZnO NNs)

A hot wall chemical vapor deposition was used to grow ZnO NNs on r-plane sapphire substrates. Gold nanoparticles (Au NPs) were used as the catalysts to direct the growth of ZnO NNs using a vapor-solid-liquid process. Self-made Au NPs with diameter ~ 5 nm were spun-coated on the surface of the r-plane sapphire substrates. Detailed procedure to prepare the Au NPs is described in former study (Shi and others 2009). Pieces of as-deposited sapphire substrates were put in an alumina boat with the same space between each other. Precursors (2.5 g ZnO / 0.36 g graphite) were put at the upstream 60 mm away from the substrates. The whole boat was then put in the center of the CVD quartz tube with 60 sccm argon flowing by heating temperature to 900^{o}C at atmospheric pressure. As-produced ZnO NNs were achieved after a typical growth time of 2 hours. Finally, ZnO NNs substrates were sputtered by Au films in different thicknesses (45 and 60 nm) by Emitech K575x Turbo Sputter Coater (EM Technologies, LTD., Kent, England) for SERS test. A S4700 Hitachi Field emission electron microscopy (FESEM,

LTD., Tokyo, Japan) and atomic force microscopy (AFM) were used to characterize the topography of ZnO nanostructures with and without gold coating.

3.3 Raman instrumentation

A Renishaw RM1000 Raman spectrometer system (Gloucestershire, UK) equipped with a Leica DMLB microscope (Wetzlar, Germany) and a 785 nm near-infrared diode laser source (maximum at 300 mW) was used in this study (Figure 5). Raman scattering signals were detected by a 578 × 385 pixels CCD array detector. The measurement was conducted with a 50× objective, a detection range from 300 to 200 cm^{-1} in the extended mode, 10 s exposure time, and 2 to 30 mW laser power.

Figure 5. A photo of Renishaw Raman spectrometer

3.4 HPLC analysis

An Agilent 1100 series HPLC system with a 1200 series automatic injector was used. The system consisted of a quaternary pump, a degasser, a column oven, and a diode array detector. The mobile phase was an 85:15 (v/v) buffer containing 10 mM citric acid and 10 mM sodium octanesulfonate (pH 3.0): acetonitrile. Test conditions: Zorbax SB-C8 (4.6 mm × 75 mm, 3.5 μm particle, Agilent) column; column temperature of 40^{o}C; flow rate of 1.0 ml/min; DAD spectra, 190 - 400 nm, detected at 236 nm.

3.5 Data analysis

Data analysis was performed using OMNIC software (ThermoFisher Scientific Inc., San Jose, CA, USA), Minitab software (Minitab Inc., State College, Pennsylvania, USA) and Delight software (D-Squared Development Inc., LaGrande, OR, USA). Pre-processing algorithms were employed to analyze the data, such as normalization, binning, smoothing, and second-derivative transformation. Normalization changes the Y-axis scale of the selected spectra to a "normal" scale in which the Y values of the data points range in absorbance units from 0 for the lowest point to 1 for the highest point. Binning reduces the number of data points in a spectrum by averaging n points into one. Smoothing eliminates high-frequency instrumental noises by averaging neighboring data points. Second-derivative transformation separates overlapping bands and removes baseline offsets.

3.5.1 Hierarchical cluster analysis and principal component analysis

Two multivariate analyses (hierarchical cluster analysis (HCA) and principal

component analysis (PCA) were used to analyze the spore spectra. A HCA dendrogram was plotted using Ward's linkage algorithm. It clusters spectra on the basis of similarity with other spectra. The spectral distance values indicate the spectral similarities. The lower the distance value between two samples indicates the higher similarity between spectral features of these two samples. PCA reduces a multidimensional data set to its most dominant features, removes random variation (noise), and retains the principal components (PC) that capture the variation between sample treatments.

3.5.2 Partial least squares

A multivariate statistical regression model, the partial least squares (PLS) model, was constructed to predict analyte concentrations in tested samples. The PLS model was validated by leave-one-out cross validation, which uses all but one sample to build a calibration model and repeats for each sample in the data set (Martens and Naes 1986). The number of PLS latent variables was optimized based on the lowest root mean square error of prediction (RMSEP) values to avoid overfitting of spectral data.

$$RMSEP = \sqrt{\frac{\sum_{i}^{n} (\hat{c}_i - c_i)^2}{n}} \qquad (3\text{-}2)$$

In this equation, n is the number of samples, $\hat{c}_i$ is the predicted melamine concentration (ppm), and c_i is the actual melamine concentration (ppm). The correlation coefficient (R) and RMSEP were used to evaluate the model. The higher the R value or the lower the RMSEP value is, the better predictability the model has.

3.6 SERS measurements

3.6.1 Analytical enhancement factor

To determine the analytical enhancement factor (AEF) of silver dendrites as SERS-active nanosubstrates, ~ 5 μL of antibiotic solution samples were deposited onto the spot of silver dendrites and bare gold-coated glass slide, respectively. AEF of SERS was calculated according to the following equation:

$$\mathrm{AEF} = I_{\mathrm{SERS}}/I_{\mathrm{RS}} \times C_{\mathrm{RS}}/C_{\mathrm{SERS}} \qquad (3\text{-}3)$$

where I_{SERS} and I_{RS} are the peak intensities in a SERS spectrum and a normal Raman spectrum, respectively. C_{SERS} and C_{RS} are the analyte concentrations in the SERS measurement and the normal Raman measurement, respectively.

3.6.2 Sensitivity

To evaluate the sensitivity of SERS, a series of concentrations of antibiotics was deposited on the spots of silver dendrites on the nanosubstrate and analyzed by Raman spectroscopy. Relationship between peak height in SERS spectra and concentrations of the sample was examined. The lowest concentration at which most characteristic peaks remain noticeable is considered as the limit of detection (LOD). The limit of quantification (LOQ) is estimated as the lowest value in the linear part of the curve.

3.6.3 Consistency

The consistency of SERS performance was evaluated in two independent experiments. In each experiment, a SERS nanosubstrate was prepared using a flat gold coated glass

slide with two identical spots of silver dendrites. SERS spectra were collected from 2 or 3 different positions within a spot. Standard deviation (SD) was calculated using standardized height intensity of the highest peak in a SERS spectrum. Relative standard deviation (RSD) was calculated according to the following equation:

$$RSD = (SD / Mean) \times 100\ \% \quad (3\text{-}4)$$

3.6.4 Shelf life

To test the shelf life of silver dendrites, a monthly test was conducted for six months. Each time, silver dendrite precipitation was transferred from the glass bottle on to a gold-coated glass slide right before testing. After the water was evaporated, 200 ppb CIP was deposited onto the nanosubstrate and its SERS spectra were acquired. Variations in the intensity and position of peaks in SERS spectra were observed and utilized in data analysis.

CHAPTER 4

RESULTS

4.1 Use of commercial Klarite substrates in SERS for detection of food contaminants

4.1.1 Morphology of Klarite substrates

Scanning electron microscopy (SEM) micrograph of the patterned area of the gold substrate shows nanotextured pyramidal subunits with ~ 1.8 µm openings of the depressions and separated by ~ 0.4 µm of the bridges with one another (Figure 6). Due to electronically connected surface, cooperative oscillations of metal conduction band electrons can be transformed into plasmons (Alexander and Le 2007).

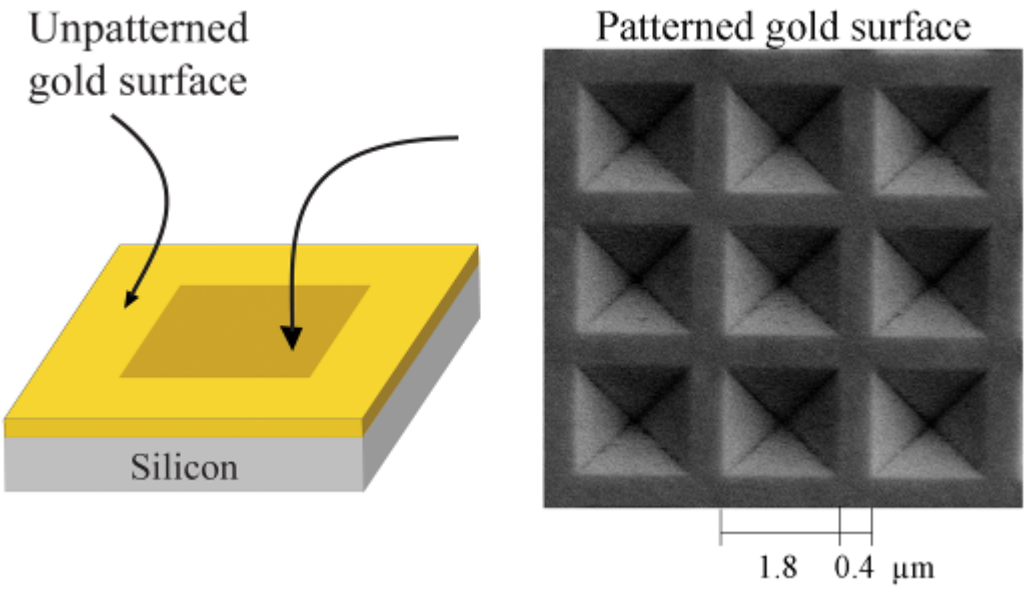

Figure 6. Scanning electron microscopy (SEM) micrograph of a Klarite gold substrate

4.1.2 SERS performance in melamine and its analogues detection

The average spectra (n = 4) of different concentrations of melamine solution are shown in Figure 7. Typical Raman peaks at 380, 582, 676, 984 cm^{-1} were observed. The most intense peak at 676 cm^{-1} is assigned to the ring breathing II mode and involves in-plane deformation of the triazine ring. The second highest peak at 984 cm^{-1} arises from the ring breathing mode I of the triazine ring (Koglin and others 1996). No peaks were observable in the SERS spectra obtained from the melamine sample with a concentration of 10^{-7} mol L^{-1} or lower.

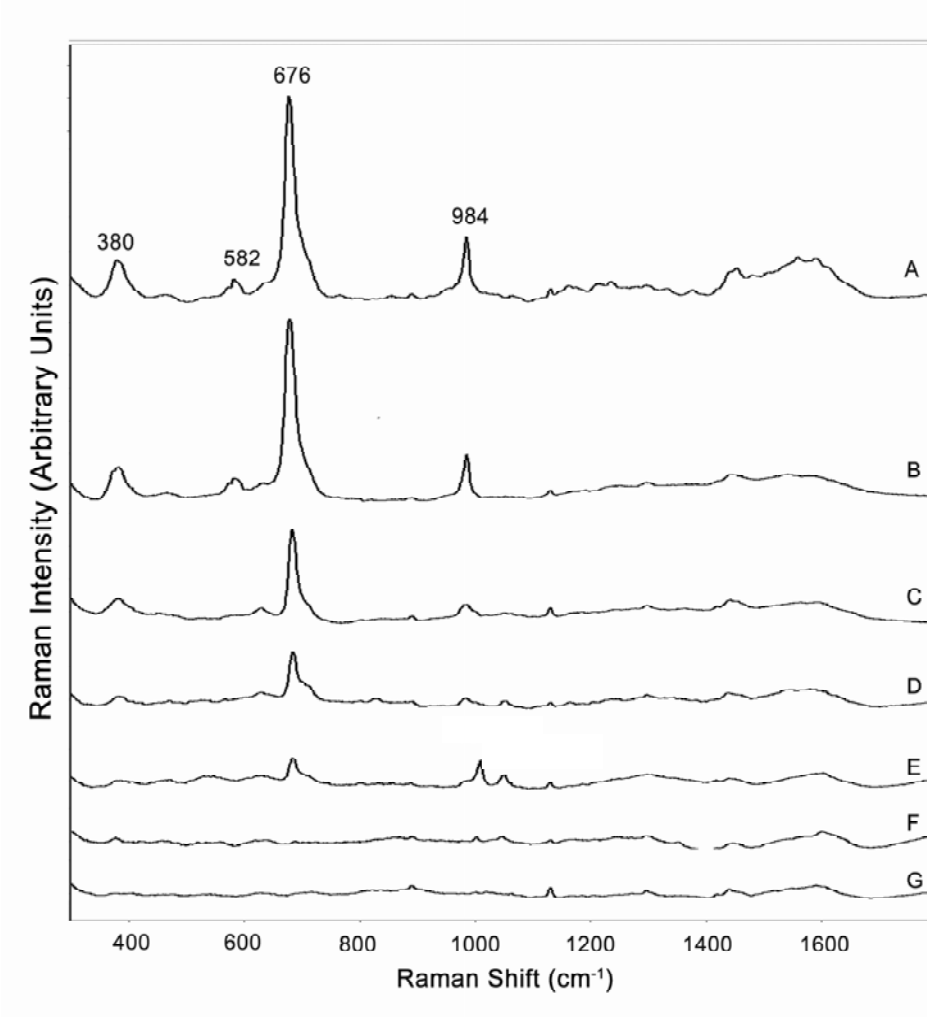

Figure 7. SERS spectra of a series of concentrations of melamine: 10^{-2} (A), 10^{-3} (B), 10^{-4} (C), 10^{-5} (D), 10^{-6} (E), 10^{-7} (F) mol L^{-1}; (G) gold substrate without the sample on a Klarite substrate

For the PLS analysis, the best performance was achieved using the full spectral region (300 – 1800 cm^{-1}) with four latent variables. Figure 8 shows the RMSEP of melamine concentration model for different latent variables. The lowest RMSEP was found for four latent variables, which indicates the optimal number of latent variable is four. Figure 9 shows the PLS prediction results by constructing the log values of predicted melamine concentrations against the log values of actual melamine concentrations. A good prediction result was obtained (R^2 = 0.93, RMSEP = 0.46).

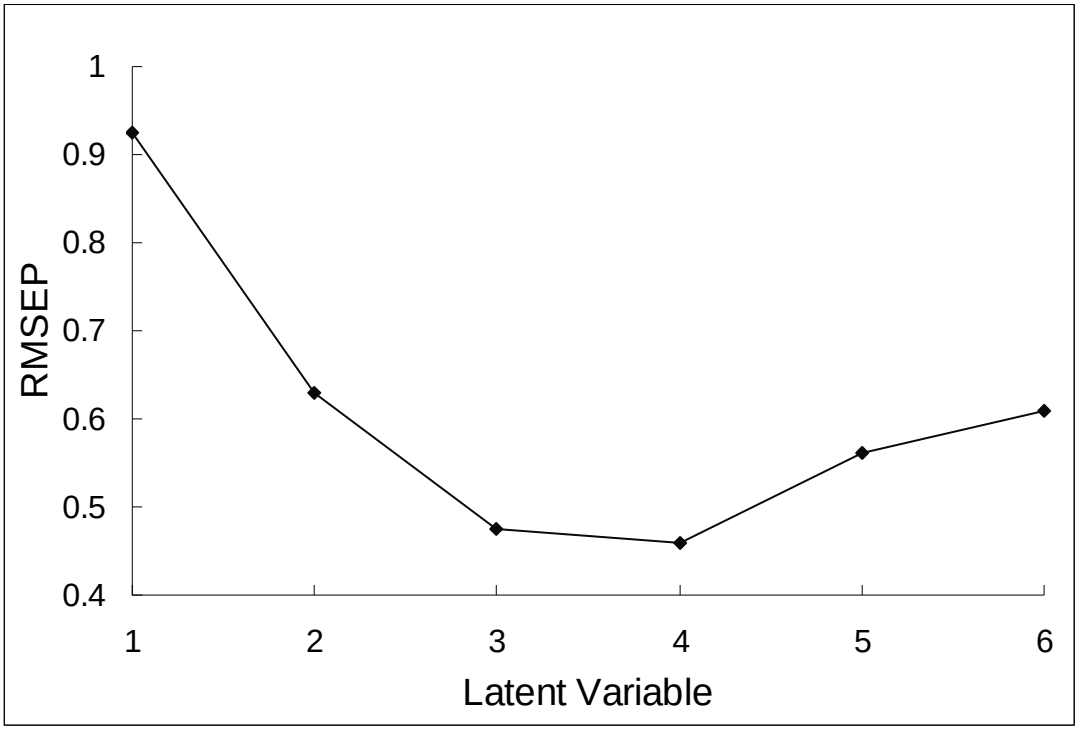

Figure 8. Root mean square error of prediction (RMSEP) of melamine concentration model for different latent variables

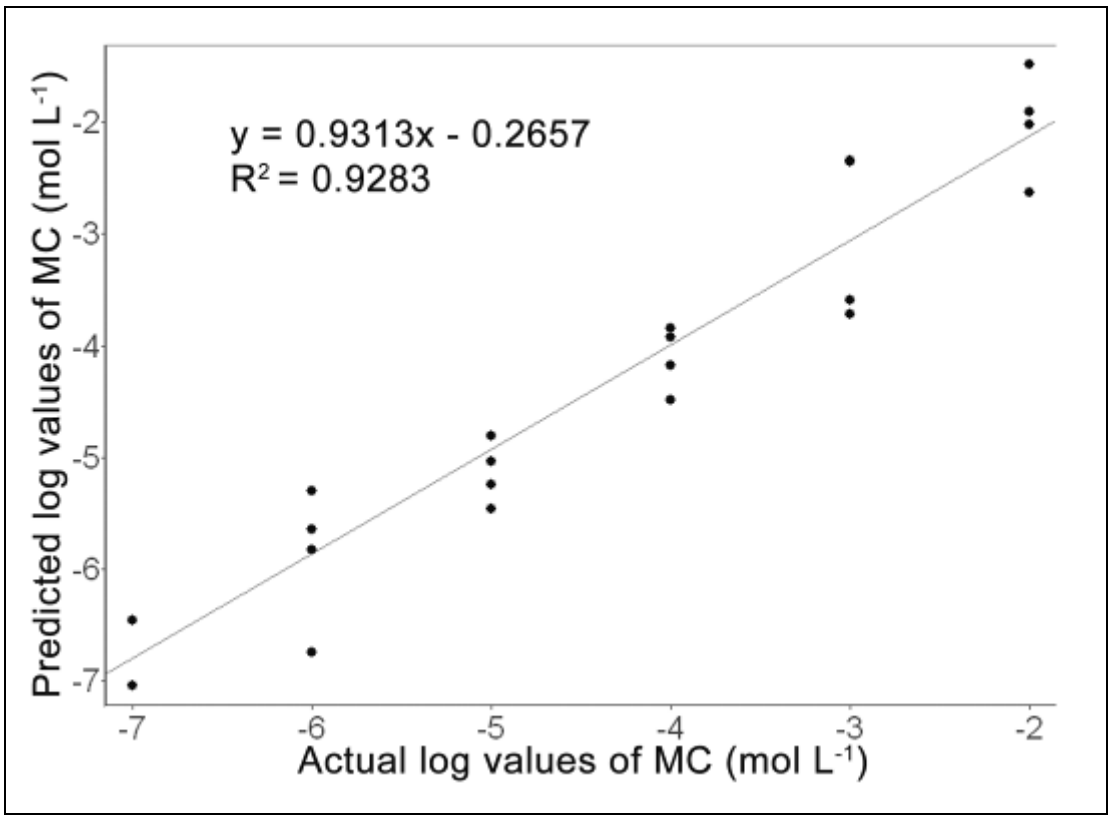

Figure 9. Partial least squares (PLS) prediction model of log values of melamine concentration (MC) (mol L^{-1})

Another prediction model was constructed based on the relationship between the intensity of the highest peak of melamine SERS spectra at around 676 cm^{-1} and log values of melamine concentrations. Theoretically, higher concentrations of test samples should result in a stronger Raman intensity. However, in reality, increasing the sample concentration past a certain level will saturate the detector. A linear regression ($R^2 = 0.96$) was found between Raman intensity and melamine concentrations (Figure 10). Therefore, based upon the results calculated by linear regression, the LOD for melamine using this SERS method is 2.6×10^{-7} mol L^{-1}, which is equivalent to approximately 33 ppb. This special model is reasonable in the case of melamine due to only one prominent featured peak was present in the melamine SERS spectra. Although it is only based on one peak, this model is applicable when applied in different complex systems since it excludes other information or interferences from the systems. Additionally, it is easier and faster to establish this model than the previous one when qualitative and partial quantitative screening of melamine is desired.

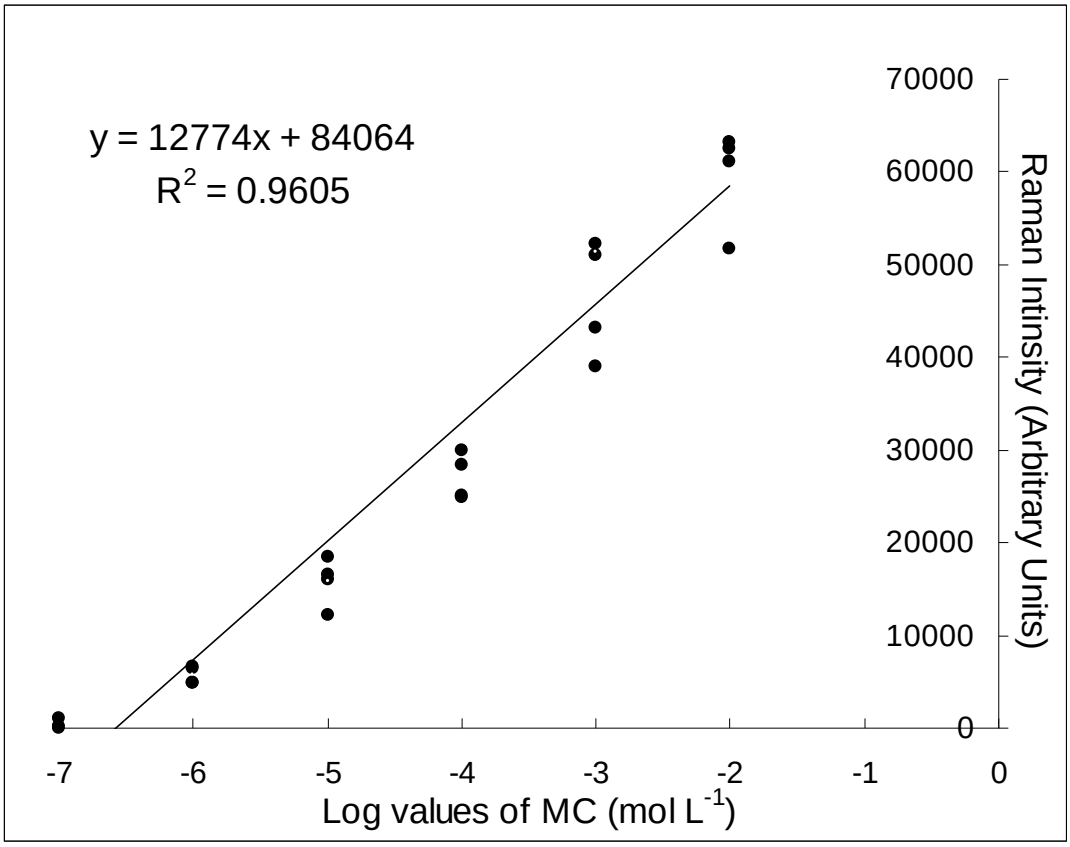

Figure 10. Relationship between Raman intensity of the highest peak at around 676 cm^{-1} and log value of melamine concentration (MC)

To determine the enhancement factor of Klarite^{TM} gold nanosubstrates for melamine, 10^{-2} and 10^{-4} mol L^{-1} of melamine solutions were deposited onto the non-active surface and active surface of the nanosubstrate, respectively. Based on the highest peak at around 676 cm^{-1}, an approximately 3×10^4 fold of signal enhancement in the SERS spectra of melamine over the normal spectra was calculated (Figure 11). Additionally, a ~ 5 cm^{-1} shift was found between these two peaks in Figure 4 (A) and (B), probably due to different concentrations and/or the influence from the nanosubstrate. The LOD of this SERS method could potentially be even lower if better performed nanosubstrates with a higher SERS enhancement factor were used.

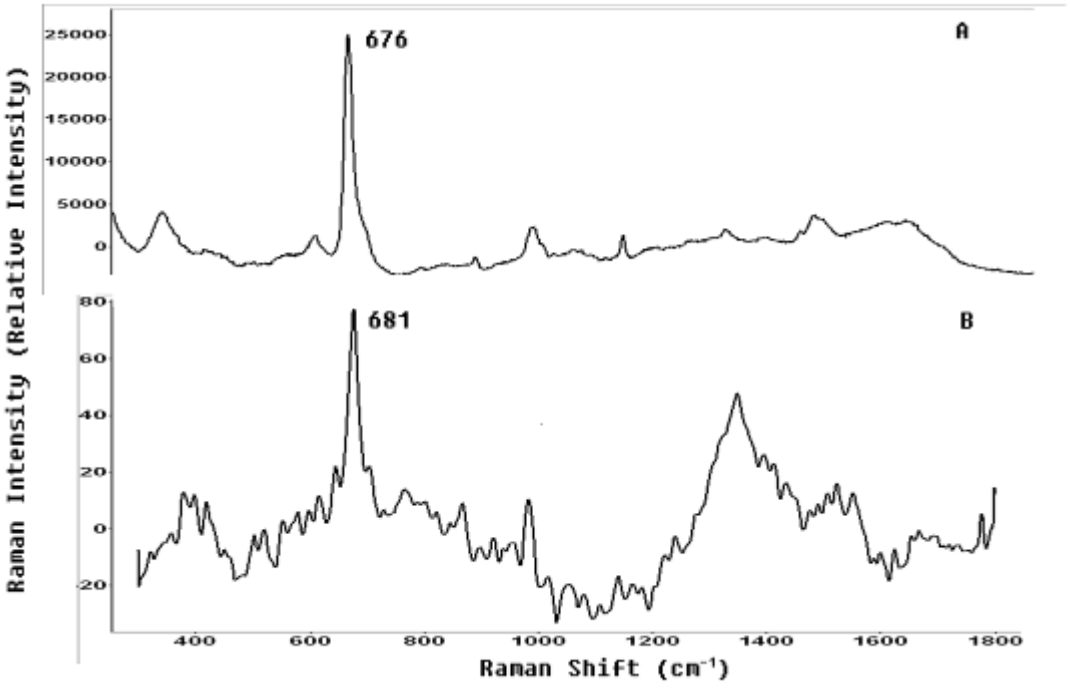

Figure 11. Raman spectrum of 10^{-4} mol L^{-1} melamine (A) on SERS-active area of gold nanosubstrate and 10^{-2} mol L^{-1} melamine (B) on non-active area of gold nanosubstrate.

SERS spectra of the solid and aqueous forms of cyanuric acid (10^{-3} mol L^{-1}) are shown in Figure 12. For cyanuric acid in the solid forms, prominent peaks were found at 525, 552, 702, 991, and 1727 cm^{-1}. However, when measuring SERS spectra of the aqueous form of cyanuric acid immediately after the chemicals dissolved completely in water, prominent peaks were found at 661, 822, 1016, 1399, 1448, and 1567 cm^{-1}. Some of those bands have been assigned before, such as 702 cm^{-1} to a ring out-of-plane bending vibration, 1016 cm^{-1} to the ring breathing, and 1727 cm^{-1} to the C=O stretching (Lewis 2001; Maheshwari and Saraf 2006). More interestingly, in less than one hour, small crystals were found in the cyanuric acid solution under a 50× objective; and the SERS spectrum of the solution changed back to that of the solid form. This may be due to the enol (cyanuric acid) – keto (isocyanuric acid) tautomerism.

It is known that free cyanuric acid in crystal forms and in neutral and acid solutions exists mainly as the keto form, while in alkali solutions, the enol form is predominant (Seifer 2002). Raman spectra of the keto form as a solid and in acid solutions and the enol form in alkali solution have been previously reported (Lewis 2001). However, in alkali solutions the compound is not present in the enol form but as a salt produced by the reaction between the enol form of cyanuric acid with the alkali. From a thermodynamics point of view, the keto-enol isomerization reaction is endothermic, indicating that the keto form is more stable than the enol form without the consideration of solvent effects (Liang and others 2004). While in aqueous solution, water molecules produce an important catalytic effect, reducing the enthalpy and energy barrier of the reaction considerably, thus the reaction rates increase significantly and the keto-enol tautomerism occurs easier (Liang and others 2007). Therefore, it is possible that immediately after cyanuric acid dissolved in water, the SERS spectrum obtained was from the enol form of cyanuric acid

due to increased energy input from the stirring; while after the stirring stopped, the unstable enol form gradually changed back to a more stable keto form.

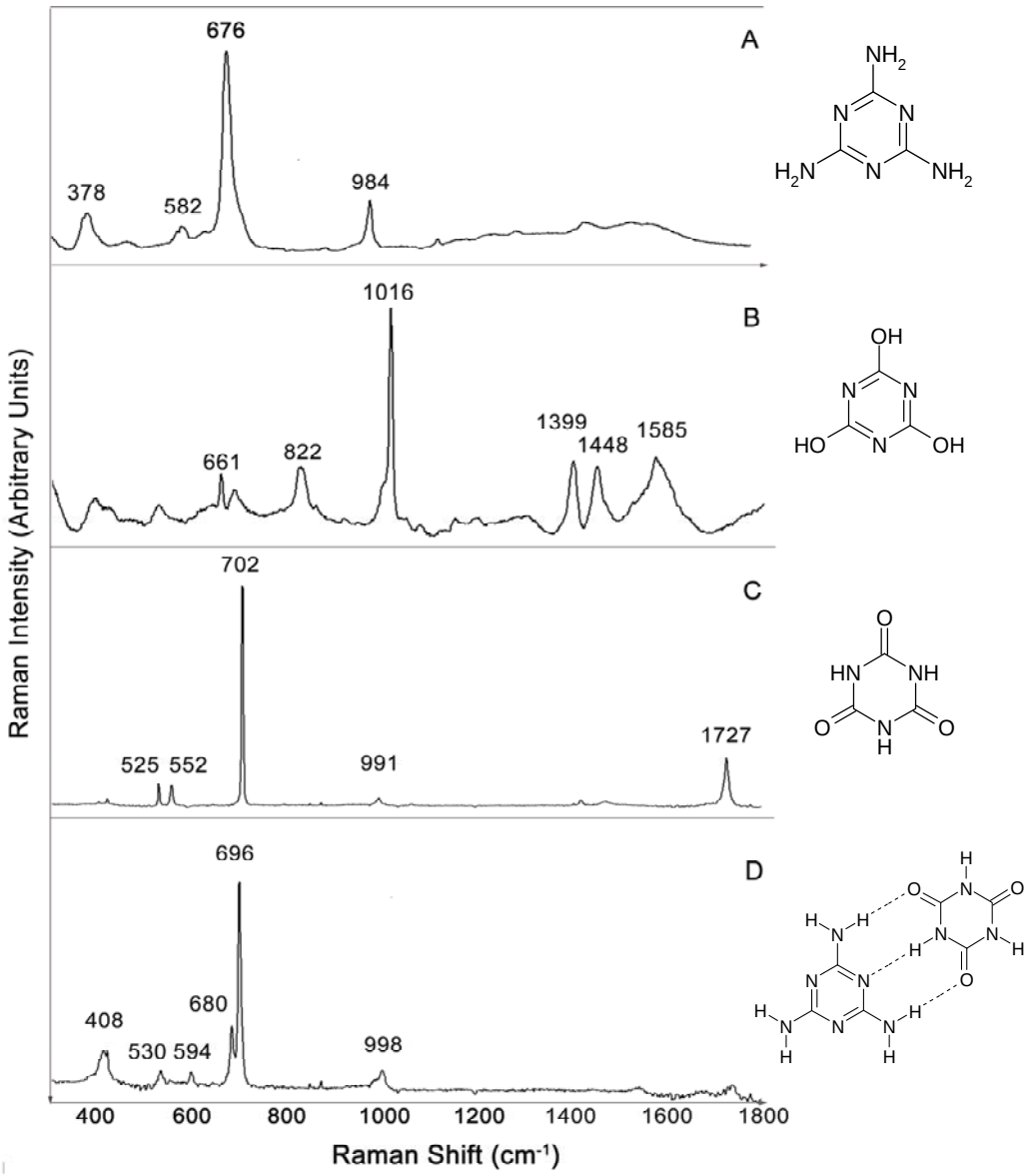

Figure 12. SERS spectra of 10^{-3} mol L^{-1} melamine (A), 10^{-3} mol L^{-1} cyanuric acid (B), solid cyanuric acid (C), melamine cyanurate (D)

When adding equal amounts (10^{-3} mol L^{-1}) of melamine and cyanuric acid together, white precipitants (melamine cyanurate) instantly formed. These spoke-like crystals were clearly observed under the 50× microscope objective and captured by a color video camera (Figure 13). The spectrum of melamine cyanurate crystals is shown in Figure 12 (D). Typical peaks at 408, 530, 594, 680, 696, and 998 cm^{-1} were readily observed. A similar spectrum of melamine cyanurate was obtained by Tseng and others (1994) using FT-Raman.

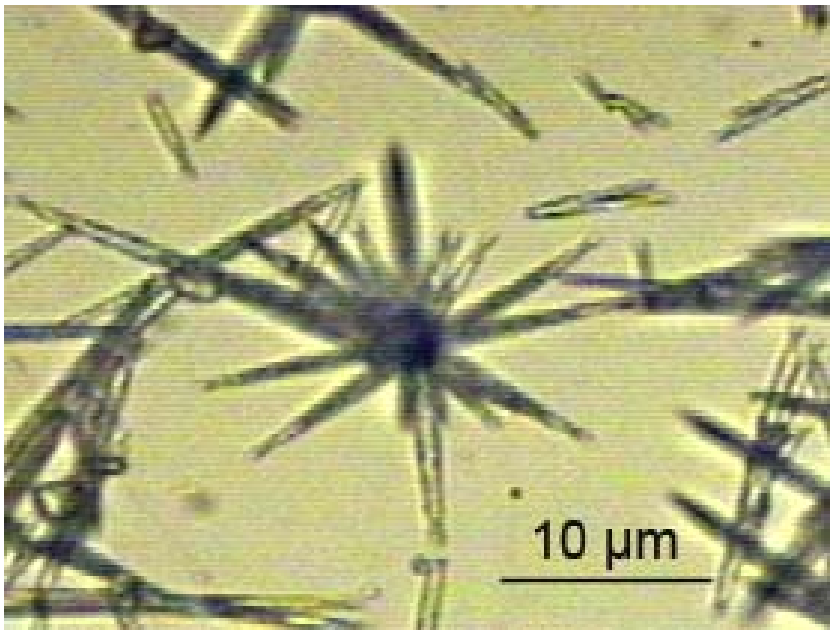

Figure 13. Spoke-like crystals were observed in the melamine cyanurate solution when equal amounts (10^{-3} mol L^{-1}) of melamine and cyanuric acid were added

4.1.3 Detection of melamine in gluten, chicken feed and processed foods using SERS and HPLC

Chicken feed and wheat gluten were selected as model food systems for studying melamine contamination since both of them were implicated in the safety incidents of imported foods in 2007. Homemade cakes and noodles were selected as food models to evaluate how food processing procedures affect melamine recovery in processed foods containing contaminated food ingredients. The spiked melamine concentrations on a dry basis for gluten, chicken feed, cake, and noodle samples are shown in Table 1.

Table 1. Recoveries of melamine concentration (%) in gluten, chicken feed, cake, and noodles using HPLC

	Spiked (%)	Quantified (%)*	Recovery (%)
Gluten	2.00	1.849 ± 0.265	92.4
	1.00	0.858 ± 0.007	85.8
	0.50	0.556 ± 0.004	111.2
	0.10	0.097 ± 0.018	97.0
Chicken feed	2.00	2.150 ± 0.050	107.5
	1.00	0.933 ± 0.026	93.3
	0.50	0.463 ± 0.024	92.6
	0.10	0.099 ± 0.004	99.0
	0.05	0.047 ± 0.009	94.0
Cake (dry basis)	1.680	1.550 ± 0.019	92.3
	0.841	0.773 ± 0.007	91.9
	0.424	0.373 ± 0.007	88.0
	0.085	0.071 ± 0.002	83.5
Noodle (dry basis)	2.153	1.710 ± 0.050	79.4
	1.088	0.867 ± 0.022	79.7
	0.547	0.536 ± 0.035	98.0
	0.110	0.090 ± 0.004	81.8

* Quantified values are shown as mean ± standard deviation (n = 2)

4.1.3.1 SERS measurement

A normal Raman spectrum of melamine in solid form is shown in Figure 14a. The most intense peak around 682 cm^{-1} is assigned to the ring breathing mode II and involves in-plane deformation of the triazine ring in melamine molecules. A barely visible peak around 989 cm^{-1} arises from the ring breathing mode I of the triazine ring (Koglin and others 1996). Normal Raman spectra of chicken feed containing 2.0% melamine and the control (melamine-free chicken feed) are shown in Figures 14b and 14c. Detecting melamine in chicken feed directly by normal Raman is challenging because melamine powders are not evenly distributed in the feed and the normal Raman signals are too weak. To solve this problem, an extraction protocol using a solution of acetonitrile in water (50% v/v) was employed, followed by the SERS measurement to acquire tremendously enhanced Raman signals of trace amounts of melamine in the extract.

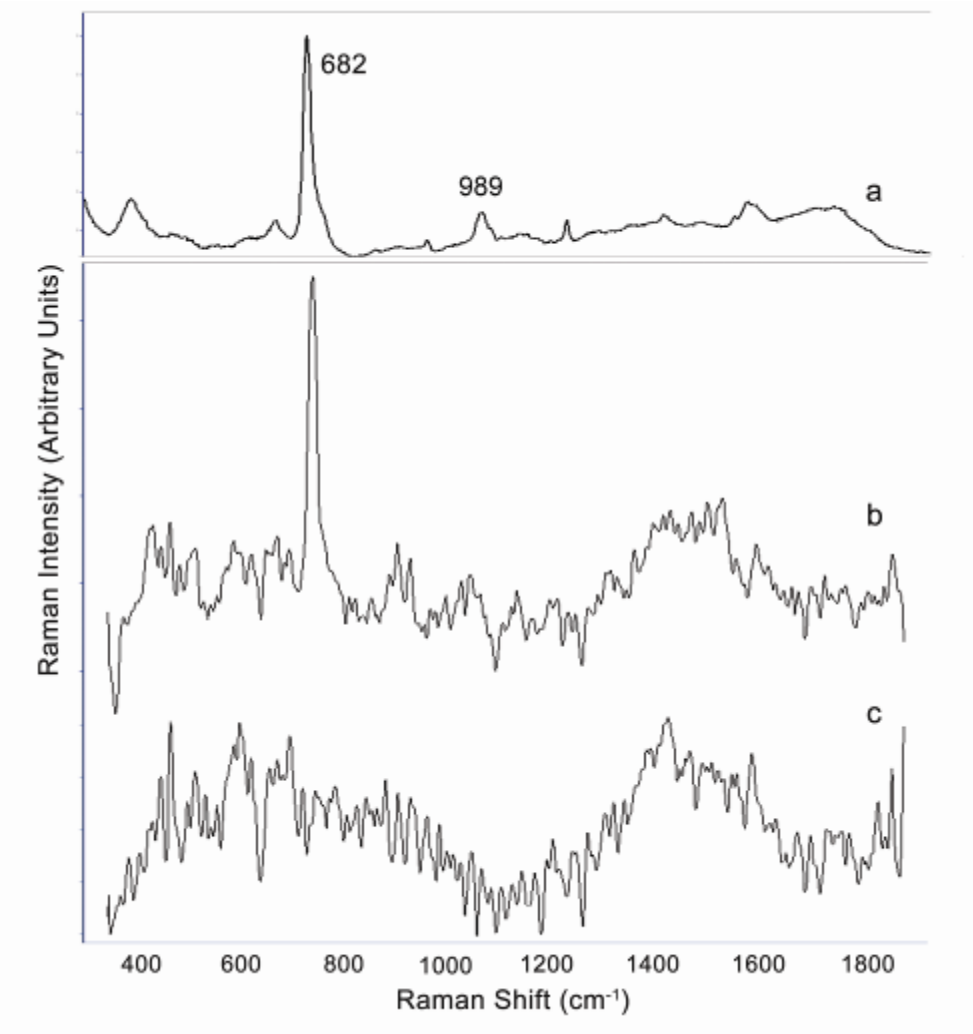

Figure 14. Normal Raman spectrum of solid melamine powders (a), chicken feed containing 2.0% melamine (b), and the control (melamine-free chicken feed) (c)

Different concentrations of melamine in wheat gluten, chicken feed, cake and noodle were extracted and analyzed by SERS. Average SERS spectra (n = 4) of melamine extracted from gluten samples are shown in Figure 15. The melamine featured peak at around 682 cm^{-1} was present in the SERS spectra collected from the extracts of samples spiked with different concentrations of melamine, but absent in the control. Similar results were obtained from chicken feed, cake and noodle samples. SERS was able to rapidly detect melamine concentrations as low as 0.1% in wheat gluten, 0.05% in chicken feed, 0.05% in cakes, and 0.07% in noodle, respectively. Lower concentrations of melamine could be detected by SERS if better performing nanosubstrates are used. These results demonstrate that SERS can effectively detect trace amounts of melamine in feed and food samples with the aid of a simple and rapid extraction procedure and Raman signal enhancement on SERS-active substrates.

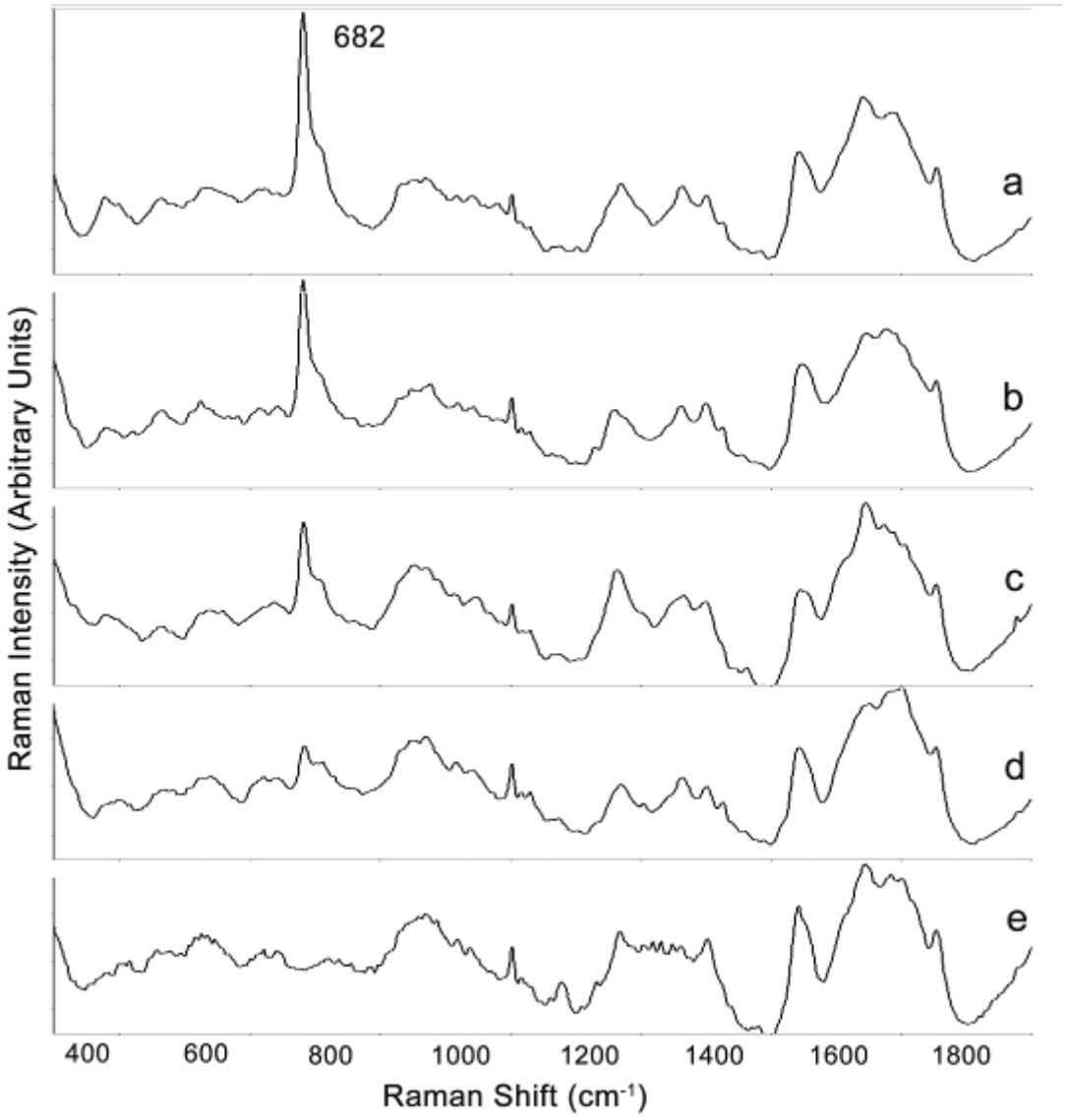

Figure 15. Average SERS spectra (n = 4) acquired from extracts of wheat gluten containing different concentrations of melamine: 2.0% (a), 1.0% (b), 0.5% (c), 0.1% (d), and 0% (e)

Figure 16 shows the RMSEP values obtained from the PLS models with different latent variables. The spectral data were pre-processed with binning at 2 cm^{-1}, smoothing at 6 cm^{-1}, and a second derivative transformation at 12 cm^{-1} in the spectral region between 500 to 1700 cm^{-1}. The lowest RMSEP value was obtained when five latent variables were used, indicating that the optimal number of latent variables is five. Figure 17 shows the PLS prediction results (n = 74) by constructing the log values of predicted melamine concentrations against the log values of spiked melamine concentrations. The prediction result was obtained with R = 0.90 and RMSEP = 0.33, indicating that satisfactory quantitative results for melamine contamination in foods by SERS could be obtained.

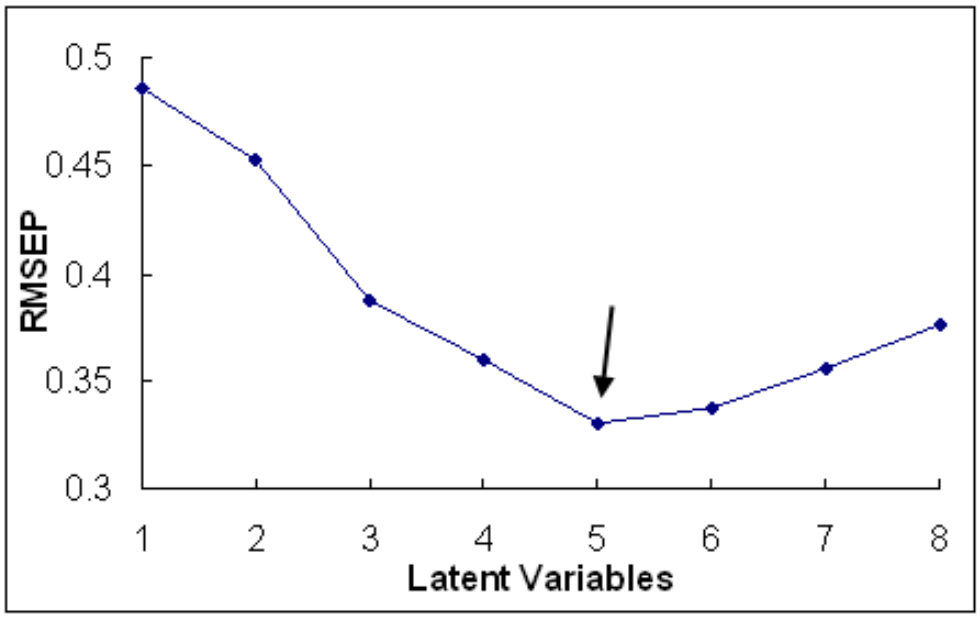

Figure 16. Root mean square error of prediction (RMSEP) values obtained from the partial least squares (PLS) models with different latent variables

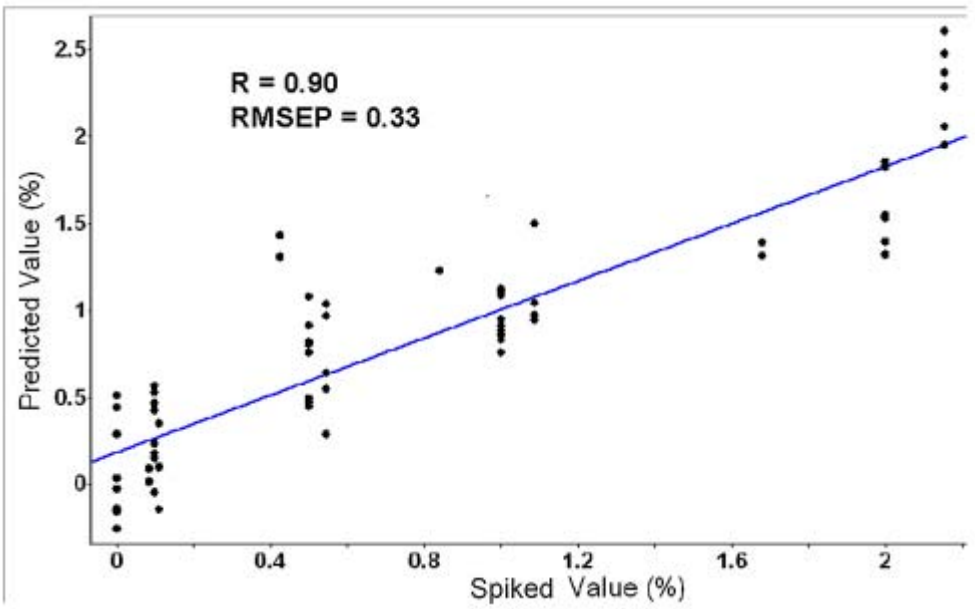

Figure 17. Predicted melamine concentration (%) vs. spiked melamine concentration (%) using the PLS model

4.1.3.2 HPLC analysis

Figure 18 shows the HPLC chromatogram of chicken feed containing 0.1% melamine and the DAD spectrum of melamine. The extraction method used in this study is a modified FDA protocol that shortens the extraction step. The LOD of using HPLC to measure melamine standard solution was 1 μg/mL. The LOQ was the same as the LOD due to linear property of the standard curve. HPLC was able to detect the lowest concentrations of melamine spiked into the samples: 0.1% melamine in wheat gluten, 0.05% in chicken feed, 0.05% in cakes, and 0.07% in noodle, respectively. The recoveries of melamine were between 85.8 – 111.2% for gluten, 92.6 – 107.5% for chicken feed, 83.5 - 92.3% for homemade cakes (dry basis), and 81.8 - 98% for raw noodles (dry basis) (Table 1). By comparison, the standard FDA method typically produces recoveries of melamine in gluten and moist pet food in the range of 90 to 110%. In simple food systems such as chicken feed and glutens, melamine can be easily extracted with 50% acetonitrile in water followed by ultra-sonicating for 2 min, instead of using a FDA protocol which takes more than 30 min. Thus our results show that the simplified extraction procedure compares favorably with more time-consuming and tedious FDA standard protocol for quantitative estimation of melamine in foods and feed ingredients. This result also indicates that food processing does not have a significant effect on melamine recovery in foods since the differences in recoveries between raw and processed foods were fairly negligible (p value > 0.05).

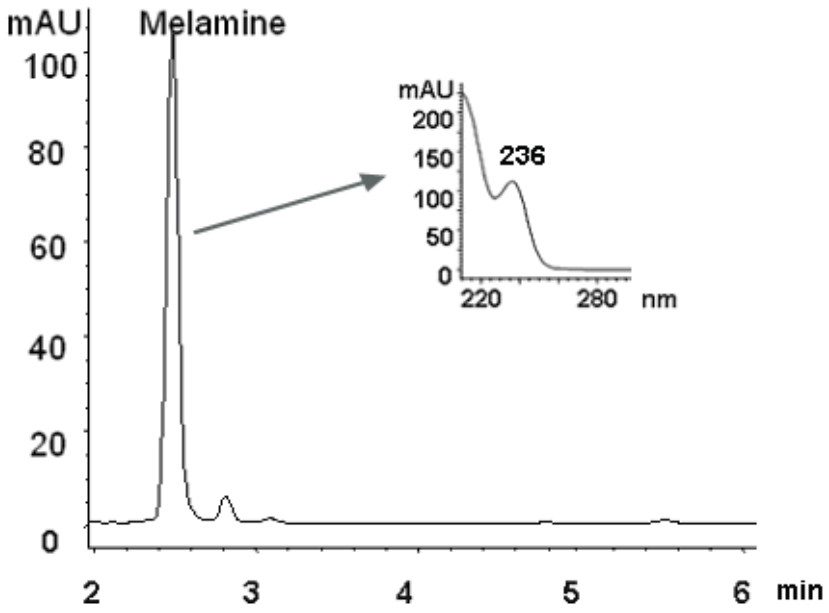

Figure 18. HPLC chromatogram of chicken feed containing 0.1% melamine and the DAD spectrum (inset)

4.1.3.3 SERS vs. HPLC

Both SERS and HPLC methods could detect melamine in tested wheat gluten, chicken feed and processed foods. The total detection time using HPLC to measure a set of 8 samples is about 3 h, compared with less than 30 min for SERS. SERS has an advantage of requiring minimum sample preparation because no centrifugation, filtration, or cleanup steps are needed; while HPLC requires complex sample pretreatment (*e.g.* centrifugation and filtration) and cleanup. Essentially, only three steps are needed for SERS measurement after sample preparation: 1) deposition of the melamine extraction solution onto the substrate; 2) evaporation of organic solvent; and 3) detection with a Raman instrument (Figure 19). In this way, SERS measurement is much faster and simpler than HPLC for melamine detection. However, SERS yields less accurate quantification results than HPLC analysis as shown by the R values (R = 0.90 for SERS; R = 0.99 for HPLC), which may be related to the substrates used in the measurements. For SERS analysis, the performance of SERS-active substrates plays an important role in melamine detection. A major challenge for SERS analysis is the difficulty in maintaining the fabrication reproducibility in substrates (Alexander and Le, 2007). Currently, only a few SERS-active substrates are commercially available in the market. Therefore, more work is needed to develop better performing and cost-effective SERS-active substrates for SERS applications. It is expected that with a better performing SERS-active substrate, lower LOD and more accurate and consistent quantification results could be obtained.

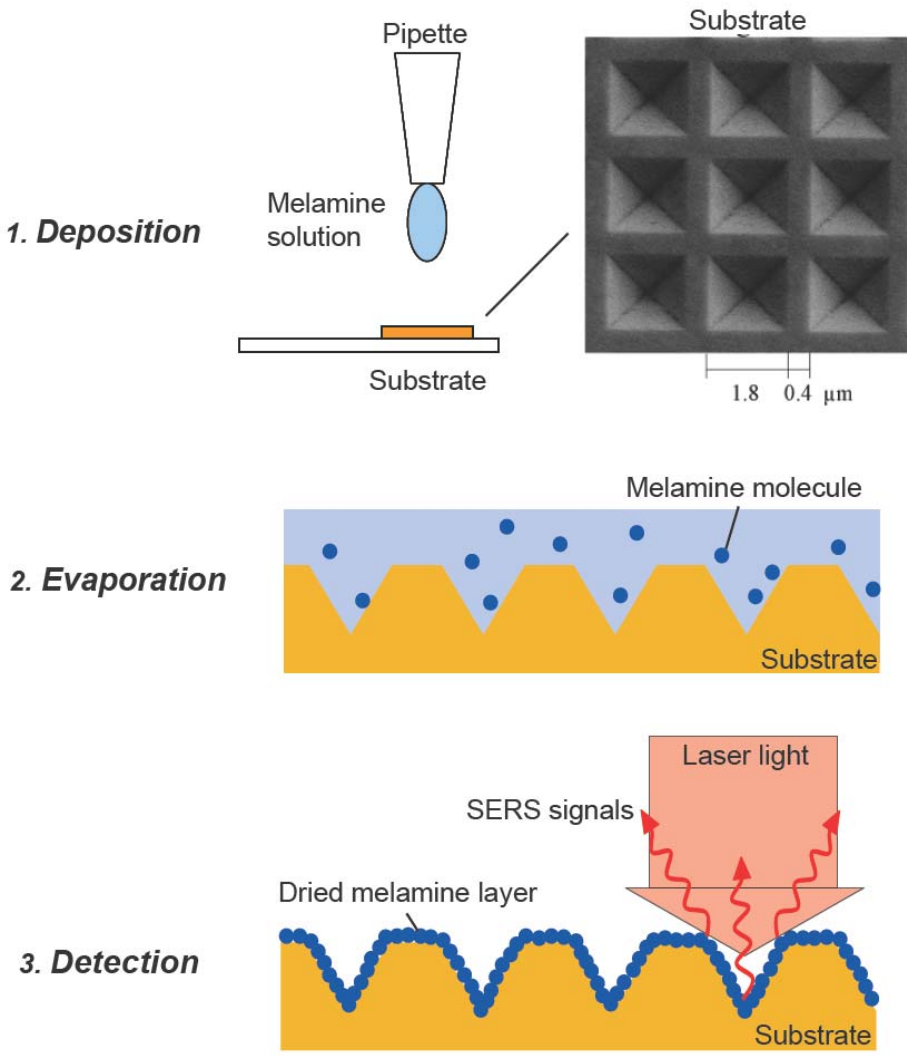

Figure 19. Structure and SEM image of a Klarite^{TM} SERS-active gold substrate and preparation of a sample on a substrate

As the first group, we propose a new protocol (Figure 20) for monitoring melamine contamination in imported foods and food ingredients by SERS coupled with HPLC: SERS is applied first to screen foods to eliminate presumptive negative samples for melamine contamination from the sample population; then HPLC is used to verify and quantify presumptive positive samples. By doing so, melamine contamination in large numbers of food and feed products could be detected accurately, quickly, and efficiently.

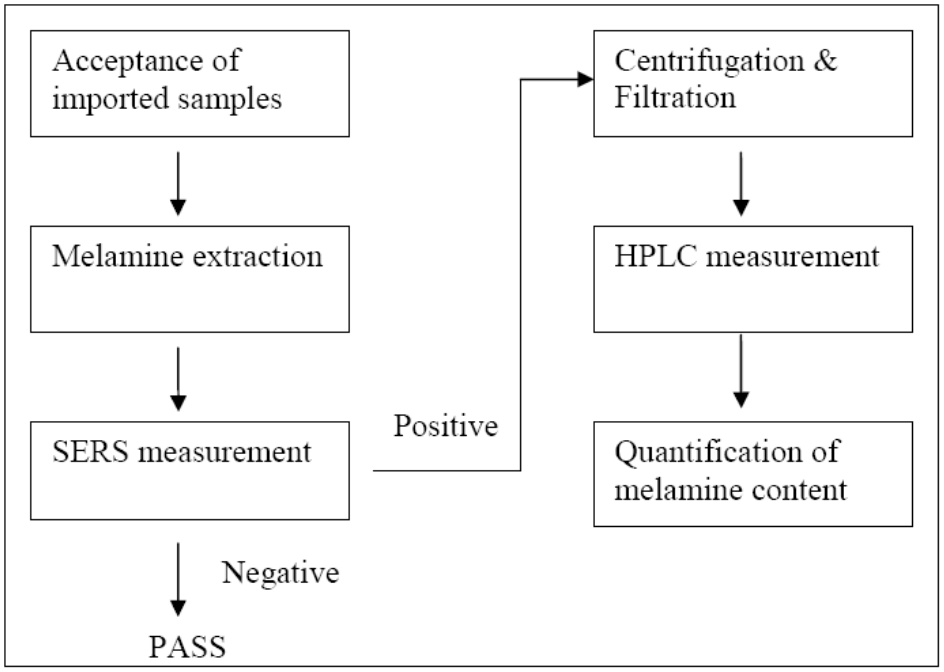

Figure 20. A proposed protocol for monitoring melamine contamination in imported foods and food ingredients by SERS and HPLC

4. 1.3.4 Conclusion

SERS is a novel and rapid analytical technique. It can be used to detect trace amounts of melamine in foods, food ingredients, and feed. SERS is much faster and simpler than HPLC, and still provides accurate results if partial quantification is needed. An applicable approach would be to use SERS to screen foods first, eliminate presumptive negative samples of melamine contamination from the sample population, and then verify presumptive positive samples using HPLC protocols. Combining these two methods could provide a more rapid and cost-effective way for monitoring melamine contamination in large numbers of food and feed products, especially imported foods and food ingredients.

4.1.4 SERS performance in single *Bacillus* spores detection

4.1.4.1 SERS spectra of dipicolinic acid

Raman spectra of DPA powder, DPA extracted from *B. subtilis* sp. spores, and dodecylamine (DDA) which was used to extract DPA are shown in Figure 21. DPA powder exhibits clear Raman peaks at 417, 647, 761, 810, 855, 998, and 1573 cm^{-1}. These peaks can be assigned to different functional groups, such as 761 cm^{-1} to the indole ring, 810 cm^{-1} to the C-H out-of-plane bend, 855 cm^{-1} to the C-C stretch or the C-O-C 1,4 glycosidic link, 998 cm^{-1} to the symmetric ring stretch, and 1573 cm^{-1} to the asymmetric O-C-O stretch (Ghiamati and others 1992; LiChan 1996; Maquelin and others 2002) (Table 2). Compared to the spectrum of DPA powder, similar peaks at 417, 810, and 998 cm^{-1} were observed readily from DPA extracted from *B. subtilis* sp. spores, suggesting

that DPA could serve as a biomarker in biochemical analysis and identification of bacterial spores.

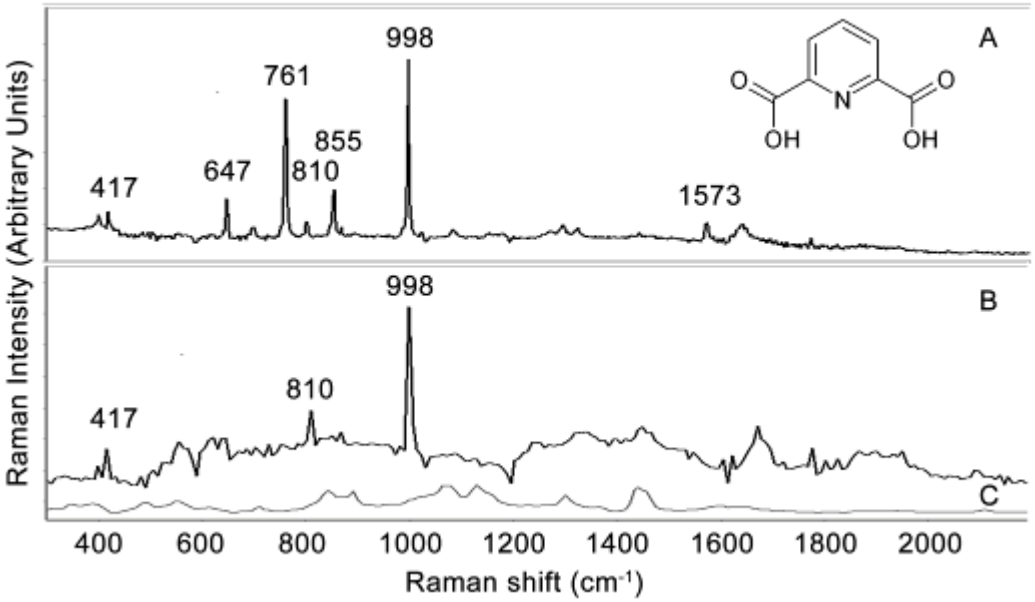

Figure 21. Raman spectra of dipicolinic acid (DPA) powder (A), DPA extracted from *B. subtilis* sp. spores (B), and 50 mM DDA (C)

Table 2. Band assignments in the Raman shift region of 300 - 2200 cm^{-1}*

Raman shift (cm^{-1})	Assignment
~ 720	Adenine
~ 761	Indole ring
~ 810	C-H out-of-plane bend
~ 855	C-C stretch, C-O-C 1,4 glycosidic link
~ 892	C-O-C stretch
~ 998	Symmetric ring stretch
~ 1298	Amide III
~ 1440	$C-H_2$ deformation
~ 1573	Asymmetric O-C-O stretch
~ 1603	Phenylalanine

*Adapted from (Ghiamati and others 1992; LiChan 1996; Maquelin and others 2002)

4.1.3.2 Spore orientations on a Klarite substrate

SEM micrograph of the patterned area of the gold substrate shows nanotextured pyramidal subunits with ~ 1.8 µm openings of the depressions and separated by ~ 0.4 µm of the bridges with one another (Figure 6). Due to electronically connected surface, cooperative oscillations of metal conduction band electrons can be transformed into plasmons (Alexander and Le 2007a). Since sizes of *Bacillus* spores are usually around 1 µm×2 µm, spores would orient themselves in a number of configurations upon the pyramidal subunits of gold nanosubstrate (Figure 22). Enhanced Raman signals of the spore arise from the surface areas closely contacted with the substrate (Figure 22). Spores in different orientations on a substrate were thought to produce equal amount of Raman signals (Alexander and Le 2007).

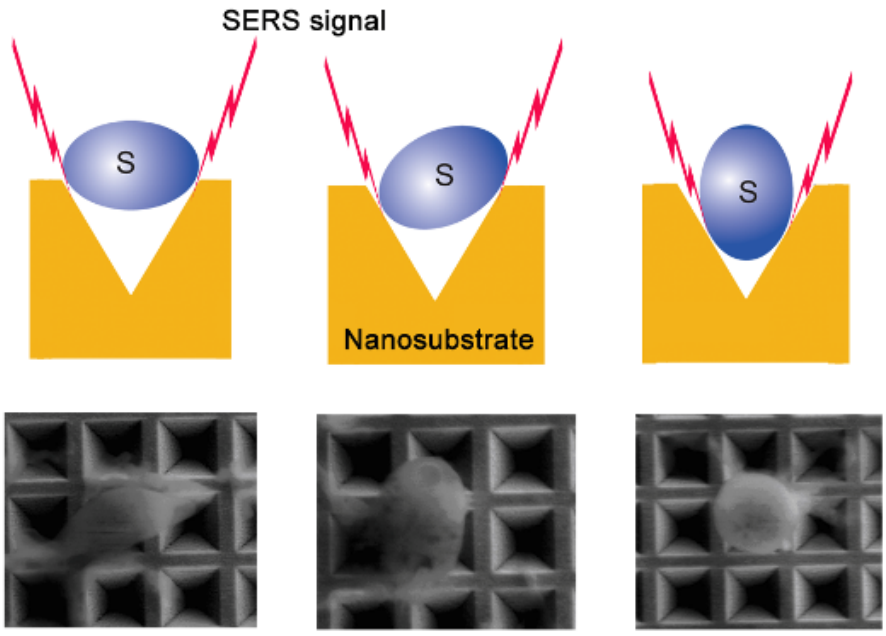

Figure 22. SEM micrographs of different orientations of a *Bacillus* spore (S) on a gold substrate

4.1.3.3 SERS performance in single spore detection

As illustrated in Figure 23, a single spore was captured optically in the area covered by the laser spot through an objective of the microscope. Spectrum of a single *B. subtilits* spore on patterned gold surface and multiple spores (10^2 to 10^3) on unpatterned gold surface of the substrate were shown in Figure 24. Raman signals acquired from a single spore on patterned area were tremendously enhanced and were much more intense than the signals acquired from multiple spores on the unpatterned area, demonstrating that SERS is capable of detecting a single bacterial spore with the aid of nanosubstrates.

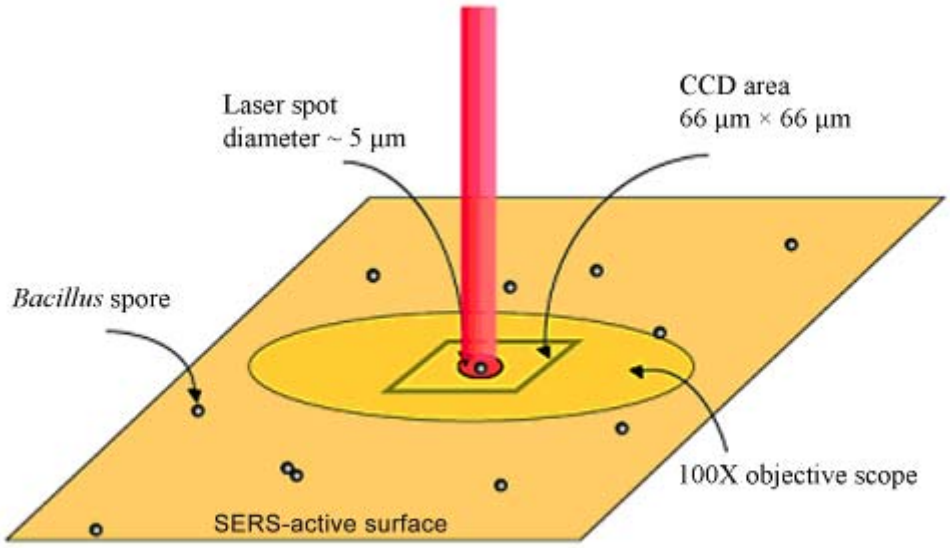

Figure 23. Schematic illustration of a single spore on a gold nanosubstrate captured by Raman microscope

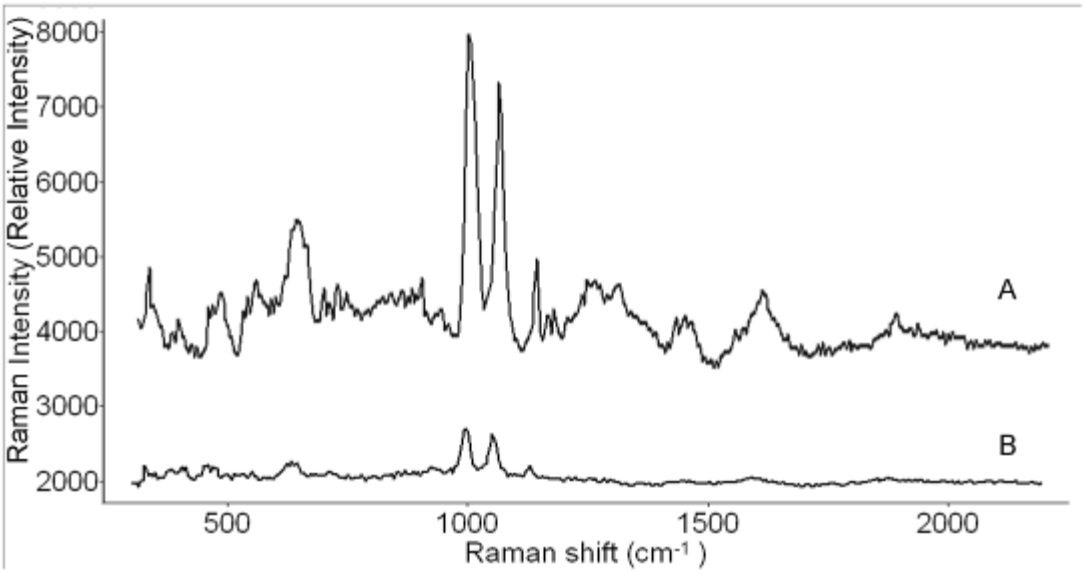

Figure 24. Raman spectrum of a single *B. subtilits* spore (A) on patterned surface and multiple spores (~ 10^3) (B) on unpatterned surface of Klarite gold substrates

4.1.4.4 Discrimination of SERS spectra

Average SERS spectra (n = 4) of spores acquired from five *Bacillus* strains (*B. cereus* ATCC 13061, *B. cereus* ATCC 10876, *B. cereus* sp., *B. subtilis* sp., and *B. stearothermophilus* sp.) are shown in Figure 25. Typical peaks at 720, 892, 998, 1132, 1298, 1440, 1603 and 1880 cm^{-1} are observed in most spectra of five spores. For instance, a peak at 720 cm^{-1} could be assigned to adenine, 892 cm^{-1} to the C-O-C stretch, 998 cm^{-1} to the symmetric ring stretch of DPA, 1298 cm^{-1} to aminde III, 1440 cm^{-1} to the $C-H_2$ deformation, and 1603 cm^{-1} to phenylalanine (Ghiamati and others 1992; LiChan 1996; Maquelin and others 2002) (Table 3). Interestingly, the peak at 892 cm^{-1} is only distinct in the spectra of *B. cereus* ATCC 13061 and *B. cereus* ATCC 10876, while the peak at 1053 cm^{-1} is distinctive for the spectra of *B. subtilis* sp. and *B. stearothermophilus* sp., but not for *B. cereus*. Additionally, a peak at 1440 cm^{-1} is present clearly in all spectra except for *B. subtilis* sp, while band around 862 cm^{-1} is only present in *B. stearothermophilus* sp. Clear differences in the intensity of normalized spectra between different *Bacillus* spores were also observed. For example, the intensity of the peak at 998 cm^{-1} in the spectrum of *B. subtilis* sp. is much higher than those of other strains. This may be due to the absence of the exosporium layer in *B. subtilis* spores, while *B. cereus* and *B. stearothermophilus* spores possess exosporium layer (Driks 1999). Therefore, *B. subtilis* spore reflects much more intense Raman signals of DPA from the sporal core than *B. cereus* and *B. stearothermophilus* spores. These differences between spectra of five *Bacillus* spores represent the differences in quantity and distribution of sporal components such as DPA, polysaccharides, proteins, phospholipids, nucleic acid, etc. The results indicate that

SERS can be used to identify and discriminate between different *Bacillus* spores based on their unique and distinct vibrational spectral information.

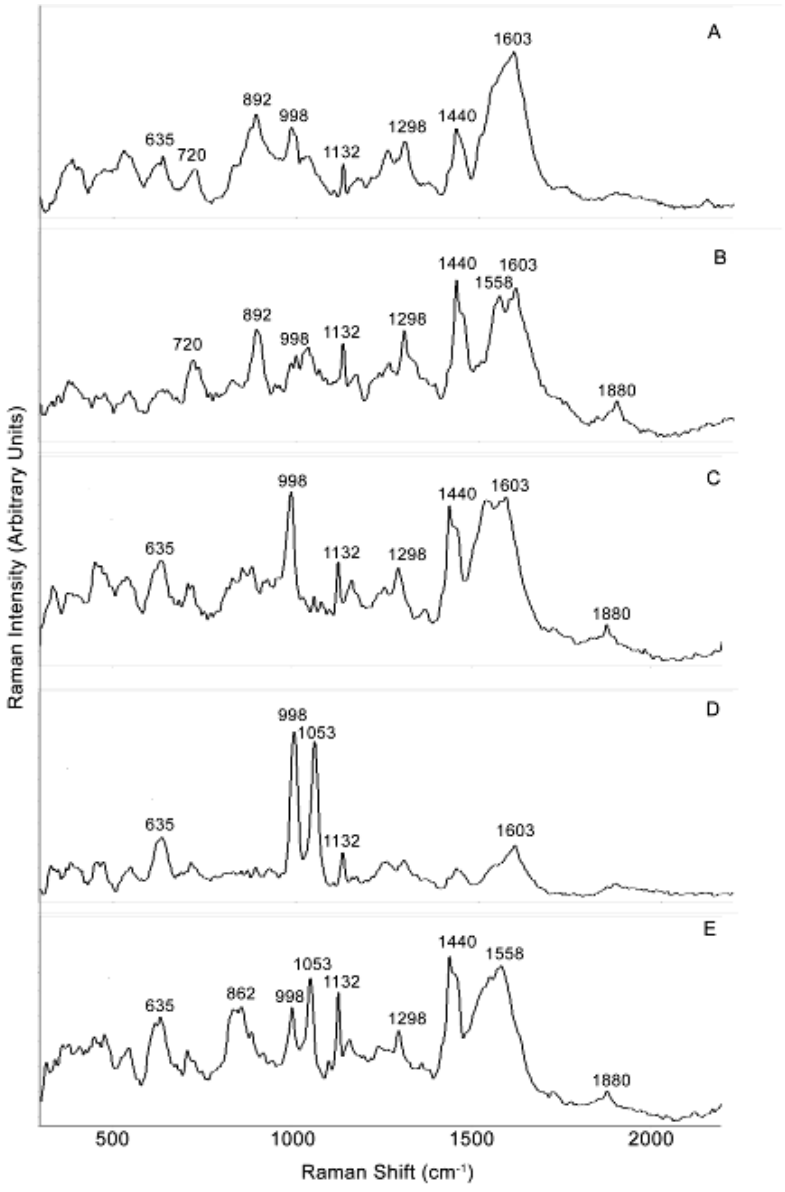

Figure 25. SERS spectra of *B. cereus* ATCC 13061 (A), *B. cereus* ATCC 10876 (B), *B. cereus* sp. (C), *B. subtilis* sp. (D), and *B. stearothermophilus* sp. (E) spores

Hierarchical cluster analysis (HCA) dendrogram (Figure 26) demonstrates the spectral similarities between the samples by deriving spectral distance based upon Ward's linkage analysis. Three clusters of *B. cereus*, *B. stearothermophilus* and *B. subtilis* spore samples were clearly distinguished. In the cluster of *B.cereus* spore samples, three *Bacillus cereus* spore samples (ATCC 13061, ATCC 10876, and *B. cereus* sp.) are close to each other but still show some differences amongst each other. Both spore samples of *B. stearothermophilus* and *B. subtilis* spore samples exhibit long distance away from *B. cereus* spore samples. This result agrees with that from the spectra (Figure 25) in which *B. subtilis* spore sample looks most different from others.

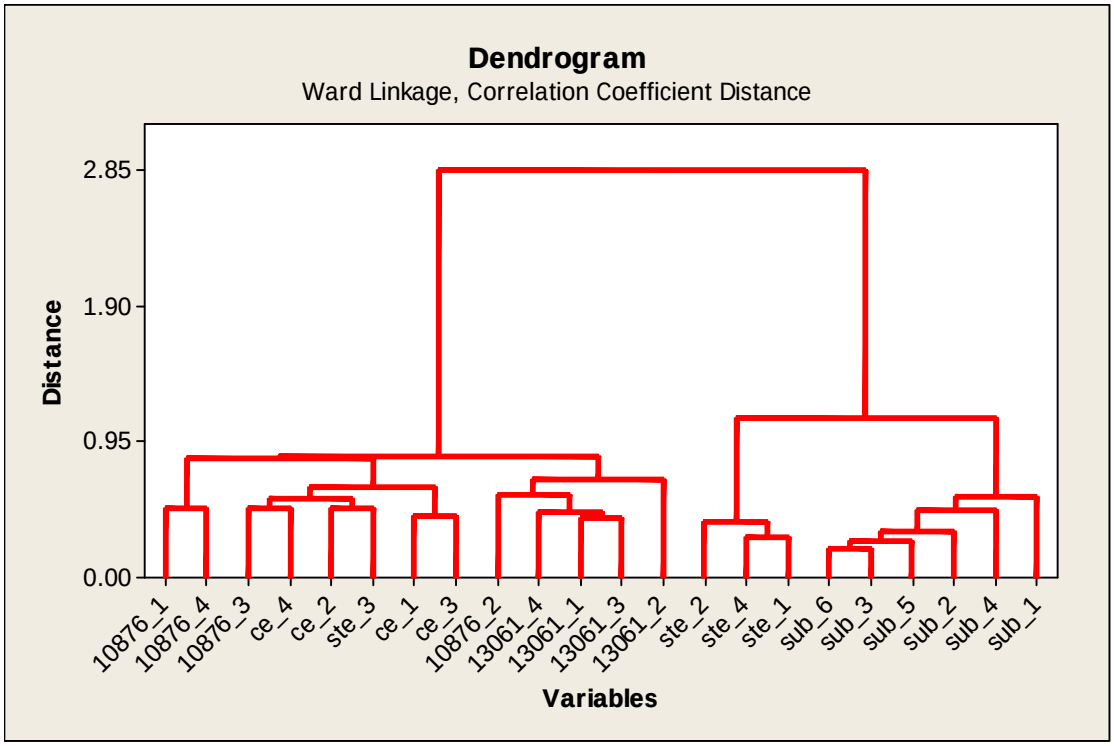

Figure 26. HCA dendrogram based on Ward's linkage of SERS spectral data of five *Bacillus* spores

PCA reduces the original set of variables into principal components (PCs) that retain its most dominant features. The first two PCs were plotted in Figure 20. Similar to the HCA result (Figure 27), segregations at the species level (*B. cereus*, *B. stearothermophilus* and *B. subtilis*) were observed clearly. Table 3 shows five PC score values generated in PCA with different Raman shift ranges. Generally, the first PC conveys the largest amount of information, followed by the second PC, and so forth. At a certain point, the variation modeled by any new PC is mostly noise (Nilsen and others 2002). The scores are composed of the weightings for each PC creating the best-fit vector for each sample (Lin and others 2004). The result obtained from the range of 900 - 1200 cm^{-1} shows higher score values than those of other ranges with a wavenumber window of 300 cm^{-1}, indicating the range of 900 - 1200 cm^{-1} explains more of the data variance than other ranges. It is noteworthy that PCA based on a short range of 950 - 1000 cm^{-1} with a wavenumber window of 50 cm^{-1}, which includes spectral information of DPA peak at 998 cm^{-1}, yields the highest score value with the first five PC scores accounting for approximately 95% of total data variance in this PCA. This result demonstrates that DPA peak contributes most to the total data variance in the PCA of SERS spectral data. *Bacillus* spores of different species exhibit unique DPA peak intensity, along with other peak information (e.g. peaks at 892, 1053, 1440 cm^{-1}), providing key information for discrimination between these spores by SERS in combination with multivariate statistical analysis.

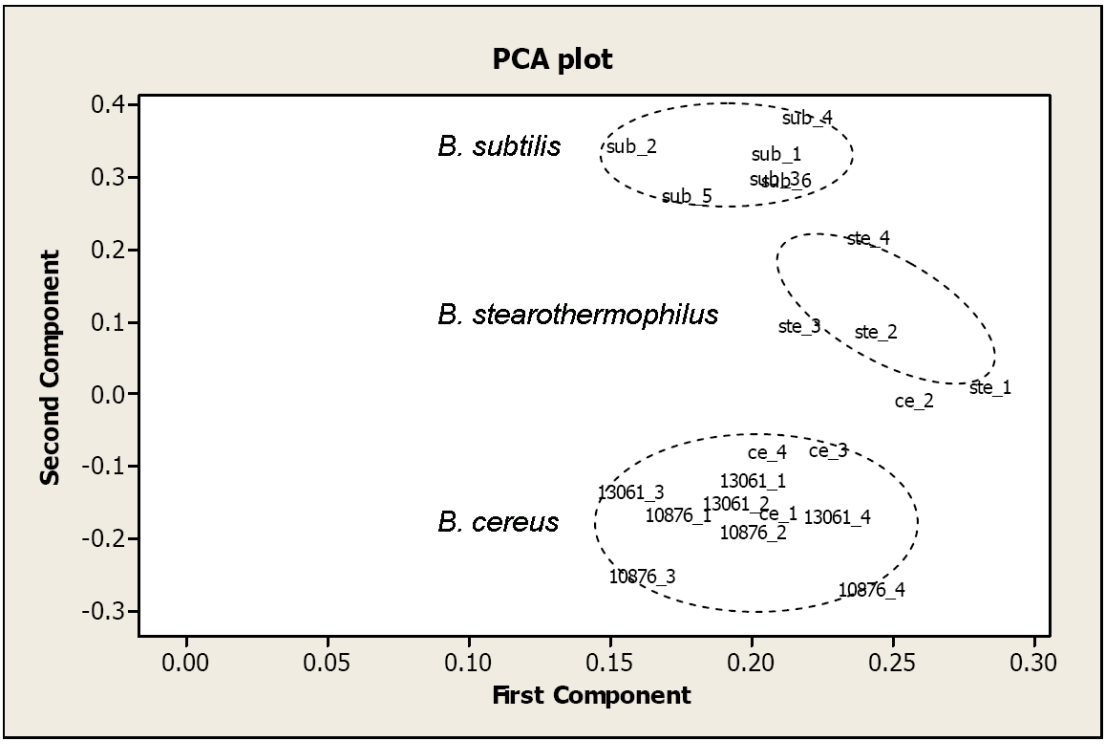

Figure 27. PCA plot based on the first two PCs of five *Bacillus* spores SERS spectra

Table 3. PC score values obtained from PCA in different Raman shift ranges

Raman shift (cm^{-1})	300-600	600-900	900-1200	(950-1000)	1200-1500	1500-1800	1800-2200
Score 1 (%)	21.89	14.49	30.34	45.70	22.86	28.49	12.14
Score 2 (%)	11.21	12.33	13.70	33.79	10.43	12.95	11.83
Score 3 (%)	10.15	7.86	13.38	7.59	7.88	8.77	9.44
Score 4 (%)	7.25	8.90	6.23	4.76	7.68	5.96	10.19
Score 5 (%)	6.40	7.24	4.59	2.90	6.37	6.31	6.18
Total (%)	56.91	50.82	68.25	94.73	55.22	62.47	49.76

4.1.4.5 Conclusion

SERS is a simple, fast, non-destructive, and ultra-sensitive technique. SERS coupled with gold nanosubstrates could provide a unique approach to detect and discriminate among different *Bacillus* spores. With the aid of the latest novel nanotechnology, the LOD of the SERS method can go down to one single spore. Distinct features were observed between spores of different *Bacillus* strains in the range of 300 - 2200 cm^{-1}. The differences in quantity and distribution of sporal components such as DPA, polysaccharides, protein, phospholipids, and nucleic acid, along with the presence or absence of exosporium, make it possible to use SERS for sensitive and selective detection of trace amount of bacterial spores. Further studies are needed to explore the potential of this technique to the analysis of agricultural and food samples.

4.2 Use of gold-coated zinc oxide nanonacklaces in SERS for detection of melamine

4.2.1 Morphology of zinc oxide nanonacklaces

FESEM images of ZnO nanostructures were shown in Figure 28. Faceted ZnO nanoneclate (NNs) were grown horizontally on sapphire substrates. These NNs were typically less than 100 nm in diameter and 10 - 20 μm in length; the density of NNs was 2 - 6 strips/μm; and the facets of the ZnO, indicative crystalline structure, could be well observed. It is known that faceted structure could provide higher Raman signals than traditional spherical one, due to its sharper curvature resulting in higher electromagnetic effect (Hao and Schatz 2004), and higher free energies for interaction with molecules resulting in higher chemical effects (Zhang and others 2005). AFM image (Figure 29) shows two-dimensional (2-D) and the sectional analysis of the ZnO NNs on r-plane

sapphire substrates. This result shows well-connected NNs structure and roughly patterned surface which can provide plenty of periodical SERS “hot-spots” which are key to enhanced Raman scattering. Detailed growth mechanisms of ZnO NNs were introduced in the previous study (Shi and others 2009). Briefly, catalysts size and the competition between surface freee energy, interfacial energy between ZnO and sapphire, and strain energy are the major factors to drive ZnO NN growth along ZnO [0001] and sapphire [10-11] and ZnO (-12-10) || sapphire (01-12) direction on r-plane sapphire. Au and Al atoms decoration and strain energy might contribute to the formation of necklace-like structures. Additionally, epitaxial relationship between r-plane sapphire and ZnO and lattice mismatch in different directions also play an important role in necklace-like structure formation.

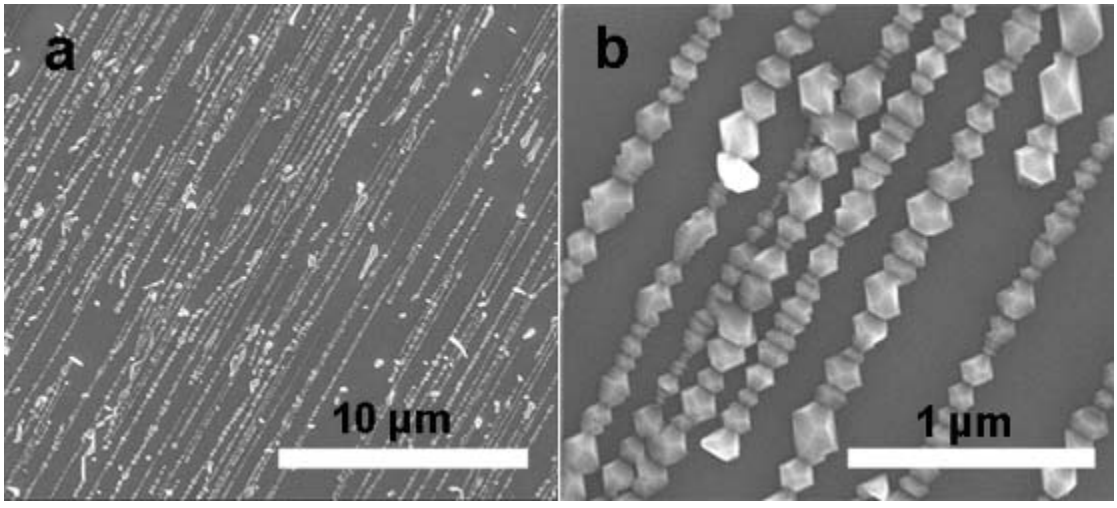

Figure 28. Field emission electron microscopy (FESEM) images of ZnO substrate 60 mm away from the precursor

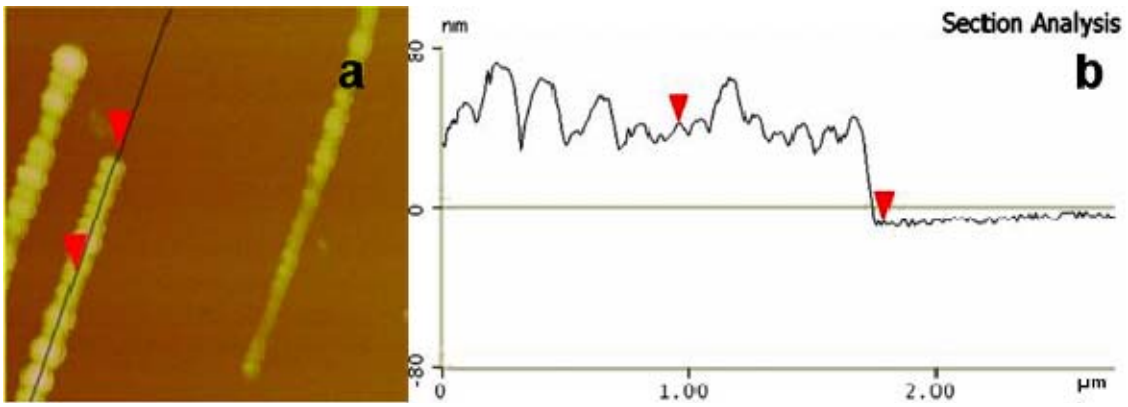

Figure 29. Atomic force microscopy (AFM) images (a) and section analysis profile of the ZnO NNs (b).

4.2.2 Characterization of Gold-coated ZnO NNs

SERS-active substrates were prepared by sputtering gold NPs onto the ZnO NN substrates. In order to evaluate the contribution of ZnO NN structure in SERS effect generation compared with gold NPs, a bare gold film sputtered on sapphire substrate was used as the control. Figure 30c shows the SERS signals of melamine from the rough gold film. It was observed that the intensity of Raman signals from the rough gold film was much lower than that from gold-coated ZnO NNs (Figure 30a). To confirm that the SERS signals were mainly from the ZnO NN structure rather than from gold NPs, an annealing procedure (250 ^{o}C, 30 sec) was applied. Figure 30d shows no SERS effect was observed from gold NP films after annealing. Figure 30b shows the SERS signals from gold-coated ZnO NNs after annealing. Compared with Figure 30b and 30c, it is evident that the SERS effect from gold-coated ZnO NNs after annealing was stronger than that from rough gold film. These results demonstrate that SERS effects came mainly from the ZnO NNs structure rather than from the rough gold film. It is well known that the plasmonic properties of SERS material mainly depend on the particle size. Larger particle size requires higher excitation wavelength in order to get plasmon resonance (Emory and others 1998; Kim and others 2009). We believe ZnO NNs with a size around 100 nm have much larger plasmon resonance under 785 nm laser than the smaller gold NPs (~10 nm), hence producing higher enhancement signals.

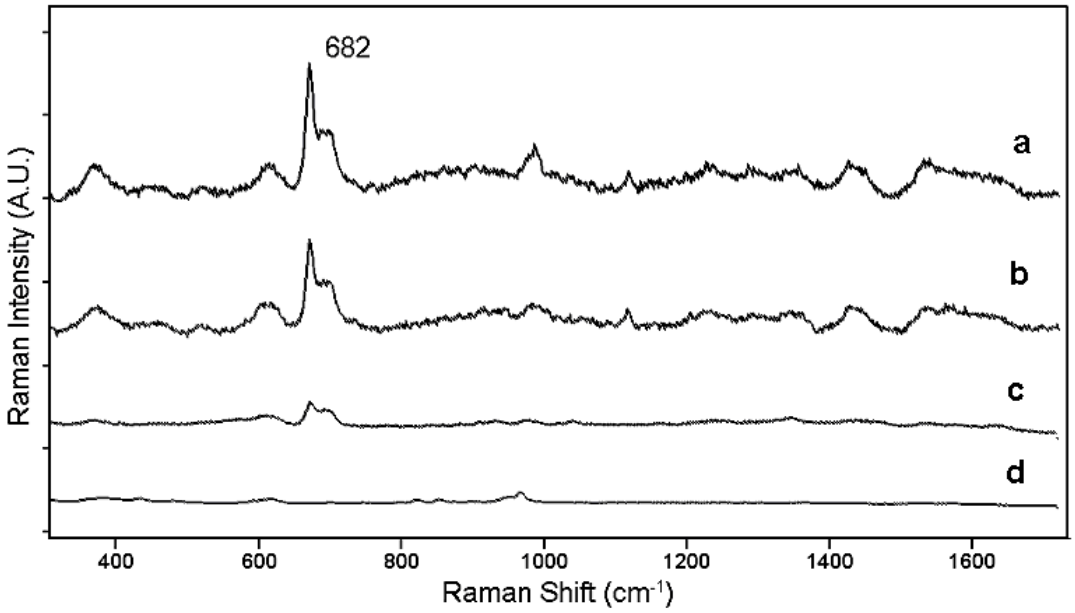

Figure 30. Average Raman spectra (n=3) of 10^{-4} mol/L melamine on a gold film coated ZnO NN substrate before (a) and after annealing (b), a gold film substrate before (c) and after annealing (d)

FESEM images of gold-coated ZnO NNs before (Figure 31a) and after (Figure 31b) the annealing procedure were obtained. Before annealing, the surface of the substrate was roughly covered with noticeable gold NPs. While after annealing, the surface of the gold NPs turned into a smooth film. These images could well explain why no SERS signals were obtained from the annealed gold film. Therefore, it was confirmed that all SERS effects were produced from NNs structure in an annealed substrate.

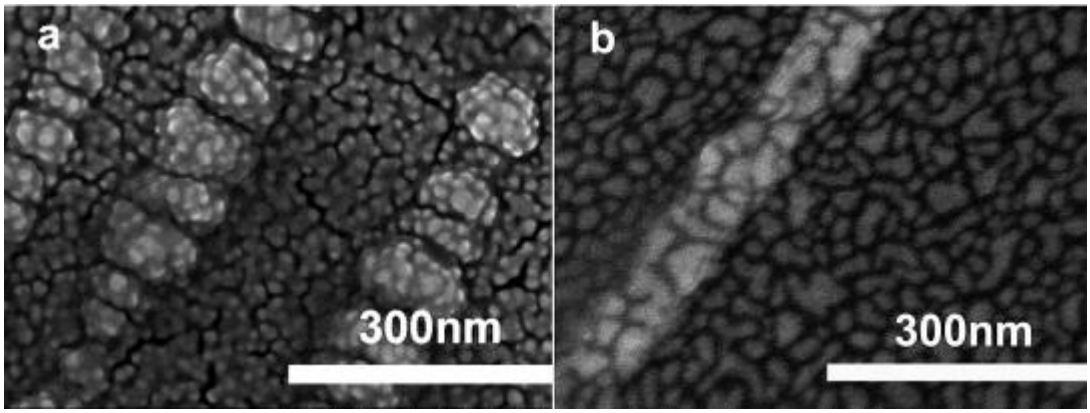

Figure 31. FESEM images of ZnO NNs coated with ~45 nm gold film before (a) and after annealing (b)

Two levels of thickness of gold coating (45 nm and 60 nm) were tested for ZnO NN substrates in this study. SERS effects of 45 nm coating were higher than that from 60 nm (Figure 32). This is because of the loss of more roughness with thicker coating, so that the SERS signals dramatically decreased.

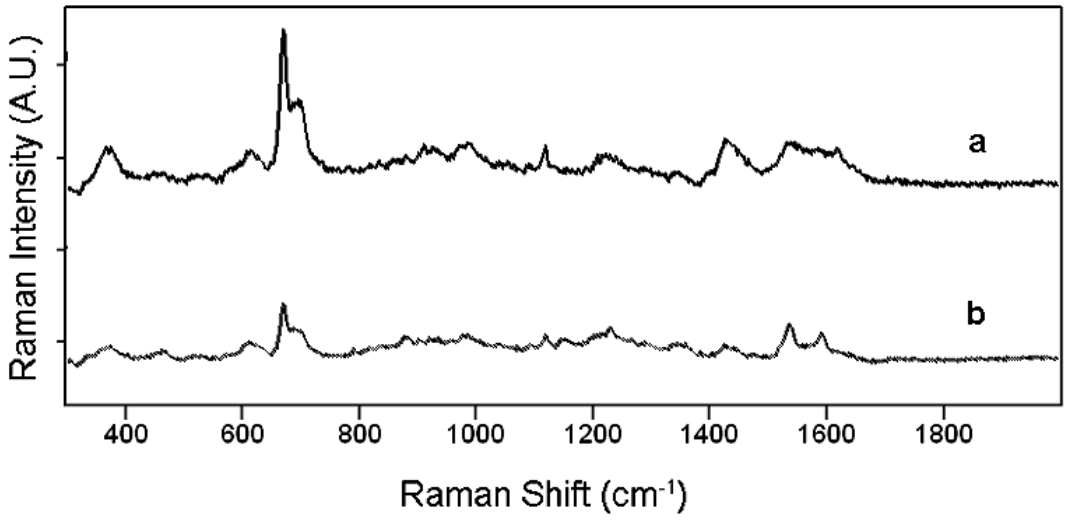

Figure 32. Average Raman spectra (n = 3) of 10^{-4} mol/L melamine on a ZnO NN substrate with 45 nm (a) and 60 nm (b) gold coating

4.2.3 SERS performance in melamine detection

Before SERS analysis, both gold-coated ZnO NN substrate and the gold film substrate were annealed to avoid SERS signals from the rough gold film. Figure 33 shows a typical SERS spectrum of melamine deposited on the surface of ZnO NN substrates, indicating low interference signals from the background of the substrate. By comparing the melamine peaks at around 683 cm^{-1} from a gold coated ZnO NN substrate with that from a flat gold film substrate, the analytical enhancement factor was calculated to be higher than 10^4 based on the equation (1). This enhancement factor is competitive with a commercial gold SERS-active substrate (He and others 2008b). Analytical enhancement factor is straightforward and can be easily measured in practical applications. However, the concentration of analyte in SERS measurement doesn't fully characterize the adsorbed molecule number, therefore, the real enhancement factor is thought to be even larger (Le Ru and others 2007).

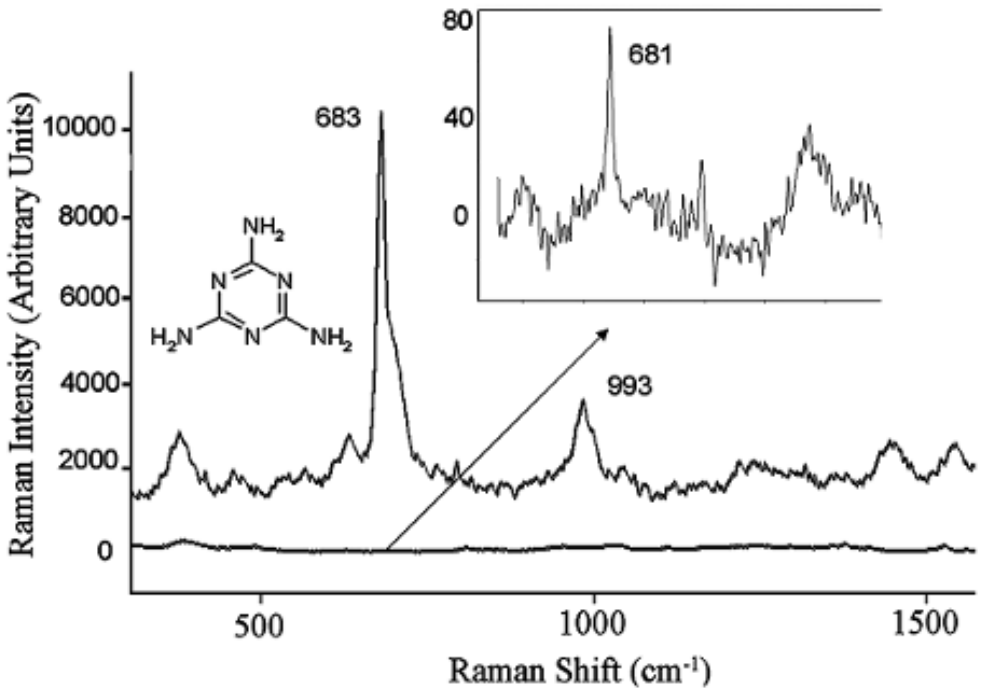

Figure 33. Average Raman spectra (n = 3) of 10^{-4} mol/L melamine on a gold coated ZnO NN substrate after annealing and 10^{-2} mol/L melamine (inset) on a gold film substrate after annealing

Different concentrations of melamine (10^{-6}, 10^{-5}, 10^{-4}, 10^{-3}, and 10^{-2} mol/L) were analyzed by gold-coated ZnO NNs. The LOD was found to be 10^{-5} mol/L (Figure 34). Figure 8 shows the concentration and signal dependence based on the melamine peak around 383 cm^{-1}. A linear regression (R^2 = 0.9561) was established between the log value of melamine concentration and Raman intensity of the peak at around 383 cm^{-1}. The error bars in Figure 8 indicate the deviation of Raman intensity of signals acquired from three randomly picked spots on the substrate. This result indicates that gold-coated ZnO NNs could produce stable and reproducible SERS signals and therefore has a potential for quantitative analysis of melamine based on its SERS spectral information.

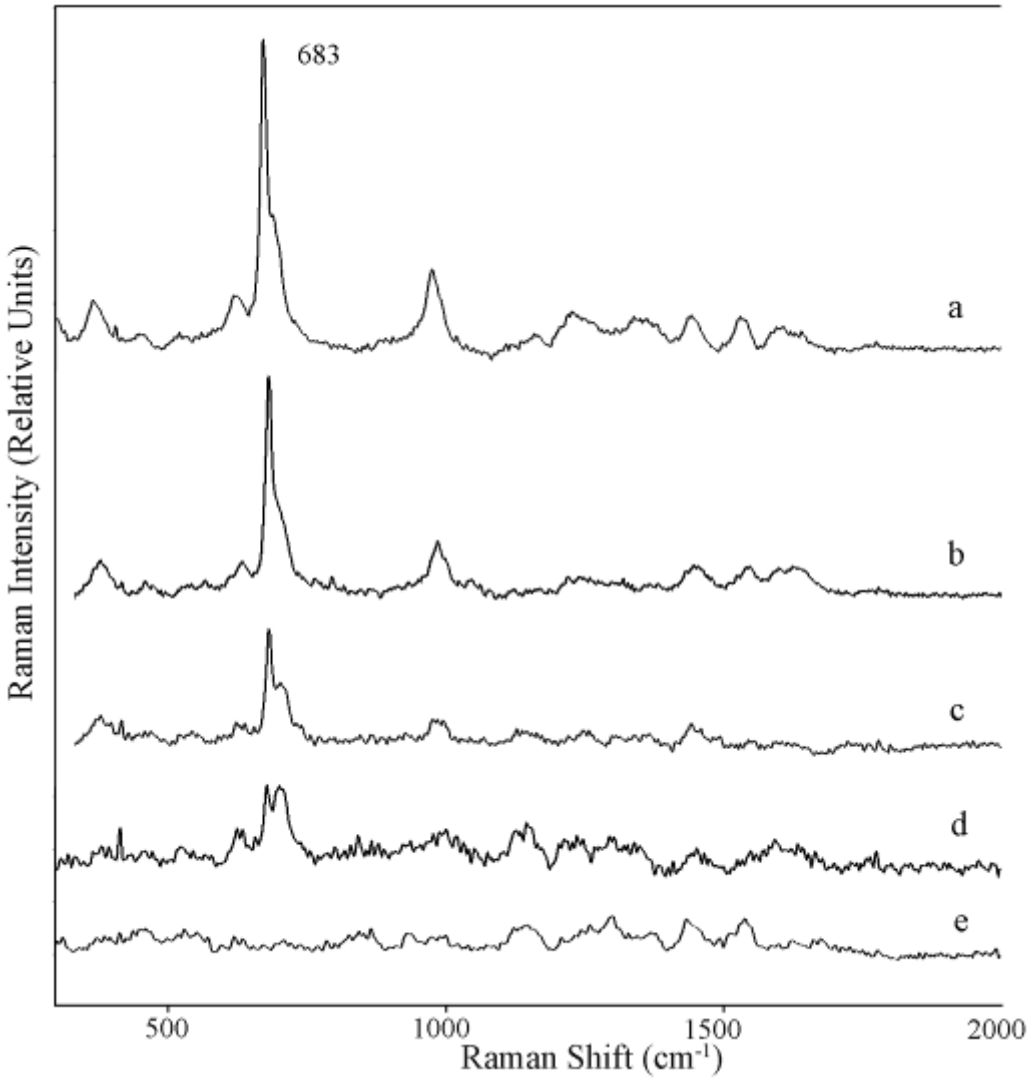

Figure 34. SERS spectra of a series concentration of melamine (10^{-6}, 10^{-5}, 10^{-4}, 10^{-3}, and 10^{-2} mol/L) deposited onto gold-coated ZnO NNs

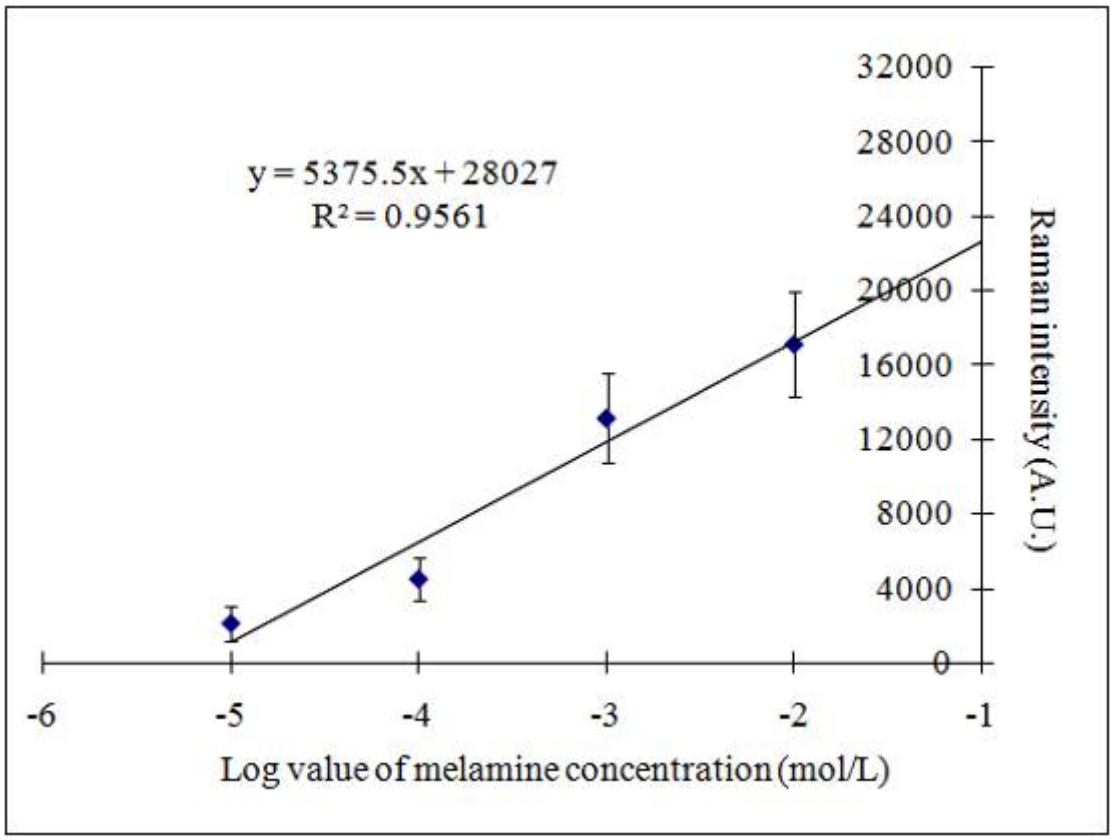

Figure 35. Relationship between log value of melamine concentration (mol/L) and Raman intensity of a melamine peak at around 683 cm^{-1} (n=3)

CV and MG were other food contaminants implicated in the 2007 seafood alert in the US (FDA 2007b). Zero tolerance policy has been set for the residues of CV and MG in fish by the US FDA (FDA 2007a). These two compounds have similar but more complex chemical structures than melamine, so they are good candidates to evaluate SERS substrates too. Distinct Raman spectra of these two chemicals were obtained (Figures 36a and 36b) and these spectra were in accord with our previous study (He and others 2008a). These results demonstrate that this new ZnO NN substrate can be used for measuring various chemicals.

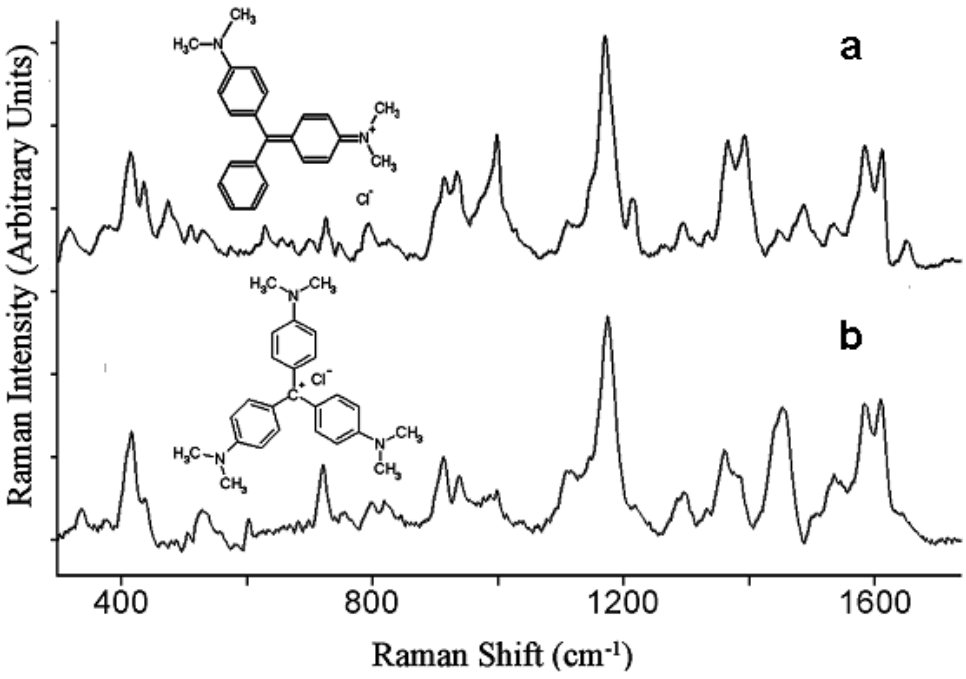

Figure 36. Average Raman spectra (n = 3) of 10^{-4} mol/L malachite green (b) and 10^{-4} mol/L crystal violet (c) on a gold-coated ZnO NN substrate after annealing

4.2.4 Other ZnO nanostructures

When sapphire substrates were put at other positions (50, 40, 30, 20 mm) away from the precursor, a different ZnO nanostructure was found. Figure 37 shows nanoblades (NBs)-like structure with a certain angle grown upon the NNs. These ZnO NBs were 200 nm - 1 μm in width and a few micrometers to a few tens micrometers in length and have multiple angles with substrates. The NBs were typically found grown out of the tip of NNs. It was observed that more ZnO NBs and NNs were grown on the sapphire substrate as they were closer to the precursor. Compared with NNs, NBs decreased more dramatically with the increasing distance away from the precursor. When substrate was placed 60 mm away from the precursor, almost all nanostructures were NNs. It was discussed in a previous study (Shi and others 2009) that the Au NPs with diameter of ~5 nm and lower density of such NPs are critical for the formation of horizontally aligned ZnO NN arrays while higher density or bigger size of Au NPs resulted in vertical ZnO NPs.

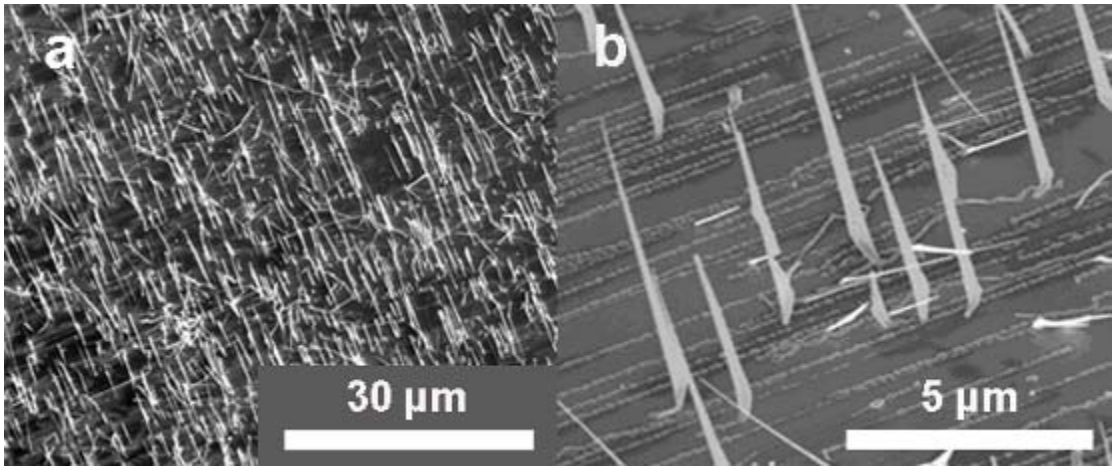

Figure 37. Field emission electron microscopy (FESEM) images of ZnO substrate 20 mm away from the precursor

SERS effects from 5 gold-coated ZnO NNs substrates at different positions were evaluated using melamine (10^{-4} mol/L). As shown in Figure 38, substrate at 40 mm position had the highest SERS effects. This result indicates that NBs structure didn't contribute but rather counteract the SERS effects. One reason is that these micrometer long tilted NBs may influence the reflectivity of Raman scattering signals. Another reason is the difficulty of controlling the coating thickness with the presence of NBs structure. Therefore, the SERS effects mainly came from the NN structure with gold coating. The denser of NN arrays, the higher SERS effects were. Decreasing of the SERS effects at further positions was due to the lower density of NNs on the sapphire substrate. It is prospective that with the high density of NNs, the whole enhancement of the gold-coated ZnO NN substrate will be improved dramatically.

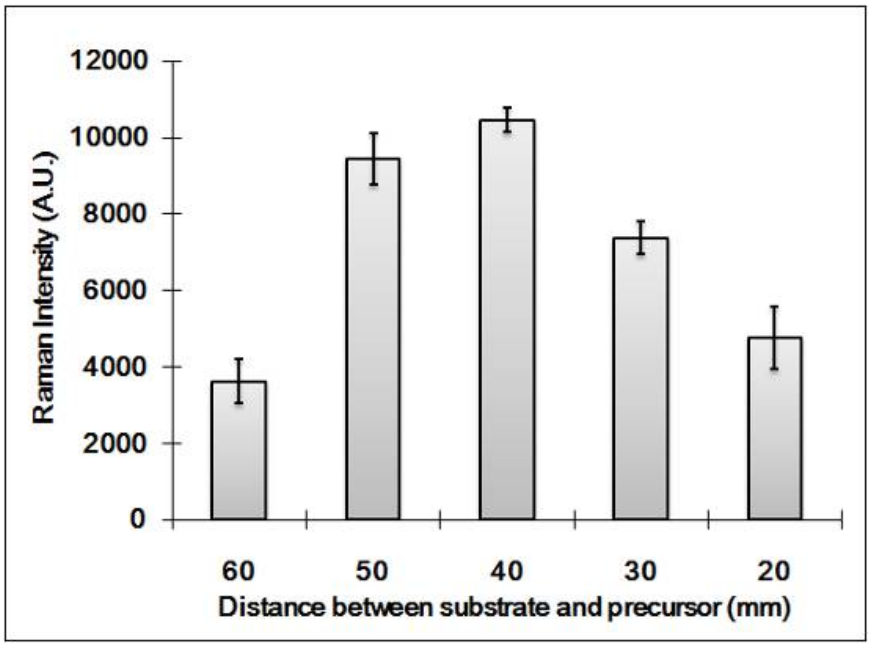

Figure 38. Raman intensity of melamine (10^{-4} mol/L) peak at around 683 cm^{-1} acquired from 5 different ZnO NN substrates (n=3). All substrates were coated with ~45 nm gold film after annealing

4.2.5 Conclusion

In summary, we reported the potential SERS application of novel faceted ZnO NN arrays that were horizontally-aligned on r-plane sapphire substrates. Our results show that gold-coated ZnO NN arrays can serve as a viable substrate for SERS applications and provide satisfactory enhancement when used to detect different analytes such as melamine and other food contaminates. It was also confirmed that the enhancement effects mainly originated from the unique faceted nanonecklace structures, instead of the nanostructures of gold films. It was found that ZnO NNs contributed to the SERS effects while ZnO NBs, when grown with larger Au NPs or higher density of Au NPs as catalysts in the CVD process, reduced the enhancement factor. We expect that ZnO NN arrays at wafer scale could be fabricated with reproducible structures by precisely controlling the experimental conditions. As a result, we believe there is a great potential for this ZnO NN substrate in the SERS applications for the detection of trace amount of food contaminates, as well as other chemicals and biochemicals. Future work will be conducted to further improve the uniformity of the density of ZnO NN arrays and optimize the thickness of the gold film. Additionally, different coating techniques will be explored for further improvement of consistency of the ZnO NN based SERS substrates.

4.3 Use of fractal-like gold nanoaggregates in SERS detection of prohibited antifungal dyes

4.3.1 Morphology of fractal-like gold nanoaggregates

SEM images (Figure 39) reveal a complex but well developed porous structure obtained from self-assembled gold nanoparticles after a brief annealing. The clustering

and aggregation of nanoparticles initially took place in an aqueous solution to form a fractal-like network and a heat-induced structural coarsening effect occurred during the annealing step, resulting in a complex porous Au structure. These porous nanostructures are expected to be useful to attract and trap analyte molecules in the close proximity of a metal surface. The pores observed under the SEM were found to be rather broad in size distribution, while the average pore size was estimated to be around 300 nm.

A previous study (Kucheyev and others 2006) reported a similar pore size of the de-alloyed nanoporous gold film to exhibit SERS effect. We believe that increasing the annealing time and/or temperature would yield larger average pore sizes as well as increasing sizes of connected nanoclusters as a result of coarsening, while the heat from annealing further purges the metal surface. It is therefore important to find the best annealing condition by precisely controlling time and temperature during annealing because the generation of the SPR is believed to be dependent on the size of Au nanoparticles as well as the pore size of Au nanoclusters.

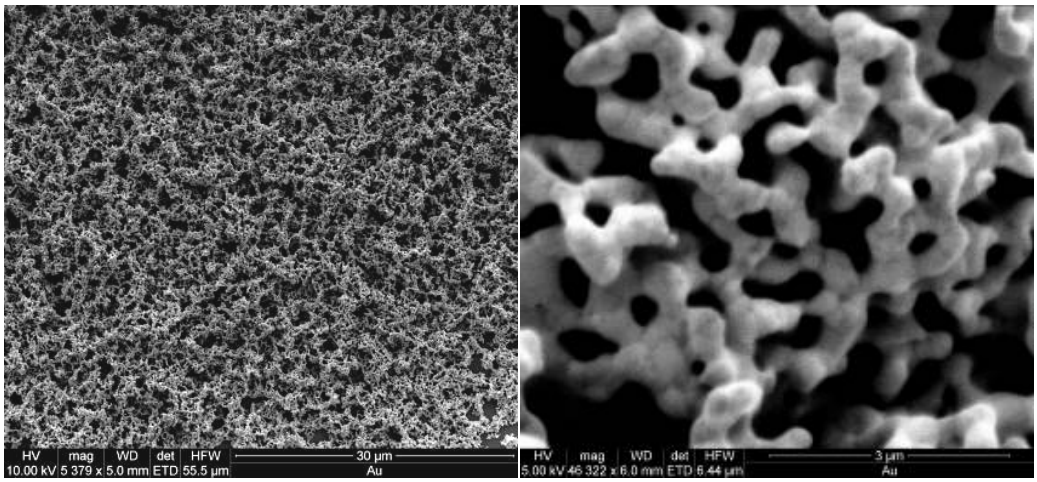

Figure 39. SEM image of a fractal-like aggregate film self-organized from gold nanoparticles. Higher magnified image of gold clusters is provided in the inset

4.3.2 SERS performance in prohibited antifungal dyes detection

4.3.2.1 SERS spectra of CV, MG, and their mixture (1:1)

CV and MG are very similar in their molecular structures. Not surprisingly, their Raman spectra are very close to each other (Figure 40). Their major peak assignments were shown in Table 4 (Liang and others 1997). One noticeable difference between these two molecules in Raman spectra could be found at the peak around 338 cm^{-1} as in-plane vibration of phenyl-C-phenyl bend which is clearly present in CV spectra but not in those of MG (Figure 40). Additionally, it was found that the ratio of peak intensity of 1171 over 1219 cm^{-1} which were assigned to be the in-plane vibrations of ring C-H and C-H rocking, respectively, was much higher in CV than that in MG. Other slight differences between relative peak intensities at several positions (e.g. 526, 724, and 916 cm^{-1}, etc) were also found between CV and MG. These differences were likely attributed to the presence of one more C_3H-N-C_3H in CV than in MG. When testing the spectra of mixed samples (1:1), the changes of peak 338 cm^{-1} and the ratio of peak intensity of 1171 over 1219 cm^{-1} were clearly observed. The intensity values were found, as expected, to be the averages of those of CV and MG. The value of the ratio of peak intensity of 1171 over 1219 cm^{-1} may be used to calculate the percentages of CV and MG in the mixture.

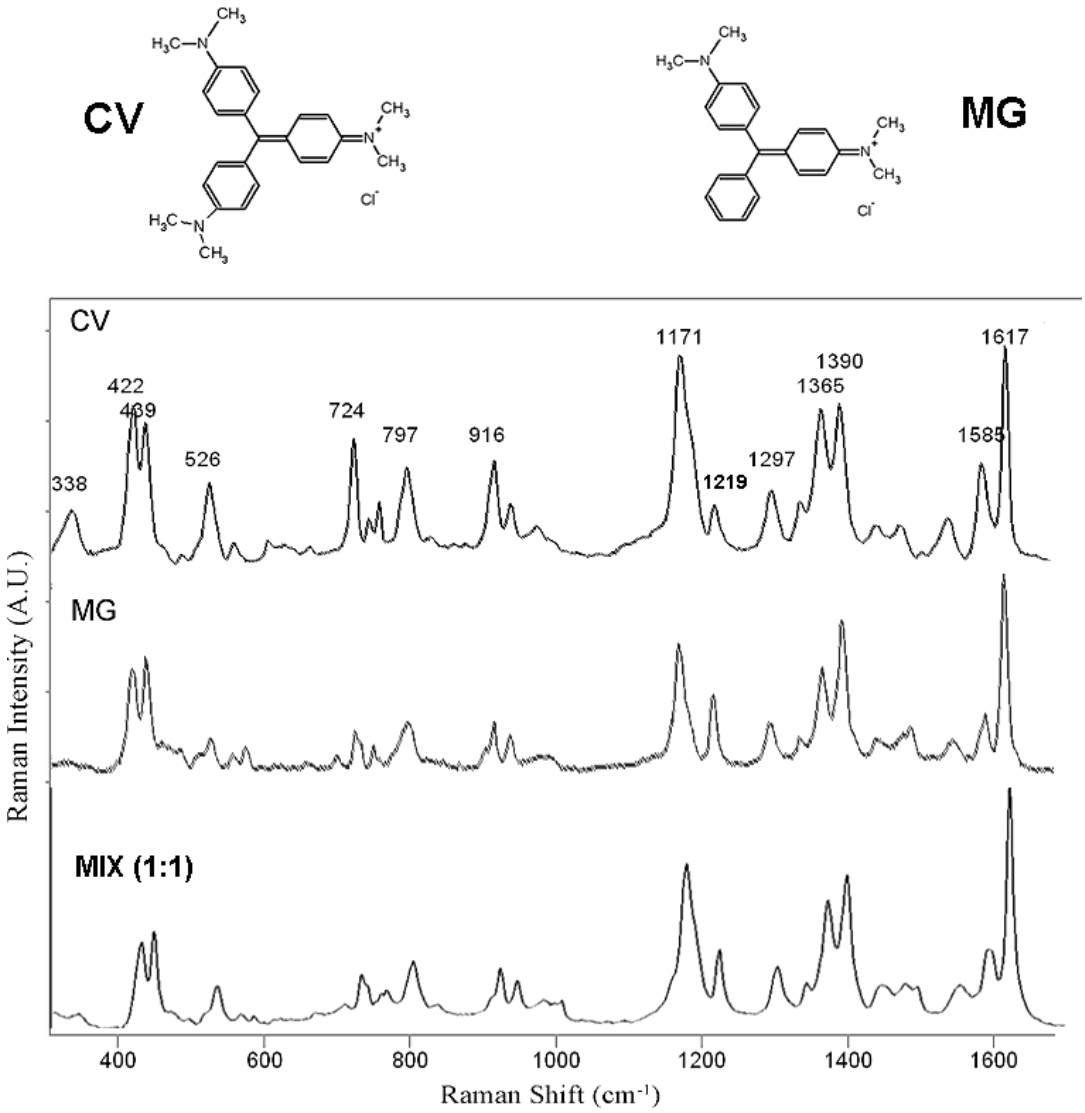

Figure 40. Average SERS spectra (n = 8) of 200 ppb CV, MG, and their mixure (1:1)

Table 4. Band assignments of peaks in CV and MG Raman spectra

Raman shift (cm^{-1})	Band assignment
~ 338	In-plane vibration of phenyl-C-phenyl
~ 422	Out-of-plane vibrations of phenyl-C-phenyl
~ 526 and 916	Ring skeletal vibration of radical orientation
~ 724 and 797	Out-of-plane vibrations of ring C-H
~ 1171	In-plane vibrations of ring C-H
~ 1219	C-H rocking
~ 1365 and 1390	N-phenyl stretching
~ 1585 and 1617	Ring C-C stretching

To differentiate these two chemicals, further analysis using PCA was conducted based upon SERS spectral data of CV, MG and the mixture (1:1) (Figure 41). PCA is a data reduction method which captures the variation between samples based on their PCs. Segregations between CV, MG, and the mixture were clearly observed. As expected, the cluster of mixed samples was positioned in the middle between the CV and MG clusters. The first five PCs explained 80% of total data variances. These results demonstrate that chemicals with similar molecular structures like CV, MG, and their mixture can be differentiated by SERS methods in conjuncture with the use of gold nanostructures.

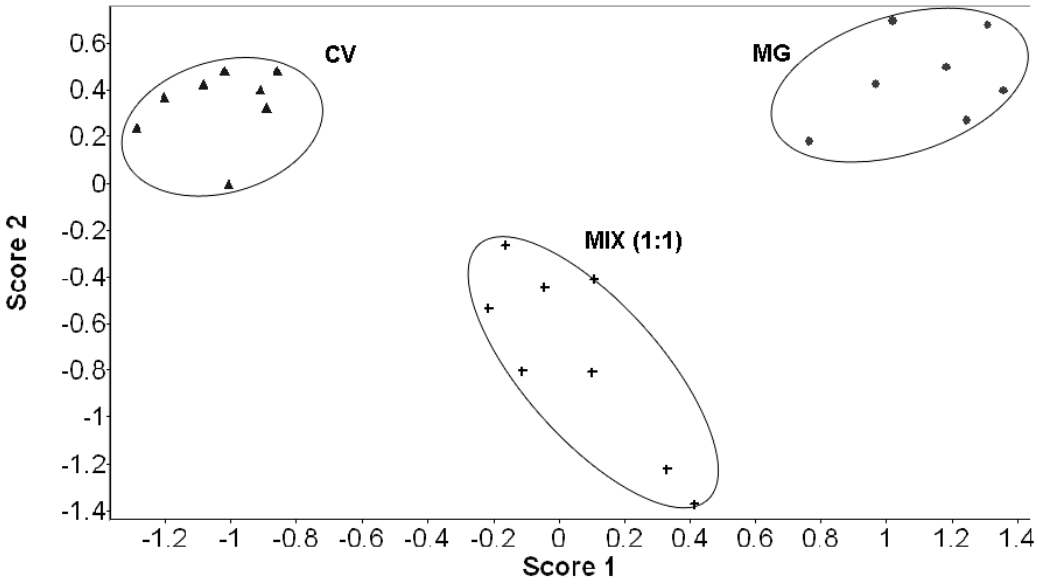

Figure 41. Two dimensional (2D) PCA plot based on the SERS spectra of MG, CV and the mixture of MG and CV (1:1)

4.3.2.2 Sensitivity of SERS measurements

To determine the enhancement factor (EF) of this fractal-like gold nanostructure as a SERS-active substrate, 2 ppb CV solution was deposited onto the fractal-like gold nanostructure and 2000 ppm CV solution onto a gold-coated flat surface, respectively. The intensity of a peak at ~ 1617 cm^{-1} in the CV Raman spectrum from the gold flat surface was ~ 500, while from gold nanostructure was ~ 20000 (Figure 42), a substantial increase in peak resolution. Based on the equation (3-3), an EF of ~ 4×10^7 for Raman signal enhancement was calculated for the gold nanostructures applied in SERS measurements. This result clearly demonstrates that SERS method coupled with the gold nanostructures is promising to serve as an ultra-sensitive and nondestructive analytical technique for chemical detection.

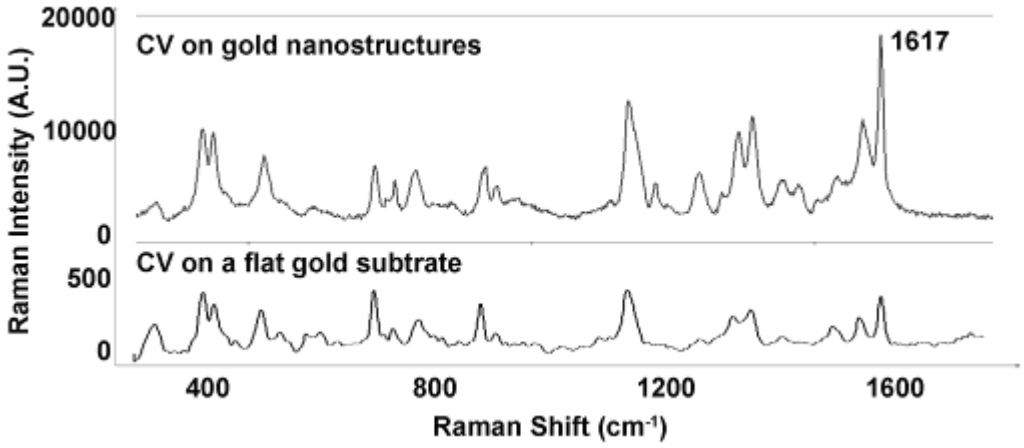

Figure 42. A SERS spectrum of 2 ppb CV on gold nanostructures and a normal Raman spectrum of 2000 ppm CV on the control (a gold-coated glass slide)

To evaluate the sensitivity and reliability of SERS and quantify different concentrations of the analyte on gold nanostructures, samples containing a series of CV concentrations (0.2, 2, 20, 200, and 2000 ppb) were deposited on the gold nanostructures and analyzed by SERS (Figure 43). As shown by the curve in Figure 5, the peak intensity at 1617 cm^{-1} increased monotonously with the increase of CV concentrations. There is a linear relationship between the log value of intensity and the log value of CV concentrations between 0.2 and 20 ppb. At higher CV concentrations, however, a saturation of peak intensities becomes evident. Curves with similar trend were reported by others using SERS (Qiu and others 2008; Tao and others 2003). Based on these results, it can be inferred that SERS activities from the gold nanostructures were well behaved at different concentration levels over 3 orders of magnitude, making it possible to quantify trace amounts of the analytes by SERS. SERS spectra of CV exhibited distinct and characteristic Raman peaks when the concentration of CV was at the ppb level. Some Raman peaks of CV were still detectable at 0.2 ppb level even though some interfering peaks due to background noises became evident. From the linear observation, the lowest detectable concentration on this gold nanostructure was estimated to be ~ 0.2 ppb, which is quite remarkable and satisfies the recommended detection level by the food safety regulations.

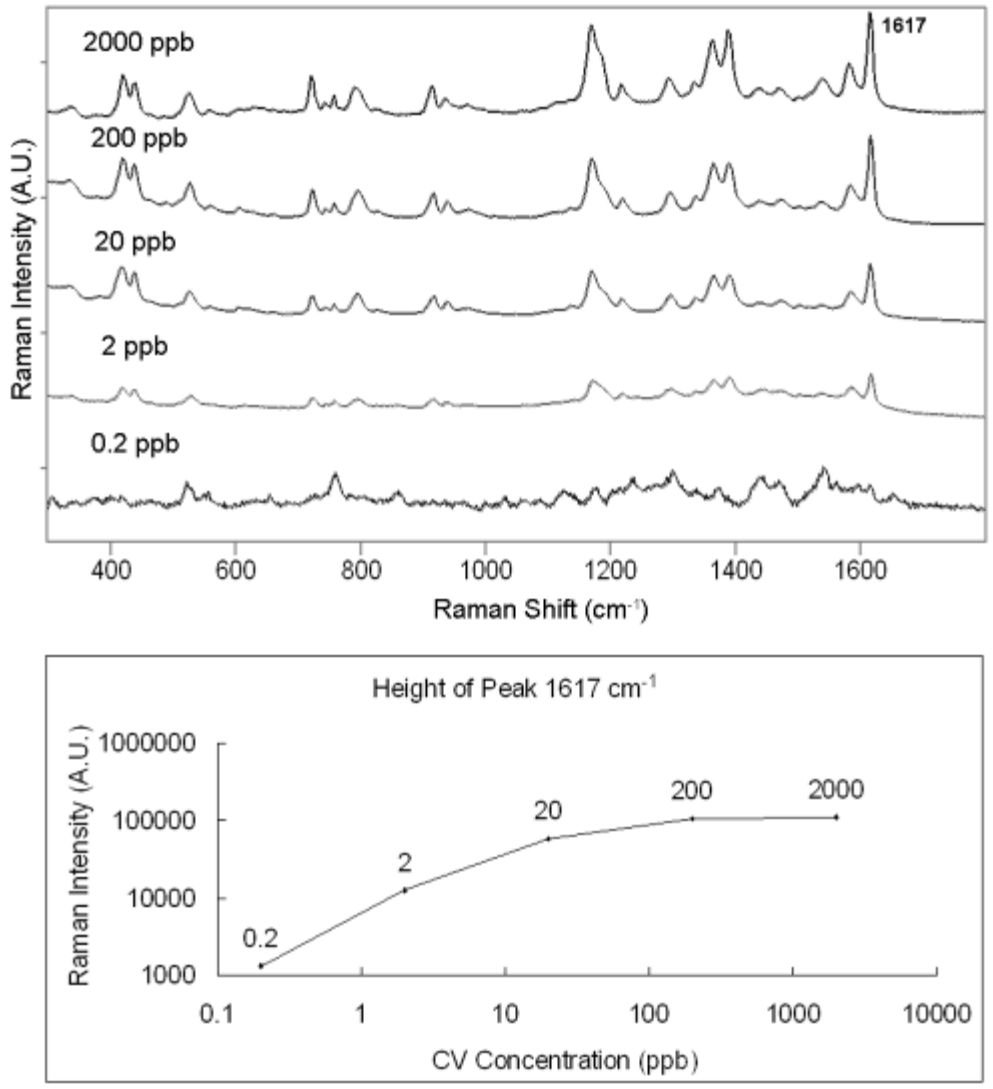

Figure 43. SERS spectra of CV at concentrations of 0.2, 2, 20, 200, and 2000 ppb on fractal-like gold nanostructures. A linear relationship between the log peak height at 1617 cm^{-1} and log CV concentration (0.2 to 20 ppb) is also shown

Currently, however, there are only a few tentative applications of SERS in solving food safety issues, most likely due to the lack of economic, effective and reliable SERS-active substrates (He and others 2007; 2008b). This preliminary study demonstrates that SERS coupled with fractal-like gold nanostructures has a great potential to serve as a promising analytical technique for the detection and characterization of trace amounts of food contaminants such as CV and MG.

It should be mentioned that our nanoparticle-based gold nanostructures are chemically very stable and physically robust. The gold nanostructures did not show any sign of degrading SERS activities when stored at ambient laboratory environment for days, washed with volatile cleaning solvents such as ethanol, or agitated in an ultrasonic cleaner for several minutes. These indicate the remarkable mechanical strength of self-organized complex nanostructures. Considering the simplicity of fabrication process and impressive ultra-high sensitivity of gold nanostructures, we expect that these self-assembled gold nanostructures will greatly promote SERS applications in detecting chemicals for food safety concerns.

Several issues about the SERS-active nanosubstrates made through the "bottom up" approach remain to be addressed. For instance, defective structural integrity over a large scale and/or poor substrate-to-substrate consistency may limit the use of these nanosubstrates for widespread applications (Alexander and Le 2007). Therefore, future studies are needed to improve the reproducibility of SERS measurements on nanosubstrates from large scale production. The multiple-interconnected gold clusters and the natural formation of pores are crucial to fabricate the high quality SERS-active nanosubstrate. Improvement of reproducibility could be achieved by fabricating nanosubstrates under optimal conditions including controlled initial nanoparticle sizes,

film thickness and annealing temperatures. In addition, work is underway in our lab to apply this ultra-sensitive SERS method to detect and characterize contaminants in real food products. The major challenge for application of SERS in real foods, besides the nanosubstrates issues stated above, is how to detect food contaminants without interferences from other components. CV and MG are expected to be easier detected due to their multiple ring structures and efficient adsorption on gold or silver surface thus producing stronger Raman signals than many other chemicals/biochemicals (Le Ru and others 2007).

4.4 Use of silver dendrites in SERS detecting restricted antibiotics

4.4.1 Characterization of a dendritic silver nanosubstrate

The morphology of silver nanostructure made by replacement reactions is mainly dependent upon silver ion concentrations. After dipping a zinc plate into a 5 mmol/L $AgNO_3$ solution for 1 min, silver aggregates were obtained, which consisted of silver nanoparticles with size around 200 nm (Figure 44A). However, the aggregate structure was not uniformly distributed on the zinc plate and the amount of aggregates was insufficient for SERS measurements. After dipping a zinc plate into a 200 mmol/L $AgNO_3$ solution for 1 min, a dendritic silver nanostructure was formed (Figure 44 B1 and B2). This structure was composed of ~50 nm silver nanoparticles that connected with each other to form symmetrical leaves on branches. The length of individual dendrite varied from 1 to 5 μm. Besides silver ion concentrations, time is also an important factor affecting the morphology, size, and production amount of silver nanostructures. For example, if the reaction time of a zinc plate in 200 mmol/L $AgNO_3$ is too short (~5 s), a

thin black silver layer was formed on the zinc plate with similar aggregate structures as that in Figure 1A. It was reported that after 50 s in 200 mmol/L $AgNO_3$ solution, a perfect dendrite structure with well-crystallized separately hexagonal plate was formed (Fang and others 2007). A strong anisotropic growth contributes the evolution of silver nanostructure to a thermodynamically stale dendrite structure. If the reaction time is too long, the silver layer on the zinc plate will be too thick and fragile to handle. Therefore, an optimum reaction time of 1 min was chosen to get a sufficient amount of silver dendrites.

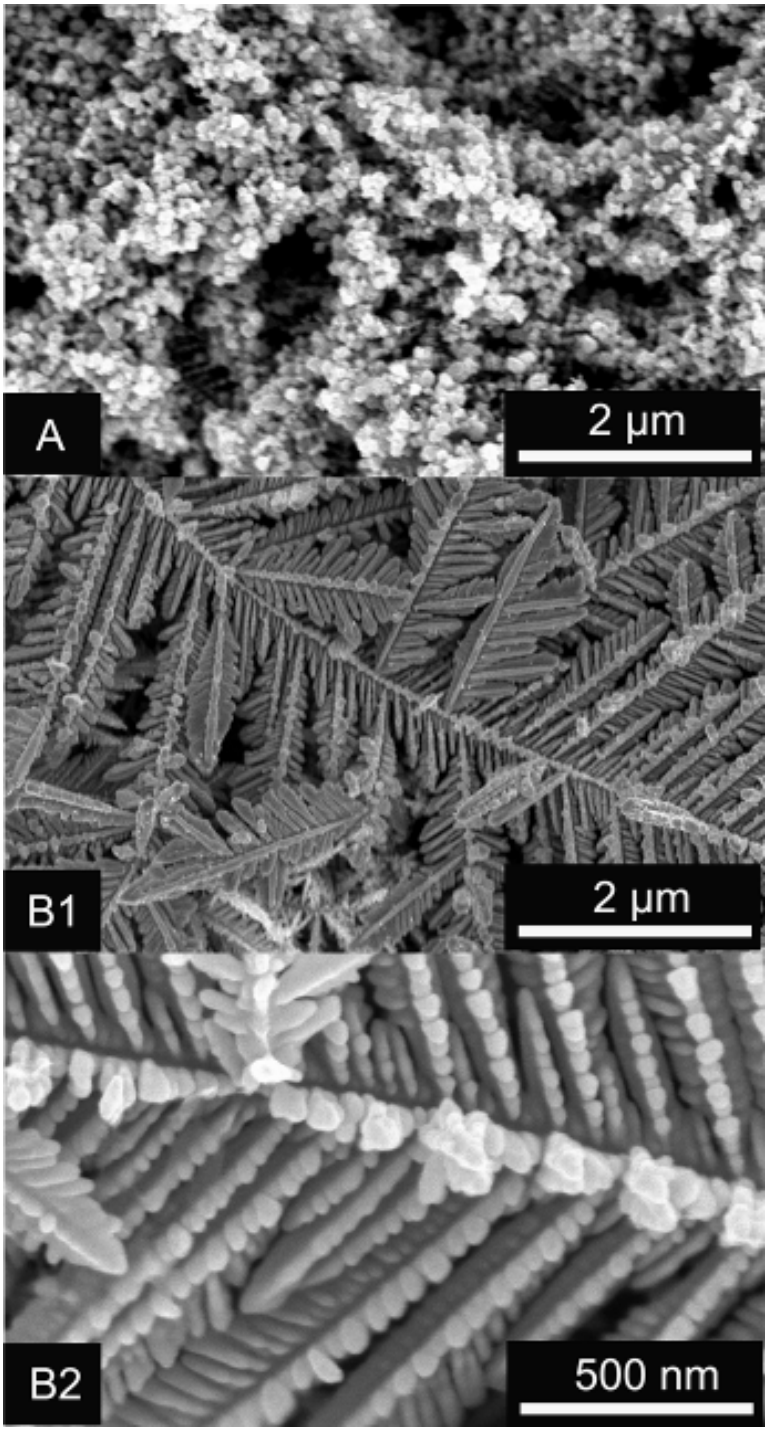

Figure 44. SEM of silver nanoparticle aggregates (A) and silver dendrites (B1 and B2)

Silver dendrite products were carefully peeled from the zinc plate with tweezers and put into a glass bottle, followed by rinsing for several times using de-ionized water. Washed silver dendrite products were stored in de-ionized water in a glass bottle (Figure 45). A dendrite silver nanosubstrate was made by transferring small amount (~3 μL) of silver dendrite precipitation from the glass bottle onto a flat gold-coated glass slide by a pipette (Figure 45). Multiple spots could be deposited onto a single slide and each spot was used to test one sample for ease of measurement and minimizing cross-contamination. The slide could be easily cleaned by erasing the silver dendrite spots and reused. This design of a SERS substrate provides an easy, convenient, and cost-effective way for SERS analysis.

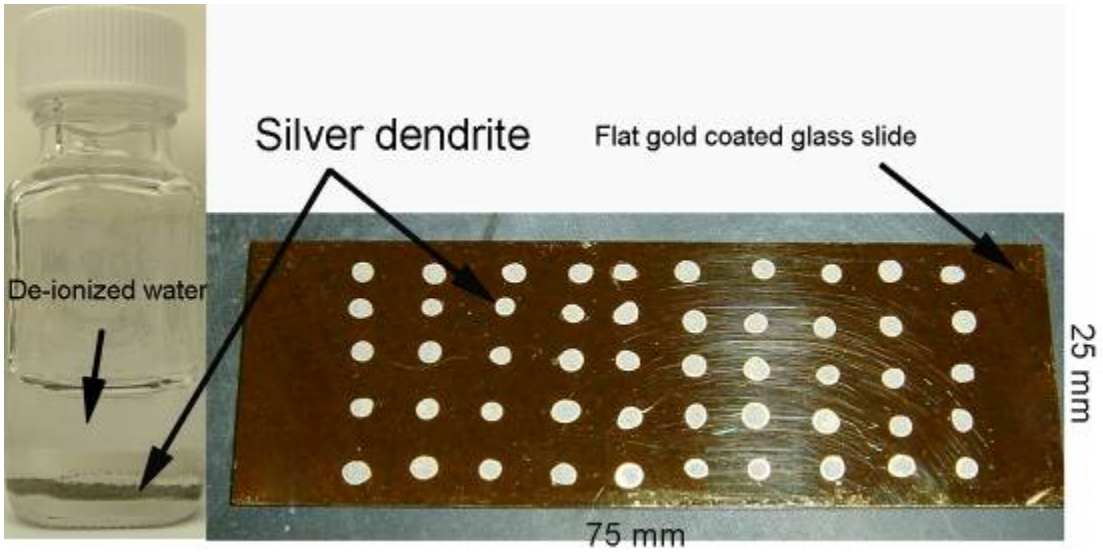

Figure 45. Silver dendrites in water and deposited on a flat gold-coated glass slide

Figure 46 shows an UV-VIS absorption spectrum of silver dendrites in de-ionized water. It is interesting to find that the absorption of the silver dendrite suspension extends over a wide range of wavelength from 400 to 800 nm. Therefore, the use of 785 nm laser excitation source in this study was appropriate to ensure the surface plasmon resonance for SERS. This result shows that silver dendrite nanostructures could accommodate a broad selection of laser excitation sources for SERS experiments. Qiu and others (Qiu and others 2008a) reported their silver fractal network absorbed a broad range of wavelength including infrared ranges. Many other studies also showed that the optimum absorption of silver nanostructures were around 400 to 500 nm (Song and others 2006; Tao and others 2003; Gao and others 2005).

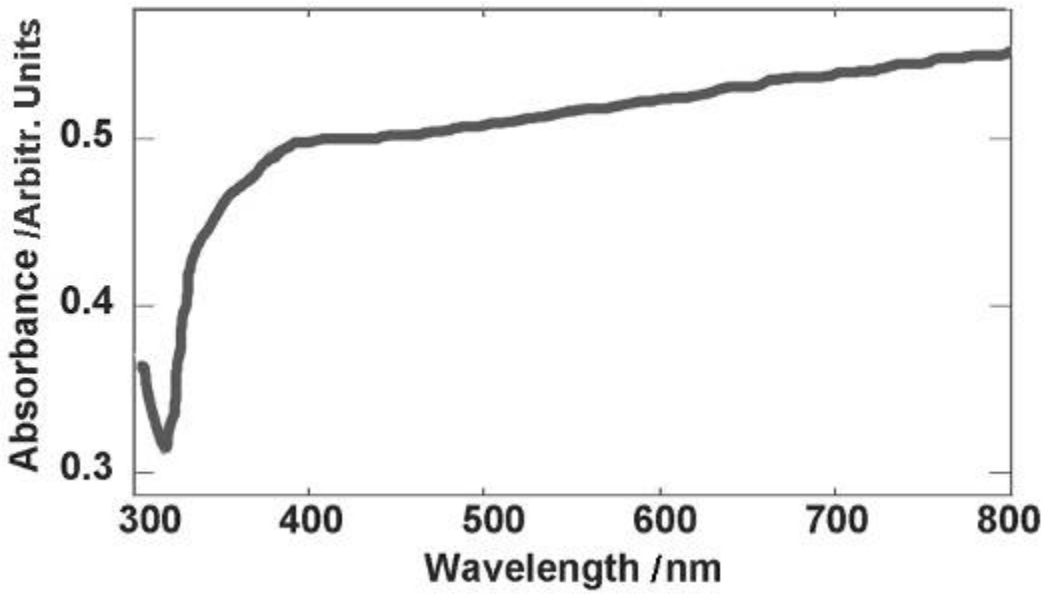

Figure 46. UV-VIS absorbance spectrum of silver dendrites

4.4.2 SERS performance in restricted antibiotics detection

4.4.2.1 Detection and discrimination of antibiotics by SERS

Three antibiotics (ENRO, CIP, and CHL) exhibit fingerprint-like SERS spectra that are related to their unique molecular structures (Figure 47). Detailed information about peak assignments could be found in some literatures (Si and others 2009; Skoulika and Constantinos 2001). For example, the 752 cm^{-1} band is attributed to methylene rocking modes. Bands around 771 cm^{-1} are characteristic of the substituted benzene ring deformation modes. Band at 1070 cm^{-1} is attributed to C-H rocking and band at 1392 cm^{-1} to symmetric O–C–O vibrations. The band around 1484 cm^{-1} is attributed to vibrations of the benzene ring, and the band at 1594 cm^{-1} attributed to benzene ring stretch, and the band at 1628 to the C=O stretch. Compared with ENRO and CHL, CIP of the same concentration exhibited 100 times more intense SERS signals. This was due to the presence of Cl^- in the solution bridging between silver dendrite nanostructures and CIP molecules, thus enhancing the attachment of CIP molecules on the surface of silver nanostructure (Ciou and others 2009). Further analysis using PCA shows clear separated clusters between different antibiotics (Figure 48).

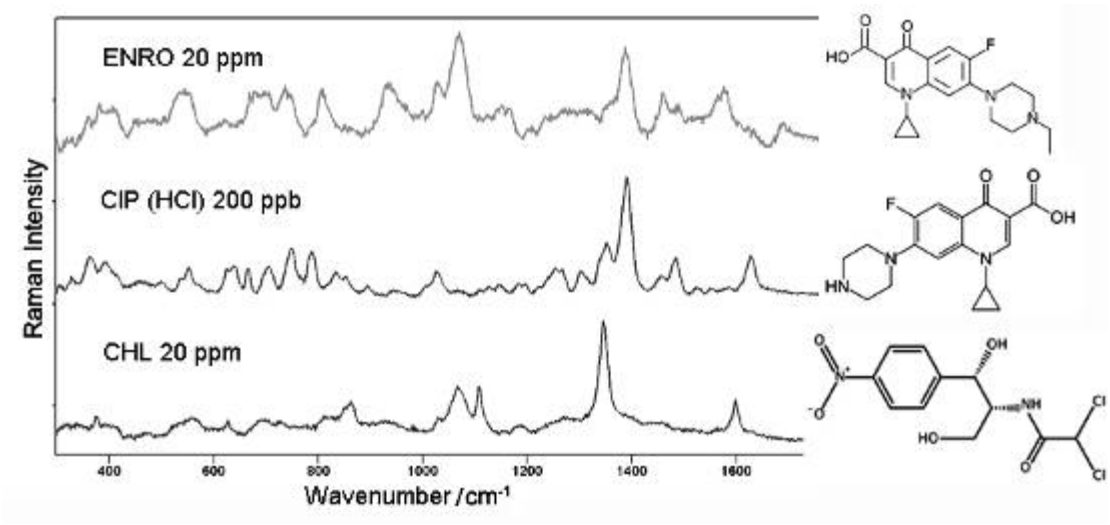

Figure 47. SERS spectra of 20 ppm enrofloxacin (ENRO), 200 ppb ciprofloxacin (CIP), and 20 ppm chloramphenicol (CHL)

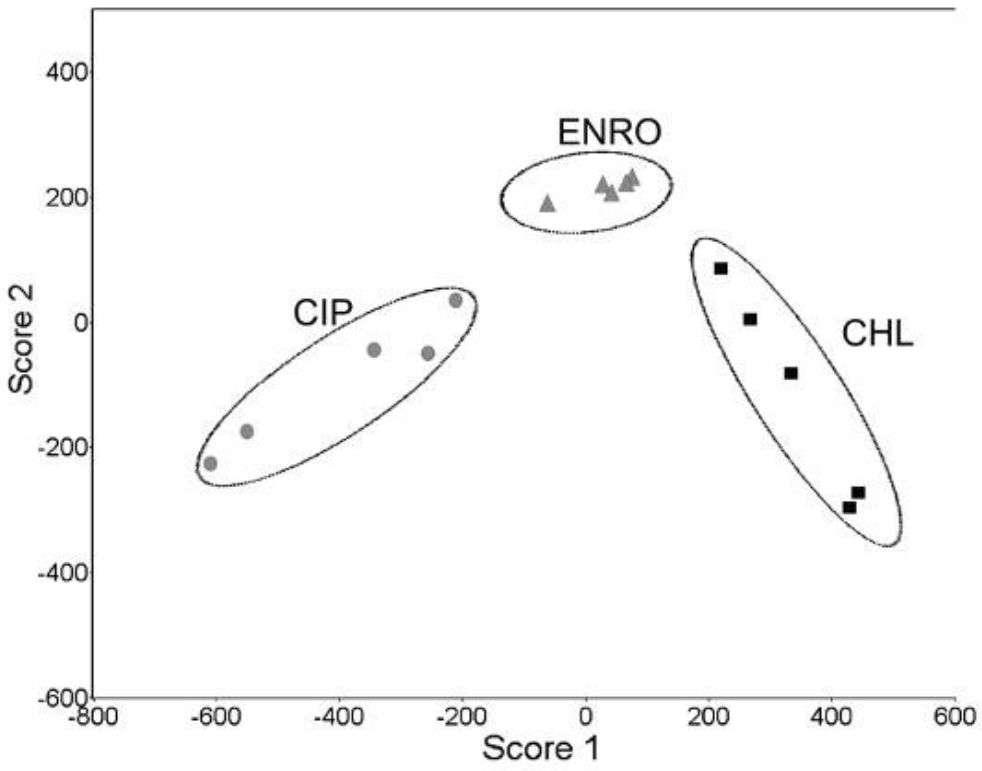

Figure 48. PCA plot of three antibiotics (enrofloxacin (ENRO), ciprofloxacin (CIP)), and chloramphenicol (CHL))

4.4.2.2 LOD and LOQ

A series of concentrations of CIP samples (20 ppb to 200 ppm) were deposited onto the spots of silver dendrites. SERS spectra of CIP (Figure 49) show distinctive and characteristic Raman peaks at various concentrations. Some Raman peaks of CIP were still discernable at 20 ppb level, even though some interfering peaks from background became more evident. A major background peak at 1074 cm^{-1} was from the NO_3^- residue on the substrate. Figure 50 shows the relationship between the concentration and the Raman peak intensity based on the CIP peak around 1392 cm^{-1}. A linear regression (R^2 = 0.98) was established using the data from samples of 20 ppb, 200 ppb, 2 ppm, and 20 ppm. Therefore, the LOD and LOQ was estimated to be around 20 ppb. Nonlinear curve was found when the concentration of CIP was above 20 ppm. This is because of saturated adsorption of CIP molecules on the silver dendrites. These results indicate that silver dendrites could be used in SERS to detect, characterize, and quantify seafood antibiotics at ppb levels based on SERS spectral information.

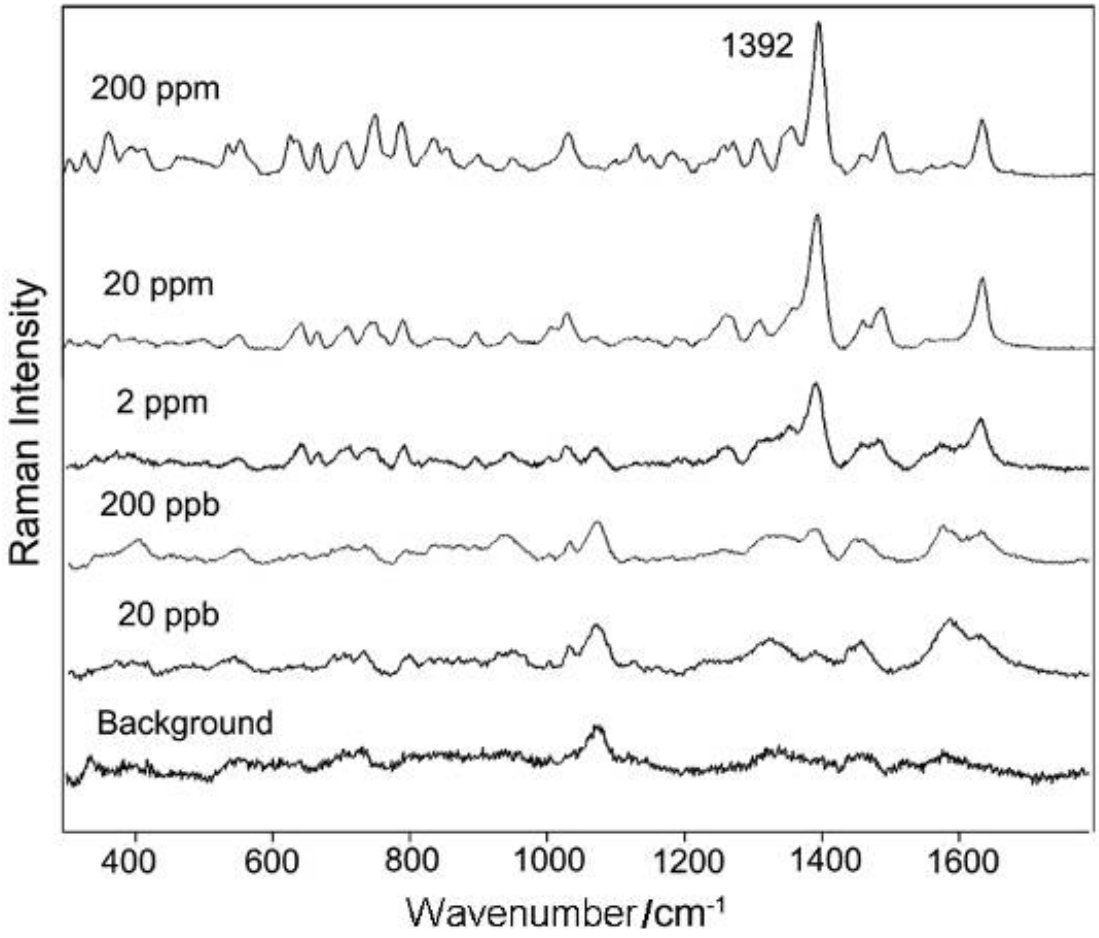

Figure 49. SERS spectra of a series of concentrations of ciprofloxacin (20 ppb to 200 ppm)

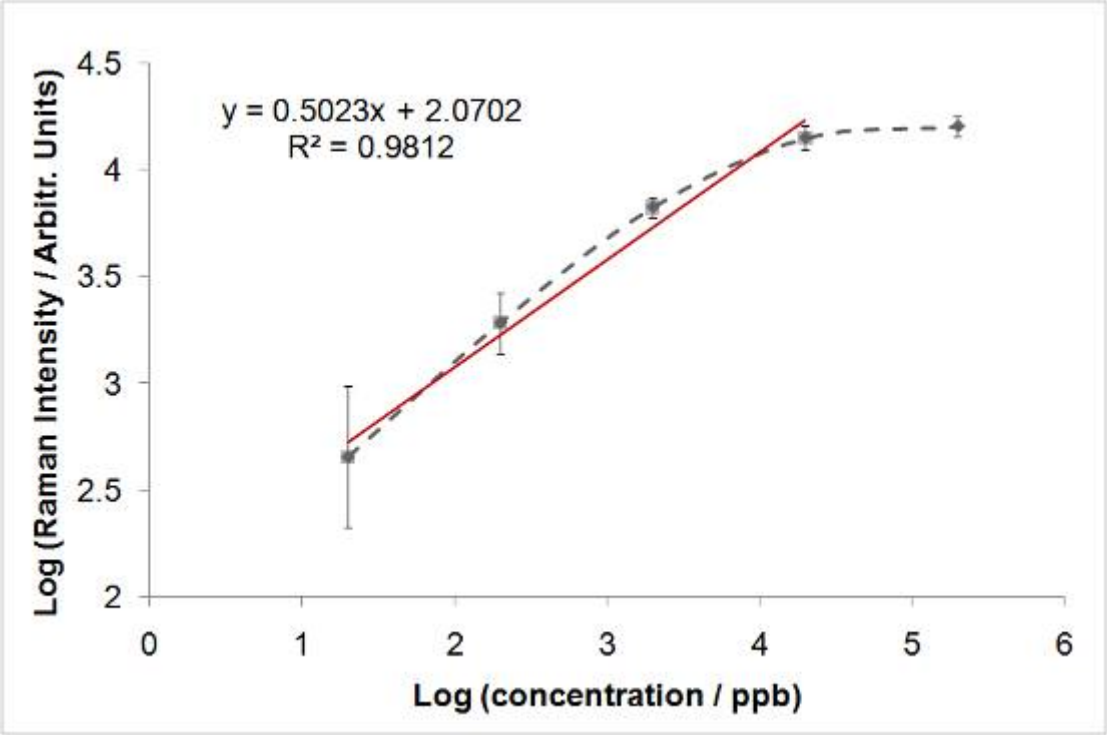

Figure 50. Relationship between the Raman intensity and concentration of ciprofloxacin solutions

4.4.2.3 Analytical enhancement factor (AEF)

By comparing the CIP peak at around 1392 cm^{-1} from a dendritic silver nanosubstrate with that from a flat gold film substrate (Figure 51), the AEF was calculated to be around 10^4 based on the equation (3-3). Measuring the AEF is a simple and straightforward way of evaluating the SERS enhancement and AEF can be easily measured in practical applications. However, it is worth mentioning that the concentration of analyte in SERS measurement doesn't fully characterize the adsorbed molecule number due to the first layer effect (Haynes and others 2005a), therefore, the real enhancement factor is thought to be even larger (Le Ru and others 2007).

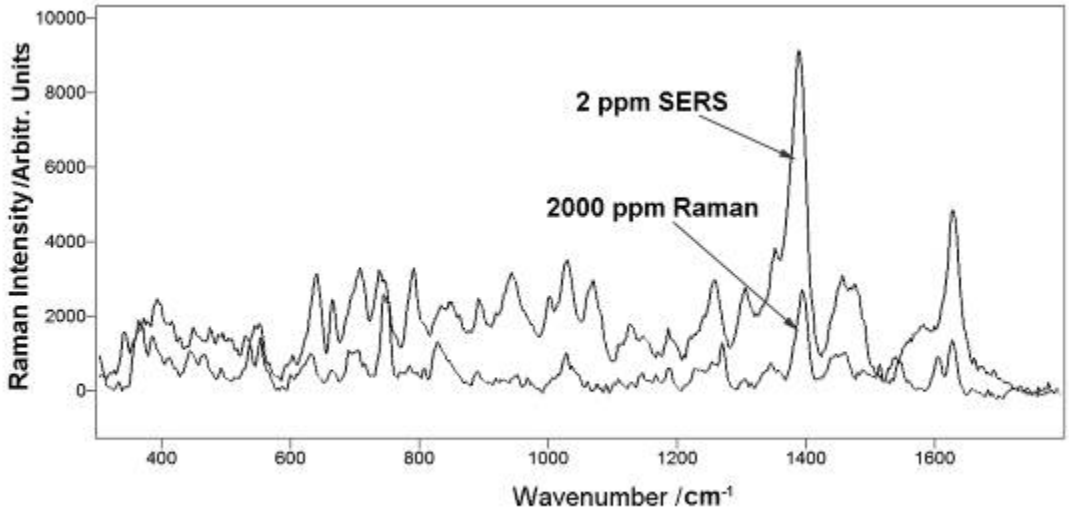

Figure 51. SERS spectra of 200 ppb ciprofloxacin on silver dendrites and 2000 ppm ciprofloxacin on a flat gold coated glass slide

4.4.2.4 Consistency test

A common problem with the "bottom-up" nanostructure is their inconsistent performance when spot-to-spot or substrate-to-substrate tests are conducted. This is mainly because of a lack of structural uniformity and integrity over the entire area of the nanostructure. In this study, consistency test was conducted in two independent experiments (nanosubstrates). On each nanosubstrate, spectra were collected from 2 to 3 different positions within a spot. Two spots were tested in each experiment. Result (Figure 52) shows a satisfactory consistency of the SERS performance. The RSD of the standardized value was calculated to be 19.6% according to equation (2). The dendritic silver network was well produced and controlled by controlling the $AgNO_3$ concentrations, the reaction time, and the way of spotting the silver dendrite precipitants on a flat slide, which provided a consistent nanostructure for SERS detection.

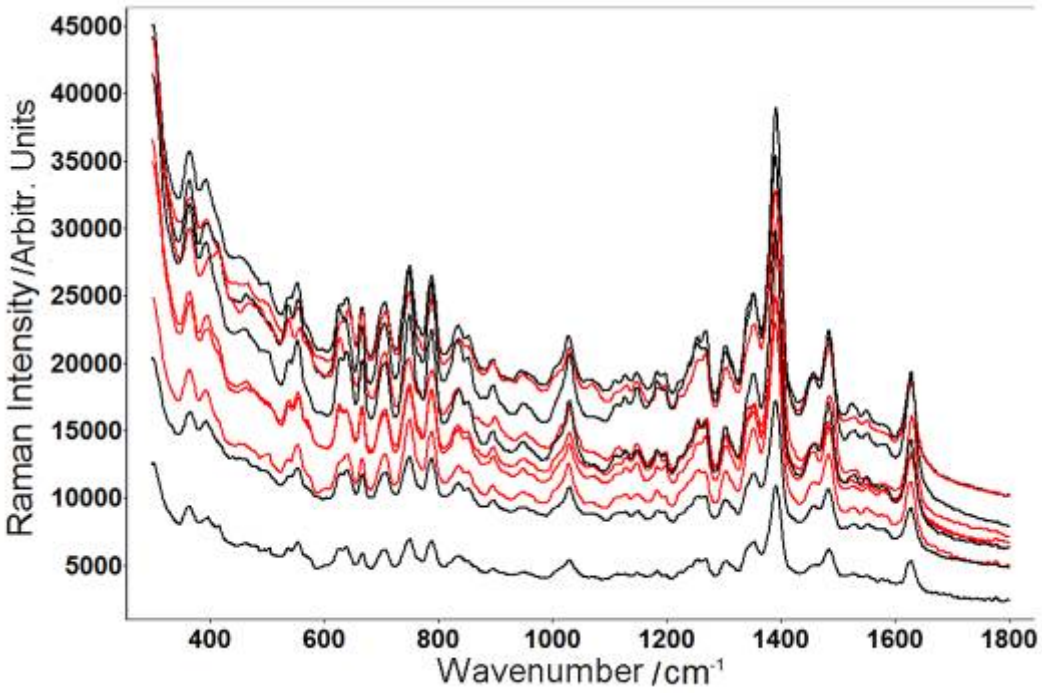

Figure 52. SERS spectra of ciprofloxacin from two independent experiments (red and black)

4.4.2.5 Shelf life test

The SERS performance of silver dendrites was tested on a monthly basis. Figure 53 shows the SERS spectra of CIP acquired from silver dendrites made and stored for 0, 3, and 6 months. No major changes were observed in either peak intensity or position of the CIP spectral peaks between these spectra, indicating excellent stability of silver dendrites in water. The low level of oxygen in water was attributed to slow down the oxidization process of silver nanomaterials, hence providing a simple and effective way to preserve the silver dendrites.

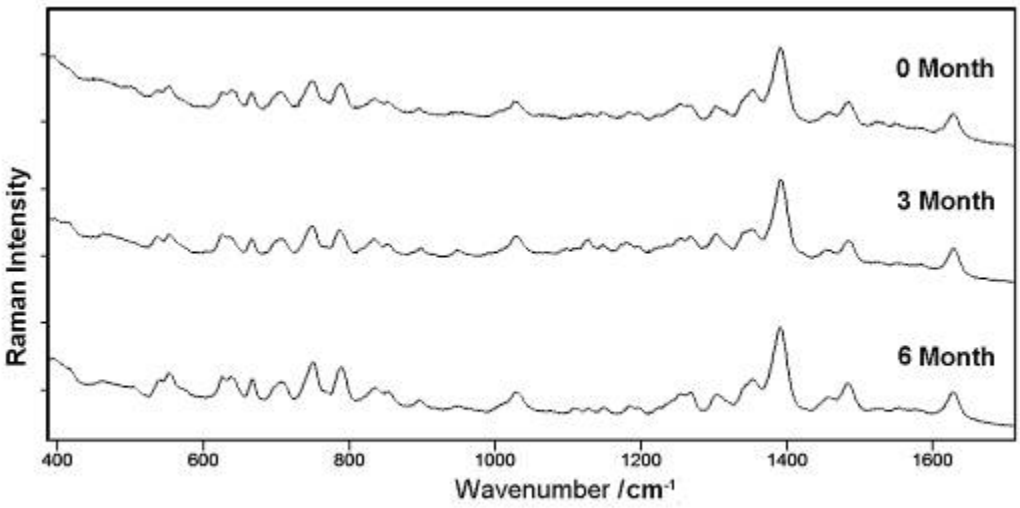

Figure 53. SERS spectra acquired from ciprofloxacin deposited onto silver dendrites that were stored for 0, 3, and 6 months

4.4.3 Conclusion

In summary, we developed a dendritic silver nanosubstrate via a simple and cost-effective method. This nanosubstrate shows satisfactory enhancement factor, consistent and stable performance in detecting trace amounts of antibiotics. Results indicate that SERS technique coupled with silver dendrites can be used for rapid and accurate detection, characterization, and quantification of antibiotics. Nevertheless, future study is needed to improve SERS sensitivity by optimizing the laser wavelength and the addition of salt concentration, exploring the feasibility of measuring other food contaminants, and applying this method in detection of chemical contaminants in real food products.

CHAPTER 5

DISCUSSION

5.1 Advantages of SERS techniques

There is a great potential for applying SERS as a routine analytical technique in rapid detection of chemical or biological contaminants in foods due to the following reasons:

1. Different chemical and microbiological samples yield unique Raman spectral patterns and the Raman intensity is related to the concentration of samples or the number of microbes. Therefore, it is possible to detect, quantify, and characterize different chemical and biological contaminants.

2. SERS is very sensitive. The LOD of SERS could reach the ppm to ppb level depending on the properties of SERS substrates and tested analyte samples. Therefore, SERS is suitable for detection of trace amount of samples.

3. SERS technique requires minimum sample preparation before measurement. Extraction of food contaminants from a food system could be simplified and large particles do not affect the final results significantly.

4. The whole procedure of SERS detection is fast due to short sample preparation time and short measurement time (less than one min for measurement).

5. The operation of SERS measurement is easy and straightforward.

6. SERS equipment is cheaper and smaller than mass spectroscopy if LC/MS or GC/MS is used. With the development of SERS substrates and the use of a portable Raman, it is possible to have cost-efficient SERS methods for on-site investigation.

5.2 Limitations and challenging issues

The limitations of SERS techniques include:

1. Only Raman-active chemicals or biochemicals yield Raman signals.

2. Food components may influence the SERS signals of target samples. The SERS signals of the target one would be greatly covered if other chemicals are more Raman-active than the target one.

3. The accuracy of SERS is lower than that of HPLC or GC due to the difficulty of controlling the uniformity of "hot spots" on the substrates.

4. Currently, there are only a few SERS substrates commercially available and they are very expensive.

5. SERS technique is still in an early developmental stage and its basic mechanism of SERS enhancement is still being studied.

SERS substrates and analytes are two critical elements in SERS testing. Challenging issues associated with these two elements are discussed below.

5.2.1 SERS substrates

A good substrate is the key in SERS testing. Any additional background peaks from the substrate will influence the measurement of samples. There are two kinds of possible peaks from a substrate. One type of peaks comes from the substrate material itself or the chemicals that involved in the substrate fabrication. This type of peaks will show up in the SERS spectra every time during measurement and is predicable. Therefore, as long as it doesn't overlap with the sample peaks, it will not influence the results. Another type of peaks come from unknown impurity from the fabrication process and is difficult to

predict. During each measurement, the peak position and intensity may vary, making it difficult to tell whether it is from the sample or from the substrate itself. Therefore, it would be better to use materials and chemicals with high quality and purity in the substrate fabrication.

5.1.2 Analytes

It is more reliable and accurate to identify a pure chemical due to the available Raman database of pure chemicals. Different chemicals or biomaterials will have their unique Raman spectral patterns. When the analyte is a mixture, however, it is difficult to make a accurate prediction of the targeted chemical in the mixture, unless the target chemical has one or several distinctive peaks (e.g. melamine peak at around 680 cm^{-1}). There are two possible reasons that can explain this. First, different chemicals may have one or several peaks at the same wavelength positions, especially for those with similar structures. Second, it is highly possible that those non-target chemicals in the mixture are more Raman-active than the target chemical, so that the signals from the non-target chemicals will overlap those from the target chemical. For SERS, it is more complicated because different chemicals will have different adsorption effect on different metal surfaces. Therefore, the selection of target chemical and appropriate solvents is very important in the SERS detection.

5.3 Future directions

Future studies need focus on the optimization of the current SERS substrates and application of those substrates in real food matrices. Many existing SERS nanosubstrates

yield inconsistent signals when spot-to-spot or substrate-to-substrate tests are conducted. This is mainly because of a lack of structural integrity and uniformity over the entire area of the substrate. In addition, it is very difficult to make a substrate with a high enhancement factor and high reproducibility concurrently. For real-world applications, reproducibility is considered more important than enhancement factors. Therefore, a nanosubstrate with a homogenous nanostructure network could produce much more consistent and reproducible signals. Different assay conditions, such as type of nanosubstrate and laser wavelength, may cause some variations in identification of samples. Therefore, a well-established database for different SERS conditions is very useful for future applications. Background signal from the food and environmental matrices is another challenge. Fortunately, many chemical contaminants are more Raman-active than biological samples. In addition, proper and simplified sample pretreatment is needed before conducting a SERS measurement.

CHAPTER 6 CONCLUSION

In conclusion, a variety of SERS substrates were developed and used including gold fractal nanoaggregates, silver dendrites, gold-coated zinc oxide nanonecklaces, and a commercial Klarite gold substrate. They were applied in SERS techniques for detection of chemical and biological samples, including melamine and its analogues, restricted antibiotics, prohibited dyes, and *Bacillus* spores. All of those SERS substrates greatly enhanced Raman scattering signals of samples. Commercial Klarite substrates could produce reproducible and satisfactory enhancement for most samples. However, they are very expensive. Gold fractal-like nanoaggregates have the highest enhancement factors among those substrates. However, inconsistent performance limited their applications in detecting food contaminants. Gold-coated zinc oxide nanonecklaces with satisfactory enhancement factors and wafer-scale fabrication face the problems of complex fabrication process and high cost. Silver dendrites are the best substrates developed in this project. They are easy-to-make, cost-effective, reproducible, stable, and with satisfactory enhancement. All of the substrates are able to detect pure samples in standard solution at the ppb level. Compared with conventional techniques such as HPLC, SERS is much faster and simpler, with great potential as a routine technique for screening large amount of food products for chemical and biological contaminants. Further study should focus on the application of this technique in real food matrices.

APPENDIX

1. Unit conversion

Percentage (%) = 10^4 parts per million (ppm) = 10^7 parts per billion (ppb)

10^{-5} mol/L melamine = 1.26×10^{-3} g/L $\approx$ 1.26 ppm

REFERENCES

Alderman DJ. 1982. *In vitro* testing of fisheries chemotherapeutants. J Fish Dis 5(2): 113-23.

Alexander TA, Le DM. 2007. Characterization of a commercialized SERS-active substrate and its application to the identification of intact *Bacillus* endospores. Appl Opt 46(18): 3878-90.

Allain LR, Vo-Dinh T. 2002. Surface-enhanced Raman scattering detection of the breast cancer susceptibility gene BRCA1 using a silver-coated microarray platform. Anal Chim Acta 469(1): 149-54.

Andersen WC, Turnipseed SB, Roybal JE. 2006. Quantitative and confirmatory analyses of malachite green and leucomalachite green residues in fish and shrimp. J Agric Food Chem 54(13): 4517-23.

Anonymous. 2004. Commission Decision 2004/25/EC as regards the setting of minimum required performance limits (MRPLs) for certain residues in food of animal origin. Official J Eur Union L6: 38-9.

Braithwaite A, Smith FJ. 1996. Chromatographic methods. 5th ed. London: Blackie Academic & Professional.

Brown CA, Jeong K-S, Poppenga RH, Puschner B, Miller DM, Ellis AE, Kang K-I, Sum S, Cistola AM, Brown SA. 2007. Outbreaks of renal failure associated with melamine and cyanuric acid in dogs and cats in 2004 and 2007. J Vet Diagn Invest 19(5): 525-31.

Brown RJC, Milton MJT. 2008. Nanostructures and nanostructured substrates for surface-enhanced Raman scattering (SERS). J Raman Spectrosc 39: 1313-26.

Cazes J, Scott RPW. 2002. Chromatography theory. Marcel Dekker, Inc.

Chan EYY, Griffiths SM, Chan CW. 2008. Public-health risks of melamine in milk products. The Lancet 372(9648): 1444-5.

Chu H, Huang Y, Zhao Y. 2008. Silver nanorod arrays as a surface-enhanced Raman scattering substrate for foodborne pathogenic bacteria detection. Appl Spectrosc 62(8): 922-31.

Cianciolo RE, Bischoff K, Ebel JG, Van Winkle TJ, Goldstein RE, Serfilippi LM. 2008. Clinicopathologic, histologic, and toxicologic findings in 70 cats inadvertently exposed to pet food contaminated with melamine and cyanuric acid. J Am Vet Med Assoc 233(5): 729-37.

Ciou S-H, Cao Y-W, Huang H-C, Su D-Y, Huang C-L. 2009. SERS enhancement factors studies of silver nanoprism and spherical nanoparticle colloids in the presence of bromide ions. J Phys Chem C 113(22): 9520-5.

Cohn E. 2008. FDA finds more traces of melamine in formula. CNN. http://www.cnn.com/2008/HEALTH/11/27/infant.formula.melamine/index.html (2/17/09)

Culp SJ, Beland FA. 1996. Malachite green: A toxicological review. J Am College Toxicol 15(3): 219-38.

Driks A. 1999. *Bacillus subtilis* spore coat. Microbiol Mol Biol Rev 63(1): 1-20.

Doering WE, Nie S. 2002. Single-molecule and single-nanoparticle SERS: examining the roles of surface active sites and chemical enhancement. J Phys Chem B 106(2): 311-7.

Emory RS, Haskins EW, Nie S. 1998. Direct observation of size-dependent optical enhancement in single metal nanoparticles. J Am Chem Soc 120: 8009-10.

Fang J, You H, Kong P, Yi Y, Song X, Ding B. 2007. Dendritic silver nanostructure growth and evolution in replacement reaction. Cryst Growth Des 7(5): 684-7.

Farquharson S, Gift AD, Maksymiuk P, Inscore FE. 2004. Rapid dipicolinic acid extraction from *Bacillus* spores detected by surface-enhanced Raman spectroscopy. Appl Spectrosc 58(3): 351-4.

FDA. 2007a. Marketing and import information on seafoods and seafood safety. http://www.fda.gov/Food/FoodSafety/Product-SpecificInformation/Seafood/ucm119105.htm (Accessed 06/25/2009)

FDA. 2007b. Questions and answers on FDA's import alert on farm-raised seafood from China. http://www.cfsan.fda.gov/~frf/seadwpe.html (Accessed 6/28/2007).

FDA. 2007c. Updated FCC Developmental melamine quantitation (HPLC-UV). http://www.fda.gov/cvm/melamine04022007.htm (Accessed 4/22/2007).

FDA. 2008a. FDA issues interim safety and risk assessment of melamine and melamine-related compounds in food. http://www.fda.gov/bbs/topics/NEWS/2008/NEW01895.html (Accessed 11/3/2008).

FDA. 2008b. Update interim safety and risk assessment of melamine and its analogues in food for humans. http://www.cfsan.fda.gov/~frf/lib4422.html (Accessed 4/19/2009).

Gao X, Gu G, Hu Z, Guo Y, Fu X, Song J. 2005. A simple method for preparation of silver dendrites. Colloids and Surfaces A 254: 57-61.

Ghiamati E, Manoharan R, Nelson WH, Sperry JF. 1992. UV resonance Raman-spectra of *Bacillus* spores. Appl Spectrosc 46(2): 357-64.

Granum PE, Lund T. 1997. *Bacillus cereus* and its food poisoning toxins. FEMS Microbiol Lett 157(2): 223-8.

Hao E, Schatz GC. 2004. Electromagnetic fields around silver nanoparticles and dimers. J Chem Phys 120(1): 357-66.

Haynes CL, McFarland AD, Van Duyne RP. 2005a. Surface-enhanced Raman spectroscopy. Anal Chem 77(17): 338a-346a.

Haynes CL, Yonzon CR, Zhang XY, Van Duyne RP. 2005b. Surface-enhanced Raman sensors: early history and the development of sensors for quantitative biowarfare agent and glucose detection. J Raman Spectrosc 36(6-7): 471-84.

He L, Kim NJ, Li H, Hu Z, Lin M. 2008a. Use of a fractal-like gold nanostructure in surface-enhanced Raman spectroscopy for detection of selected food contaminants. J Agric Food Chem 56(21): 9843-7.

He L, Liu Y, Lin M, Awika J, Ledoux DR, Li H, Mustapha A. 2008b. A new approach to measure melamine, cyanuric acid, and melamine cyanurate using surface enhanced Raman spectroscopy coupled with gold nanosubstrates. Sens Instrumen Food Qual 2(1): 66-71.

He L, Liu Y, Lin M, Mustapha A, Wang Y. 2007. Detecting single Bacillus spores by surface enhanced Raman spectroscopy (SERS) Sens Instrumen Food Qual 2: 247-53.

Ingelfinger JR. 2008. Melamine and the global implications of food contamination. N Engl J Med 359(26): 2745-8.

Inglesby TV, O'Toole T, Henderson DA, Bartlett JG, Ascher MS, Eitzen E, Friedlander AM, Gerberding J, Hauer J, Hughes J, McDade J, Osterholm MT, Parker G, Perl TM, Russell PK, Tonat K. 2002. Anthrax as a biological weapon, 2002: updated recommendations for management. JAMA 287(17): 2236-52.

Janssen FW, Lund AJ, Anderson LE. 1958. Colorimetric assay for dipicolinic acid in bacterial spores. Science 127(3288): 26-7.

Kim YN, Yoo SH, Oh CS. 2009. Fabrication of SERS-active patterned gold nanoparticle films by electron irradiation and postpyrolysis. J Phys Chem C 113(2): 618-23.

Kneipp K, Kneipp H, Itzkan I, Dasari RR, Feld MS. 2002. Surface-enhanced Raman scattering and biophysics. J Phys-Condens Matter 14(18): R597-624.

Kneipp K, Kneipp H. 2006. Single molecule Raman scattering. Appl Spectrosc 60(12): 322A-34A.

Koglin E, Kip BJ, Meier RJ. 1996. Adsorption and displacement of melamine at the Ag/electrolyte interface probed by surface-enhanced Raman microprobe spectroscopy. J Phys Chem 100(12): 5078-89.

Kroll RG, Gilmour A, Sussman M. 1993. New techniques in food and beverage microbiology. Oxford: Blackwell.

Le Ru EC, Blackie E, Etchegoin PG. 2007. Surface enhanced Raman scattering enhancement factors: a comprehensive study. J Phys Chem C 111: 13794-803.

Lewis DM. 2001. FT-IR and FT-Raman spectroscopic studies of 2,4,6-trichloro-s-triazine and its hydroxy derivatives. Advin Colour Sciand Technol 4(2): 59.

Liang EJ, Ye XL, Kiefer W. 1997. Surface-enhanced Raman spectroscopy of crystal violet in the presence of halide and halate ions with near-infrared wavelength excitation. J Phys Chem A 101(40): 7330-5.

Liang XQ, Pu XM, Zhou HW, Wong NB, Tian AN. 2007. Keto-enol tautomerization of cyanuric acid in the gas phase and in water and methanol. J Mol Struct-Theochem 816(1-3): 125-36.

Liang XQ, Zheng WX, Wong NB, Li JS, Tian AM. 2004. Theoretical study on the mechanism of keto-enol isomerization for cyanuric acid and cyameluric acid. J Mol Structure-Theochem 672(1-3): 151-9.

Li-Chan ECY. 1996. The applications of Raman spectroscopy in food science. Trends Food Sci Technol 7(11): 361-70.

Lin J, Smith MP, Chapin KC, Baik HS, Bennett GN, Foster JW. 1996. Mechanisms of acid resistance in enterohemorrhagic Escherichia coli. Appl Environ Microbiol 62(9): 3094-100.

Lin M, Al-Holy M, Al-Qadiri H, Kang DH, Cavinato AG, Huang Y, Rasco BA. 2004. Discrimination of intact and injured Listeria monocytogenes by Fourier transform infrared spectroscopy and principal component analysis. J Agric Food Chem 52(19): 5769-72.

Lin M, He L, Awika J, Yang L, Ledoux DR, Li H, Mustapha A. 2008. Detection of melamine in gluten, chicken feed, and processed foods using surface enhanced Raman spectroscopy and HPLC. J Food Sci 73(8): T129-34.

Litzau JJ, Mercer GE, Mulligan KJ. 2008. GC-MS Screen for the presence of melamine, ammeline, ammelide, and cyanuric acid. FDA Laboratory Information Bulletin No. 442324.

Martens H, Naes T. 1986.Multivariate calibration. New York: JohnWiley & Sons, Inc.

Maheshwari V, Saraf RF. 2006. Mineralization of monodispersed CdS nanoparticles on polyelectrolyte superstructure forming an electroluminescent "necklace-of-beads". Langmuir 22(21): 8623-6.

Maquelin K, Kirschner C, Choo-Smith LP, van den Braak N, Endtz HP, Naumann D, Puppels GJ. 2002. Identification of medically relevant microorganisms by vibrational spectroscopy. J Microbiol Methods 51(3): 255-71.

McCreery RL. 2000. Raman spectroscopy for chemical analysis. Wiley-Interscience.

Mendoza M. 2009. Associated Press. Consumer group says FDA melamine guidelines unsafe.

Mishra S, Ojha AK, Singh D, Prasad RR, Srivastava SK, Singh RK. 2007. Concentration-dependent surface-enhanced Raman scattering and molecular dynamic study of dimethyl formamide. J Raman Spectrosc 38(11): 1454-60.

MSNBC. 2007. Tainted food killed 224 pets in latest tally. http://www.msnbc.msn.com/id/22028878/from/ET/, 11/29/2007. .

Nastasijevic I, Mitrovic R, Buncic S. 2008. Occurrence of Escherichia coli O157 on hides of slaughtered cattle. Lett Appl Microbiol 46(1): 126-31.

Nilsen H, Esaiassen M, Heia K, Sigernes F. 2002. Visible/near-infrared spectroscopy: A new tool for the evaluation of fish freshness? J Food Sci 67(5): 1821-6.

Panicker CY, Varghese HT, Philip D. 2006. FT-IR, FT-Raman and SERS spectra of Vitamin C. Spectrochimica Acta Part a-Molecular and Biomolecular Spectrosc 65(3-4): 802-4.

Peica N, Lehene C, Leopold N, Cozar O, Kiefer W. 2007. Raman and surface-enhanced Raman studies of the food additive sodium benzoate. J Opt Adv Mater 9(9): 2943-8.

Peica N, Pavel I, Pinzaru SC, Rastogi VK, Kiefer W. 2005. Vibrational characterization of E102 food additive by Raman and surface-enhanced Raman spectroscopy and theoretical studies. J Raman Spectrosc 36(6-7): 657-66.

Perdigao LMA, Champness NR, Beton PH. 2006. Surface self-assembly of the cyanuric acid-melamine hydrogen bonded network. Chem Commun (5): 538-40.

Qiu T, Wu XL, Shen JC, Xia Y, Shen PN, Chu PK. 2008. Silver fractal networks for surface-enhanced Raman scattering substrates. Appl Surf Sci 254: 6399-402.

Rasco BA, Bledsoe GE. 2005. Bioterrorism and foods safety. Boca Raton, FL: CRC Press.

Riley LW, Remis RS, Helgerson SD, McGee HB, Wells JG, Davis BR, Hebert RJ, Olcott ES, Johnson LM, Hargrett NT, Blake PA, Cohen ML. 1983. Hemorrhagic colitis associated with a rare *Escherichia coli* serotype. N Engl J Med 308(12): 681-5.

Roybal JE, Walker CC, Pfenning AP, Turnipseed SB, Gonzales SA, Hurlbut JA. 2003. Concurrent determination of four fluoroquinolones; ciprofloxacin, enrofloxacin, sarafloxacin and difloxacin in atlantic salmon tissue by LC with fluorescence detection. Food and Drug Administration http://www.cfsan.fda.gov/seafood1.html.

Sauer G, Brehm G, Schneider S. 2004. Preparation of SERS-active gold film electrodes via electrocrystallization: their characterization and application with NIR excitation. J. Raman Spectrosc 35: 568-76.

Seifer GB. 2002. Cyanuric acid and cyanurates. Russ J Coord Chem 28(5): 301-24.

Shi J, Sun X, Zhang J, Lian J, Yu Q, Lin M, Li H. 2009. Epitaxial growth of horizontally aligned zinc oxide nanonecklaces arrays on r-plane sapphire. J Appl Phys. Forthcoming.

Si MZ, Kang YP, Zhang ZG. 2009. Surface-enhanced Raman scattering (SERS) spectra of chloramphenicol in Ag colloids prepared by microwave heating method. Raman Spectroscopy. Forthcoming.

Skoulika SG, Constantinos AG. 2001. Rapid quantitative determination of ciprofloxacin in pharmaceuticals by use of solid-state FT-Raman spectroscopy. Spectrosc Tech 55(9): 1259-65.

Smith KE, Besser JM, Hedberg CW, Leano FT, Bender JB, Wicklund JH, Johnson BP, Moore KA, Osterholm MT. 1999. Quinolone-resistant *Campylobacter jejuni* infections in Minnesota, 1992-1998. New Eng J Med 340(20): 1525-32.

Smoker M, Krynitsky AJ. 2008. Interim method for determination of melamine and cyanuric acid residues in foods using LC-MS/MS: Version 1.0. FDA Laboratory Information Bulletin No. 4422.

Song W, Cheng Y, Jia H, Xu W, Zhao B. 2006. Surface enhanced Raman scattering based on silver dendrites substrate. J Colloid Interface Sci 298(2): 765-8.

Sugita T, Ishiwata H, Yoshihira K. 1990. Release of Formaldehyde and Melamine from Tableware Made of Melamine Formaldehyde Resin. Food Addit Contam 7(1): 21-7.

Tao A, Kim F, Hess C, Goldberger J, He R, Sun Y, Xia Y, Yang P. 2003. Langmuir-blodgett silver nanowire monolayers for molecular sensing using surface-enhanced Raman spectroscopy Nano Lett 3(9): 1229-33.

Teslova T, Corredor C, Livingstone R, Spataru T, Birke RL, Lombardi JR, Canamares MV, Leona M. 2007. Raman and surface-enhanced Raman spectra of flavone and several hydroxy derivatives. J Raman Spectrosc 38(7): 802-18.

Tseng CH, Mann CK, Vickers TJ. 1994. Ft-Raman determination of melamine and melamine-cyanurate in nylon. Appl Spectrosc 48(4): 535-7.

Turnbull PCB. 1996. Bacillus. In: Baron, S., editor). Medical Microbiology. 4th ed. California: Addision-Wesley Publishing Company.

Turnipseed SB, Walker CC, Roybal JE, Pfenning AP, Hurlbut JA. 1998. Confirmation of fluoroquinolones in catfish muscle by electrospray liquid chromatography mass spectrometry. J AOAC Int 81(3): 554-62.

USAToday. 2007. U.S. food imports outrun FDA resources. http://www.usatoday.com/money/industries/food/2007-03-18-food-safety-usat_N.htm (Accessed 12/19/2007).

Willets KA, VanDuyne RP. 2007. Localized surface plasmon resonance spectroscopy and sensing Annu Rev Phy Chem 58: 267-97.

Wang Y, Li YS, Zhang ZX, An DQ. 2004. SERS spectra of vitamin A acid in silver solution. Guang Pu Xue Yu Guang Pu Fen Xi 24(11): 1376-8.

Wu LP, Li YF, Huang CZ, Zhang Q. 2006. Visual detection of Sudan dyes based on the plasmon resonance light scattering signals of silver nanoparticles. Anal Chem 78(15): 5570-7.

Xin H, Stone R. 2008. Tainted milk scandal: Chinese probe unmasks high-tech adulteration with melamine. Sci 322(5906): 1310-1.

Xu L, Fang Y. 2004. Raman spectroscopy of p-hydroxybenzoic acid aqueous solution and surface-unenhanced Raman scattering on silver colloid with ultraviolet excitation. J Colloid Interface Sci 274(1): 122-5.

Yi W, Bei W, Wang QG. 1990. Crystal-structure of melamine cyanuric acid complex (1-1) trihydrochloride, MCA.3HCl. J Crystallogr Spectrosc Res 20(1): 79-84.

Zhang J, Li X, Sun X, Li Y. 2005. Surface enhanced Raman scattering effects of silver colloids with different shapes. J Phys Chem 109(25): 12544-8.

VITA

Lili He was born in Hangzhou, Zhejiang, China on March 5, 1982. She is the only child in the family. She earned her Bachelor's degree in Plant Protection from Zhejiang University, China, in 2004 and Master's degree in Plant Pathology from Zhejiang University, China, in 2006. Then she got married and moved to Washington State University, US to pursue her doctoral degree in Food Science. After one year study, she transferred to University of Missouri, Columbia, US to continue her PhD study in Food Science and got reunion with her husband. In 2009, she received her doctoral degree with 6 publications.